Title
Dynamics of Early Afterdepolarization (EAD)-mediated Arrhythmias

Author
Chang, Marvin G

Publication Date
2012

Peer reviewed|Thesis/dissertation

UNIVERSITY OF CALIFORNIA

Los Angeles

Dynamics of Early Afterdepolarization (EAD)-mediated Arrhythmias

A dissertation submitted in partial satisfaction of the

requirements for the degree Doctor of Philosophy

in Molecular, Cellular, & Integrative Physiology

by

Marvin G. Chang

2012

ABSTRACT OF THE DISSERTATION

Dynamics of Early Afterdepolarization (EAD)-mediated Arrhythmias

by

Marvin G. Chang

Doctor of Philosophy in Molecular, Cellular, & Integrative Physiology

University of California, Los Angeles, 2012

Professor James N. Weiss, Chair

This dissertation is dedicated to understanding the dynamical mechanisms underlying early afterdepolarization (EAD)-mediated arrhythmias. EADs are a richly mined area of research that has resulted in little therapeutic benefit at the bedside since their first description in the early 1980's. In an effort to provide a fresh perspective on EADs, I take an experimental and computational non-linear dynamics approach to studying these arrhythmias that plague millions worldwide and are associated with significant cost burden and high mortality. Here, I show that the dual Hopf-homoclinic bifurcation mechanism for generating EADs may be responsible for EAD-mediated arrhythmias in cardiac disease, providing new therapeutic targets and expanding the current concept of reduced repolarization

reserve. Also, I provide evidence that certain pathological cardiac tissue substrates may exhibit the unique dynamical property of bistability (ie. switch-like behavior) in the form of biexcitability, the ability to switch between I_{Na}- and I_{Ca}-mediated propagation. This unique property of biexcitability may provide significant mechanistic insight into the seemingly paradoxical properties of certain EAD-mediated arrhythmias such as Torsades de Pointes (TdP), that is uniquely characterized by a slow rate and undulating QRS complexes on ECG. Lastly, I show that activation of K_{ATP} channels (inward rectifying K channels that open when cellular ATP levels fall) "flips the switch" from I_{Ca}- to I_{Na}-mediated propagation. Consistent with clinical observations of TdP and polymorphic ventricular tachycardia (PVT), the majority of I_{Ca}-dependent reentries spontaneously terminate following K_{ATP} channel activation, with a minority of I_{Ca}-dependent reentries converting to I_{Na}-dependent reentries. These results suggest that in the clinical setting, K_{ATP} channels may serve as an "emergency repolarization reserve" to spontaneously terminate most episodes of I_{Ca}-dependent arrhythmias such as PVT and TdP, but may also facilitate the occasional degeneration of these arrhythmias to I_{Na}-dependent VT/VF. These findings provide a fresh perspective on EAD-mediated arrhtyhmias that may lead to novel therapeutics at the bedside.

The dissertation of Marvin G. Chang is approved.

Kenneth D. Philipson

Riccardo Olcese

Zhilin Qu

Jau-Nian Chen

James N. Weiss, Committee Chair

University of California, Los Angeles

2012

I dedicate this thesis to my family

for their endless love, support, and encouragement

and

all my friends, colleagues, and teachers

who have invested in me.

TABLE OF CONTENTS

ABSTRACT OF THE DISSERTATION ..... **II**
TABLE OF CONTENTS ..... **VI**
FIGURES/TABLES LIST ..... **VIII**
ACKNOWLEDGEMENTS ..... **X**
VITA ..... **XIV**
1. INTRODUCTION **1**
1.1 STATEMENT OF THE PROBLEM 1
1.2 ORGANIZATION OF THE DISSERTATION 5
2. BACKGROUND **6**
2.1 THE CARDIAC ACTION POTENTIAL 6
2.3.1 Normal Conduction in the Heart *13*
2.4.1 Delayed Afterdepolarizations (DADs) *15*
2.4.2 Early Afterdepolarizations (EADS) *16*
2.5 NON-LINEAR DYNAMICS IN BIOLOGY 19
2.5.1 Poincare-Andronov-Hopf Bifurcation *22*
2.5.2 Homoclinic Bifurcation *33*
2.6 EXPERIMENTAL DISSECTION OF TISSUE LEVEL ARRHYTHMIAS 35
2.6.1 Optical Mapping *36*
2.6.2 Neonatal Rat Ventricular Myocyte (NRVM) Monolayers *39*
3. THE DYNAMICS UNDERLYING EARLY AFTERDEPOLARIZATION-MEDIATED TRIGGERED ACTIVITY IN CARDIAC MONOLAYERS **42**
3.1 ABSTRACT 42
3.2 INTRODUCTION 44
3.3 MATERIALS AND METHODS 47
3.4 RESULTS 51
3.4.1 BayK8644 and isoproterenol induce bursts of EAD-mediated triggered activity *51*
3.4.2 EAD bursts depend on LTCC, but not on Na^+ channels, SR Ca^{2+} cycling, or Ca^{2+} overload per se *54*
3.4.3 Excessively decreased repolarization reserve suppresses EADs *57*
3.4.4 EAD bursting in a detailed action potential model *59*
3.5 DISCUSSION 61
3.5.1 Hopf bifurcation mechanism of EAD formation *62*
3.5.2 Spontaneous termination of EAD bursts *64*

3.5.3 Limitations and Conclusions *65*
3.6 SUPPLEMENTAL MATERIALS 67
3.6.1 Supplemental methods *67*

4. BISTABLE WAVE PROPAGATION AND EAD-MEDIATED CARDIAC ARRHYTHMIAS 73

4.1 ABSTRACT 73
4.2 INTRODUCTION 75
4.3 MATERIAL AND METHODS 77
4.4 RESULTS 78
4.4.1 Bistable wave conduction in a homogeneous tissue model *78*
4.4.2 Co-existence of I_{Na}-mediated and $I_{Ca,L}$-mediated conduction in the same homogeneous tissue *86*
4.4.3 TdP and PVT due to $I_{Ca,L}$-mediated and I_{Na}-mediated conductions in a heterogeneous tissue model *86*
4.4.4 Experimental evidence of bi-excitability *89*
4.5 DISCUSSION AND CONCLUSIONS 92
4.5.1 EADs and bi-excitability *93*
4.5.2 Bi-excitability and cardiac arrhythmias *95*
4.5.3 Limitations *96*
4.6 SUPPLEMENTAL MATERIAL 97
4.6.1 Supplemental Methods *97*
4.6.1 Supplemental Figures *102*

5 FLIPPING THE SWITCH: K_{ATP} CHANNEL MEDIATED CONVERSION OF I_{CA}-MEDIATED TO I_{NA}-MEDIATED CARDIAC CONDUCTION 104

5.1 ABSTRACT 104
5.2 INTRODUCTION 106
5.3 METHODS 107
5.4 RESULTS 110
5.4.1 Effects of pinacidil on $I_{Ca,L}$-mediated reentry in NRVM monolayers *110*
5.4.2 Computer simulations in 2D tissue *117*
5.5 DISCUSSION AND CONCLUSIONS 122
5.5.1 Pro- and Anti-Arrhythmic Effects of I_{KATP} Activation on EAD-mediated Arrhythmias *123*
5.5.2 Limitations *126*

6 CONCLUDING REMARKS 127

7 BIBLIOGRAPHY 129

FIGURES/TABLES LIST

FIGURE 2-1. BASIC CARDIAC ACTION POTENTIAL 6
FIGURE 2-2. EXCITATION CONTRACTION COUPLING. ACTION POTENTIAL RESULTS IN OPENING OF L-TYPE Ca^{2+} CHANNELS (LTCC) 9
FIGURE 2-3. MOLECULAR MECHANISM OF MUSCLE CONTRACTION 12
FIGURE 2-4. AFTERDEPOLARIZATIONS. ABNORMAL OSCILLATIONS THAT OCCUR EITHER DURING (EAD) OR FOLLOWING REPOLARIZATION (DAD) OF THE ACTION POTENTIAL 15
FIGURE 2-5. DELAYED AFTER DEPOLARIZATION (DAD) 16
FIGURE 2-6. EAD WITH MULTIPLE OSCILLATIONS 17
FIGURE 2-7 NONLINEAR DYNAMICS IN DISSECTING BOTH A QUALITATIVE AND QUANTITATIVE MECHANISM 21
FIGURE 2-8 SADDLE NODE 34
FIGURE 2-9 HOPF-HOMOCLINIC BIFURCATION MECHANISM 35
FIGURE 2-10 OPTICAL MAPPING SETUP 37
FIGURE 2-11 VOLTAGE MAPS OF ELECTRICAL WAVE PROPAGATION IN A CARDIAC MONOLAYER. OPTICAL MAPPING ALLOWS SUFFICIENT SPATIAL AND TEMPORAL RESOLUTION TO STUDY "ARRHYTHMIAS IN A DISH" 38
FIGURE 2-13. CULTURED NRVMS EXHIBIT ROBUST Ca^{2+}-INDUCED Ca^{2+}-RELEASE 40
FIGURE 2-14 CULTURED NRVMS RESEMBLE ADULT MYOCYTES. FLUORESCENT MICROSCOPY IMAGE OF A DAY 11 NRVM-ONLY MONOLAYER STAINED FOR A-ACTININ 40
FIGURE 3-1. VOLTAGE AND Ca^{2+} BURSTS INDUCED BY BAYK8644 AND ISOPROTERENOL 52
FIGURE 3-2. BAYK8644 AND ISOPROTERENOL INDUCES BURSTS OF FOCAL ACTIVITY RESEMBLING POLYMORPHIC VT 53
FIGURE 3-3. EAD BURSTS ARE ABOLISHED BY Ca^{2+} CHANNEL BLOCKADE BUT OCCUR INDEPENDENTLY OF SR Ca^{2+} CYCLING AND Na^{+} CHANNEL BLOCKADE 55
FIGURE 3-4. EAD BURSTS ARE PROLONGED FOLLOWING CHELATION OF INTRACELLULAR Ca^{2+} ..56
FIGURE 3-5. EAD BURSTS DEPEND ON LTCC AND NOT Ca^{2+} OVERLOAD PER SE. OUABAIN AND HIGH Ca^{2+} (3.6MM) PRODUCED REPETITIVE FOCAL ACTIVITY BUT NOT BURSTS 57
FIGURE 3-6. EAD BURSTS ABOLISHED BY REDUCING REPOLARIZATION RESERVE. EITHER BLOCKING THE K^{+} CURRENTS WITH 4-AP (10MM) (PANEL A), OR OVEREXPRESSING THE MUTANT CA-INSENSITIVE CALMODULIN CaM_{1234} WITH $AdCaM_{1234}$ ABOLISHED BURSTS 59
FIGURE 3-7. COMPUTER SIMULATION OF EAD BURSTS IN A DETAILED AP MODEL 61
FIGURE S3-1. FLUORESCENT MICROSCOPY IMAGE OF A DAY 11 NRVM-ONLY MONOLAYER STAINED FOR A-ACTININ 69
FIGURE S3-2. LARGE Ca^{2+} TRANSIENTS ARE OBSERVED (VIA OPTICAL MAPPING) FOLLOWING STIMULATION DURING SUPERFUSION WITH NORMAL TYRODE (1.8 MM Ca^{2+}) THAT ARE ABOLISHED AFTER DISABLING THE SR WITH 10 MM CAFFEINE 69
FIGURE S3-3. TABLEAU OF RECORDING CHANNELS (SPACED 1 MM APART) FROM RIGHT LOWER QUADRANT OF OPTICAL MAPPING PHOTODIODE ARRAY ILLUSTRATING THAT VOLTAGE BURSTS OCCUR ON A MACROSCOPIC SCALE (>1 MM) AND ARE SYNCHRONIZED. 70

FIGURE S3-4. RELATIVE INTRACELLULAR Ca^{2+} CONCENTRATION, ΔF, UNDER DIFFERENT CONDITIONS 71
FIGURE S3-5. THE INFLUENCE OF PARAMETER VALUES ON THE DURATION AND FREQUENCY OF BURSTING 72
FIGURE 4-1. NORMAL AND ABNORMAL CARDIAC DEPOLARIZATIONS OF SINGLE-CELL MODELS 80
FIGURE 4-2. BISTABLE SPIRAL WAVES IN A HOMOGENEOUS TISSUE MODEL 83
FIGURE 4-3. CO-EXISTENCE OF I_{NA}-MEDIATED AND $I_{CA,L}$-MEDIATED CONDUCTIONS 84
FIGURE 4-4. PREVENTION OF FULL REPOLARIZATION IN A SINGLE CELL BY PERIODIC SIMULATION 85
FIGURE 4-5. BI-EXCITABILITY CAUSING TDP AND PVT IN HETEROGENEOUS TISSUE MODEL 88
FIGURE 4-6. BI-EXCITABLE WAVE PROPAGATION IN EXPERIMENTS OF NRVM MONOLAYERS SUPERFUSED WITH BAYK8644 AND ISOPROTERENOL 91
TABLE S4-1. PARAMETERS CHANGED FROM THE ORIGINAL MODEL BY MAHAJAN ET AL 100
FIGURE S4-1. INDUCTION OF REENTRY BY EADS IN A 2D HETEROGENEOUS TISSUE MODEL AFTER A SINGLE S1 STIMULUS 102
FIGURE S4-2. NRVM MONOLAYER EXPERIMENTS SHOWING TERMINATION OF REENTRY BY NITRENDIPINE BUT NOT TTX 103
FIGURE 5-1. EAD-MEDIATED ARRHYTHMIAS INDUCED BY BAYK4688 + ISOPROTERENOL IN NRVM MONOLAYERS 111
FIGURE 5-2. EAD-MEDIATED REENTRY AROUND A CENTRAL OBSTACLE IN AN NRVM MONOLAYER 112
FIGURE 5-3. EFFECT OF THE K_{ATP} CHANNEL AGONIST PINACIDIL IN NRVM MONOLAYERS WITH COMPLEX SUSTAINED EAD-MEDIATED ARRHYTHMIAS 113
FIGURE 5-4. EFFECTS OF THE K_{ATP} CHANNEL AGONIST PINACIDIL IN NRVM MONOLAYERS WITH COMPLEX SUSTAINED EAD-MEDIATED ARRHYTHMIAS 114
FIGURE 5-5. EFFECTS OF PINACIDIL ON EAD-MEDIATED REENTRY AROUND A CENTRAL OBSTACLE IN AN NRVM MONOLAYER 116
FIGURE 5-6. EFFECTS OF PINACIDIL ON CONDUCTION VELOCITY OF EAD-MEDIATED REENTRY AROUND A CENTRAL OBSTACLE IN NRVM MONOLAYERS 117
FIGURE 5-7. EFFECT OF I_{KATP} ACTIVATION ON $I_{CA,L}$-MEDIATED REENTRY IN SIMULATED 2D HETEROGENEOUS CARDIAC TISSUE (300 X 300 MYOCYTES) 118
SUPPLEMENTAL MOVIE 5-1. TERMINATION OF $I_{CA,L}$-MEDIATED REENTRY BY SLOW ACTIVATION OF I_{KATP} OVER 5 MINUTES (FIRST 90 S SHOWN) 121
SUPPLEMENTAL MOVIE 5-2. CONVERSION OF $I_{CA,L}$-MEDIATED REENTRY TO I_{NA}-MEDIATED REENTRY BY RAPID ACTIVATION OF I_{KATP} OVER 50 MS 121

Acknowledgements

It is a great pleasure to thank the many people who have made this dissertation possible. In writing this thesis, it was often times not only difficult but almost impossible to restrain myself from using the “editorial we" in place of "I" (customary for a single author dissertation), because it truly was a journey of many rather than a journey of one.

Special recognition goes to Dr. Jim Weiss, my Ph.D. supervisor and chair of my committee, for his support and guidance. His invaluable advice related to not just science but life in general, will serve me well in the future. I am appreciative of his fostering a laidback yet collaborative and productive research environment with freedom of scientific inquiry. Research never felt like “work”, and for that I am truly grateful.

Special recognition also goes to Drs. Alan Garfinkel, Zhilin Qu, and Enno de Lange for their close mentorship in the area of non-linear dynamics. As an experimentalist at heart and by training, and a stubborn one too, Drs. Garfinkel, Qu, and de Lange “showed me the light.” Without them, I would have never been able to attain such a high appreciation for dynamics in scientific inquiry. Now, thanks to them, dynamics is now a part of my scientific arsenal that will undoubtedly be useful in my future studies.

Dr. Alan Garfinkel, whose invaluable mentorship cannot be understated because without it much of this work would not have been possible, is the board

certified spin artist that I consult whenever I have problems explaining difficult concepts to a general audience. He has a gift for explaining everyone's project better than they can explain it themselves. This is inarguably one of the most important skills a scientist can have, and I am truly grateful for his mentorship in both the spoken and written word, and non-linear dynamics in general.

Dr. Zhilin Qu is the mastermind of the PRL paper[1] that I have grown to love over the past couple years. I thank him for the tremendous amount of patience he exhibited in explaining the technical details of that work, and non-linear dynamics in general. Somehow, he always managed to do it with a smile on his face despite how frustrated he might have been at times (explaining non-linear dynamics to an experimentalist is never an easy task, even for a professional!).

Dr. Enno de Lange is my computational counterpart. He is truly a rainmaker when it comes to computational simulations. There are very few people in this world who can perform simulations as efficient, and as well as he can. It was always a pleasure to watch him work -- always a "method to his madness" in attacking problems that many others might solve by "bruit force." I am truly grateful for all that he has taught me about non-linear dynamics, and his contributions to my projects. Without him, much of this dissertation would not have been possible. I am truly blessed to have worked with this man.

I would also like to also give special thanks to Dr. Guillaume Calmettes, who has generously provided technical assistance for many of my projects, including in

writing this dissertation. His enthusiasm for science is contagious. Lucky for me, I sit right next to him in the lab!

Gratitude is expressed to Mr. John Parker for his engineering expertise, Dr. Scott John for his virology expertise, and all the of the members of the CVRL for their helpful discussions and guidance, especially Drs. Hrayr Karagueuzian and Riccardo Olcese.

Gratitude is also expressed to Dr. Jim Tidball, the Chair of the Molecular, Cellular, & Integrative Physiology (MCIP) program at UCLA, for his strong support of students and fostering a positive academic environment. It is no mistake that under his tenure, UCLA MCIP is the top physiology graduate program in the country [2].

I am immensely grateful for the mentorship I received early in my training from Drs. Leslie Tung, Roselle Abraham, and Eduardo Marbán. They truly taught me the art of doing science, which has been invaluable in my work at UCLA. There is no doubt that I am a much more developed, efficient, and independent scientist at this stage in my training because of their guidance and support.

I am also very grateful to Drs. Ken Philipson, Zhilin Qu, Riccardo Olcese, and Jau-nian Chen, and Jim Weiss, for generously volunteering their time and energies to serve on my committee.

Lastly, I would like to thank my parents. Everything I know and everything I am, I owe to my parents. Their unending support and sacrifices have made all this possible.

This dissertation work was financially supported by NIH/NHLBI P01 HL078931, R01 HL103662, NIH MSTP T32 GM008042 and NIH MCIP T32 GM065823, a postdoctoral fellowship award from the American Heart Association, Western States Affiliate, a fellowship award for advanced researchers from the Swiss Foundation for Grants in Biology and Medicine, and the Laubisch and Kawata Endowments.

VITA

EDUCATION

08/2007 to present	David Geffen School of Medicine at UCLA Molecular Cellular & Integrative Physiology, Los Angeles, CA MD/PhD, 2013, expected date of completion
	• PhD Thesis on *"Dynamics of Early Afterdepolarization (EAD)-mediated Arrhythmias"* (defended 08/2011)
9/2000 to 10/2006	Johns Hopkins University, Baltimore, MD BS/MSE, Biomedical Engineering (Electrical Engineering concentration)

HONORS AND AWARDS

2011-Present	Ad hoc reviewer, *Journal of the American College of Cardiology (JACC)*
2011-Present	Ad hoc reviewer, *Circulation: Arrhythmia and Electrophysiology*
2011	Best Poster Award, Molecular Cellular & Integrative Physiology Retreat
2006	Young Investigator Award Finalist, Heart Rhythm
2004	Tau Beta Pi (Engineering Honor Society)
2004	Alpha Eta Mu Beta (Biomed. Engineering Honor Society)

RESEARCH EXPERIENCE

6/2008 to Present	Drs. James N. Weiss, Zhilin Qu, and Alan Garfinkel, UCLA, Los Angeles, CA *Dynamics of Early Afterdepolarization (EAD)-mediated Arrhythmias*
8/2007 to 4/2008	Dr. Eduardo Marbán, UCLA/CSMC, Los Angeles, CA *Role of abnormal Ca^{2+} cycling in arrhythmia dynamics and failed defibrillation*

9/2004 to 7/2007	Drs. M. Roselle Abraham and Eduardo Marbán, Johns Hopkins University, Baltimore, MD *Antiarrhythmic Gene therapy and Electrophysiological characterization of in vitro models of skeletal myoblast and mesenchymal stem cell transplantation*
05/2002 to 07/2007	Dr. Leslie Tung, Johns Hopkins University, Baltimore, MD *Development of optical instrumentation for the study of voltage and calcium wave propagation in cardiac tissue*

WORK EXPERIENCE

09/2010 to 05/2011	Professional Development/Grad School Survival Committee, Molecular Cellular & Integrative Physiology, UCLA, Los Angeles, CA
12/2005 to 05/2007	Volunteer, Emergency Room, Johns Hopkins Hospital, Baltimore, MD
02/2004 to 12/2005	Teaching Assistant and Grader, BME Dept., Johns Hopkins University, Baltimore, MD
09/2003 to 05/2004	Graduate Student Rep., Graduate Academic Council, Johns Hopkins University, Baltimore, MD

PUBLICATIONS

1. Abraham MR*, Henrikson CA*, Tung L, **Chang MG**, Aon M, Xue T, Li RA, O' Rourke B, Marbán E. Antiarrhythmic engineering of skeletal myoblasts for cardiac transplantation. ***Circulation Research.*** 97(2):159-167, 2005. (*equally contributing authors).

2. **Chang MG**, Tung L, Sekar RB, Chang CY, Cysyk J, Dong P, Marbán E, Abraham MR. Proarrhythmic potential of mesenchymal stem cell transplantation revealed in an in vitro coculture model. ***Circulation***. 113(15):1832-1841, 2006.

3. Lin JW, Garber L, Qi YR, **Chang MG**, Cysyk J, Tung L. Region of slowed conduction acts as core for spiral wave reentry in cardiac cell monolayers. ***Am J Physiol Heart Circ Physiol***. 294(1):H58-65, 2008.

4. **Chang MG***, Zhang Y*, Chang CY, Xu L, Emokpae R, Tung L, Marbán E, Abraham MR. Spiral waves and reentry dynamics in an in vitro model of the healed infarct border zone. ***Circulation Research***. 105(11):1062-1071, 2009. (*equally contributing authors).

5. Chen F, De Diego C, **Chang MG**, McHarg JL, John S, Klitzner TS, Weiss JN. Atrioventricular conduction and arrhythmias at the initiation of beating in embryonic mouse hearts. ***Developmental Dynamics***. 239(7):1941-1949, 2010.

6. **Chang MG*,** Sato D*, de Lange E*, Lee JH, Karagueuzian HS, Garfinkel A, Weiss JN, Qu Z. Bi-excitable Wave Dynamics and Cardiac Arrhythmias. ***Heart Rhythm***. 9(1):115-22, 2012. (*equally contributing authors).

7. **Chang MG***, Chang CY*, de Lange E*, Xu X, O'Rourke B, Karagueuzian HS, Tung L, Marbán E, Garfinkel A, Weiss JN, Qu Z, Abraham MR. The Dynamics of Early Afterdepolarization-Mediated Triggered Activity in Cardiac Monolayers. ***Biophysical Journal*.** 102(12):2706-14, 2012. (*equally contributing authors).

ABSTRACTS

1. **Chang MG**, Emokpae R, Zhang Y, Tung L, Marbán E, Abraham MR. Co-culture of mesenchymal stem cells and neonatal rat ventricular myocytes produces an arrhythmic substrate. Presented at ***Heart Rhythm (oral presentation)***, New Orleans, LA, May 2005.

2. **Chang MG**, Zhang Y, Emokpae R, Marbán E, Tung L, Abraham MR. Effects of Increasing I_{Ca} on Spiral Wave Dynamics: Results from a 2-D Experimental Model. Presented at ***Heart Rhythm***, New Orleans, LA, May 2005.

3. **Chang MG**, Cysyk J, Zhang Y, Qi YR, Tung L, Abraham MR. Electrophysiological characterization of *in vitro* model of cellular cardiomyoplasty. Presented at ***Biomedical Engineering Society (oral presentation)***, Baltimore, MD, Sept 2005.

4. Kizana E, Cingolani E, **Chang MG**, Ramirez G, Ginn SL, Abraham MR, Marbán E, Alexander IE. Gene Transfer of a "Poison Pill" Connexin43 Mutant Attenuates Coupling in Cardiomyocytes: Novel Basis for Modulation of Cardiac Conduction by Gene Therapy. Presented at ***American Heart Association***, Dallas, TX, Nov 2005.

5. **Chang MG**, Cysyk J, Zhang Y, Chang CY, Marbán E, Tung L, Abraham MR. Effects of Lidocaine and Nitrendipine on Spiral Wave Dynamics in a 2-D myocyte co-culture model of stable re-entry. Presented at ***American Heart Association***, Dallas, TX, Nov 2005.

6. **Chang MG**, Zhang Y, Cysyk J, Tung L, Marbán E, Abraham MR. Reentrant Arrhythmias Are Easily Induced In in vitro Models of MSC Transplantation. Presented at ***American Heart Association (oral presentation)***, Dallas, TX, Nov 2005.

7. **Chang MG**, Tung L, Sekar RB, Cysyk J, Qi YR, Xu L, Marbán E, Abraham MR. Calcium Overload Induces Tachyarrhythmias in a 2D Ventricular Myocyte Experimental Model. Presented at ***Heart Rhythm***, Boston, MA, May 2006.

8. **Chang MG**, Chang CY, Xu L, Sekar RB, Cysyk J, Marbán E, Tung L, Abraham MR. Role of Sarcoplasmic Reticulum Calcium Cycling in Arrhythmias in a 2-D Experimental Model of Calcium Overload. Presented at ***American Heart Association***, Chicago, IL, Nov 2006.

9. Chang CY, **Chang MG**, Xu L, Aon M, Zauher M, Marbán E, Tung L, Abrama MR. Novel bursting behavior is observed in ventricular myocytes in the presence of Ca2+ overload. Presented at ***Heart Rhythm***, Denver, CO, May 2007.

10. **Chang MG**, Xu L, Chang CY, Cysyk J, Marbán E, Tung L, Abraham MR. Field Stimulation Produces Fibrillatory Activity in a 2-D Experimental Model of Calcium Overload. Presented at ***Heart Rhythm (oral presentation)***, Denver, CO, May 2007.

11. **Chang MG**, Chang CY, Xu L, Tung L, Abraham MR, Marbán E. Pro-arrhythmic effect of monophasic field stimulation revealed in a 2-D experimental model of up-regulated mode 2 gating and calcium overload. Presented at ***Western Student Medical Research Forum (oral presentation)***, Monterey, CA, Feb 2008.

1. Introduction

1.1 Statement of the Problem

Early Afterdepolarization (EAD)-mediated arrhythmias such as Torsades de Pointes are often times the trigger for sudden cardiac death (SCD), a major killer in developed countries. These arrhythmias often complicate conditions such as heart failure, increased catecholamines, and both acquired and drug Long QT syndrome (LQTS). In fact, the association of EAD-mediated arrhythmias with SCD is so strong that every drug regardless of its clinical use is assessed for drug acquired LQTS prior to market release, with a QT prolongation of 5 ms raising significant regulatory concern[3].

While much work has been done in the past couple decades to understand EADs, this work has yielded little in the form of clinically effective therapies for EAD-mediated arrhythmias. Clearly, a fresh new perspective on EAD-mediated arrhythmias is needed if there is to be an impact on patients at the bedside. In an attempt to provide a fresh new perspective on EADs, I have collaborated extensively with non-linear dynamicists in our group to drive my research at the bench. The strengths of non-linear dynamics is its ability to provide incredible insight into areas of research that have already been richly mined by other experimentalists (often times before I could walk or talk, much less hold a pipette), and/or are too complex (or impossible) to study just experimentally.

Fortunately, nonlinear dynamics can be readily applied to arrhythmia research because of the advent of patch clamping technology that has allowed the measurement of necessary membrane properties to construct realistic cardiac myocyte cell models. The UCLA Cardiovascular Research Laboratory (CVRL) is an ideal environment to undertake such a systems biology approach towards biomedical research, given that it is one of the few labs in the world that fosters truly close collaboration between experimentalists and dynamicists to understand complex electrical problems in the heart.

This conducive environment present in the CVRL has made it possible to answer the following three questions that comprise my thesis:

1. *What is the role of the Hopf-Homoclinic Bifurcation Mechanism in a robust in vitro model of EAD bursts?*

   Recent theoretical work by our group[1] detailed the role of the Hopf and Homoclinic bifurcations[4] in the dynamical mechanism of EADs. It offers the tantalizing possibility of suppressing EADs by targeting the kinetics of specific ion channels rather than their magnitude (often associated with lackluster clinical efficacy, severe side effects, and significant consequences related to excitation-contraction coupling). In this study, I characterize a robust *in vitro* model of EAD bursts in the context of the Hopf-Homoclinic bifurcation mechanism. Also, I dissect the physiological mechanism of EAD bursts in a more physiological action potential model that includes detailed

Ca^{2+} handling and ionic fluxes (absent in the phenomenological Luo-Rudy I model previously used). It is my hope that this new perspective of EAD-mediated arrhythmias may lead to clinically effective therapies if it can be understood and appreciated by those outside the physics and nonlinear dynamics community.

2. *What is the role of bi-excitability in the heart as it relates to arrhythmias?*

It is well known that certain cardiac tissue substrates can support either I_{Na} or I_{Ca} propagation but not both at the same time. Normal atrial and ventricular tissue is solely dependent on I_{Na} for propagation, while the AV node, ischemic tissue, and infarct border zone are solely dependent on I_{Ca}[5-7]. In other words, it has never been shown that a specific cardiac substrate can exhibit the property known as bi-excitability – the ability to support both I_{Na}- and I_{Ca}-dependent propagation at the same time, or switch between the two types of propagation under the influence of a variable that does not affect the intrinsic properties of the substrate (e.g., cell-to-cell coupling, ion channels). In this study, I provide experimental and theoretical evidence that certain pathological substrates may exhibit bi-excitability, and support spiral waves driven by a I_{Ca} rotor that is resistant to Na channel blockers but vulnerable to Ca^{2+} channel blockers. Our simulations suggest that spiral waves driven by I_{Ca} rotors in this bi-excitable substrate may give rise to the

unique EKG signature (slowly undulated QRS complexes) observed during episodes of Torsades de Pointes.

3. *What is the role of K_{ATP} channel in bi-excitable tissue and its relevance to Torsades de Pointes.*

In this study, I show that bi-excitability may also explain other characteristic features of Torsades de Pointes in addition to its unique EKG signature, most notably the clinical observation that most episodes of Torsades de Pointes spontaneously terminate, while others degenerate into VF and sudden cardiac death. I hypothesized that the K_{ATP} channel may play a role in both clinical outcomes of Torsades de Pointes by providing sufficient repolarization reserve to switch the tissue from the I_{Ca} to the I_{Na} state, resulting in either spontaneous termination (unexcited I_{Na} state) or induce VF (driven by I_{Na}). Consistent with clinical observations, K_{ATP} activation (via pinacadil) spontaneously terminated the majority of I_{Ca}-dependent spiral waves, with a minority of reentries increasing in complexity and switching from I_{Ca}- to I_{Na}-dependent spiral waves. Simulations revealed that the probabilistic nature of the outcomes were dependent on the presence of a I_{Na}-mediated wavefront in the arm of the I_{Ca} rotor at the time of K_{ATP} channel activation. These results suggest that K_{ATP} activation in bi-excitable tissue may underlie the clinical outcomes (spontaneous termination and VF) observed following episodes of Torsades de Pointes.

1.2 Organization of the dissertation

This dissertation is oragnized as follows:

- *Chapter 2* provides a brief overview of cardiac electrophysiology and non-linear dynamics, with the purpose of providing those with expertise outside these areas the necessary knowledge to understand the studies outlined in Chapters 3-5. Readers may want to skip particular sections of Chapter 2 that detail topics that they are familiar with.
- *Chapters 3-5* details the studies performed to answer the questions above.
    - *Chapter 3* details the role of the Hopf-Homoclinic bifurcation mechamism in a robust *in vitro* model of EAD bursts.
    - *Chapter 4* details the role of bi-excitability in the heart as it relates to arrhythmias.
    - *Chapter 5* details the role of the K_{ATP} channel in bi-excitable tissue and its relevance to *Torsades de Pointes*
- *Chapter 6* discusses the implications of these studies.

2. Background

The goal of this chapter is to provide a brief and sufficient overview of cardiac electrophysiology and nonlinear dynamics to understand the studies detailed in the following chapters. It is outside the scope of this dissertation to provide a complete overview of each of the topics covered in this chapter, but readers are encouraged to refer to sources referenced in this chapter for more detailed information. Readers may also consider skipping sections of this chapter that cover topics of significant familiarity.

2.1 The Cardiac Action Potential

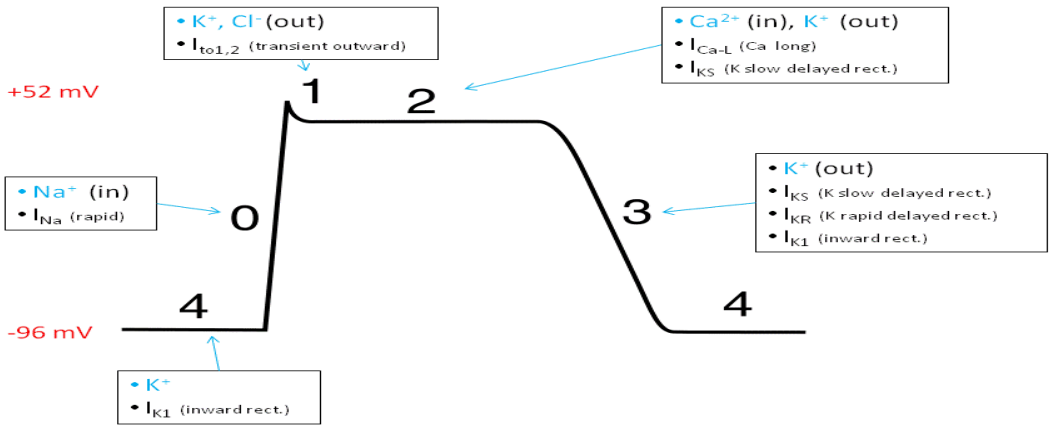

Figure 2-1. Basic Cardiac Action Potential. Major outward and inward currents are labeled for each phase of the action potential. Figure reprinted from [8].

No review of cardiac electrophysiology would be complete without a brief overview of the cardiac action potential[9, 10]. An "all or none" action potential (Fig. 2-1) occurs when a cardiac myocyte's membrane potential (V_m) is depolarized above a certain threshold (either via current injected from a neighboring myocyte or an external stimulus) that results in activation of Na^+ channels, and the sharp upstroke (Phase 0) of the action potential. It is worth noting that because the inactivation of the Na^+ channel is highly dependent on both voltage and time, the V_m threshold that results in this "all or none" response varies depending on the rate that V_m rises (dV_m/dt).

Following the upstroke of the action potential, a transient outward K^+ channel opens very briefly (hence the name, transient), with the L-type Ca^{2+} channels (LTCC) opening just shortly after. This timing delay between the currents provided by the opening of the transient outward K^+ channel (I_{to}) and the LTCC (I_{Ca}) is responsible for the notch (Phase 1) observed just after the upstroke of the action potential in species such as rabbit, guinea pic, and humans. The plateau (Phase 2) phase follows the notch of the action potential, and occurs as a result of a balance between the currents of the inward Ca^{2+} channel and outward K^+ channels. The action potential repolarizes (Phase 3) when this balance is disrupted, and outward K^+ currents exceed the inward Ca^{2+} current. This occurs because of (1) activation of K^+ channels that increase in magnitude faster at higher V_m (ie. the plateau phase) with time, and (2) inactivation of the LTCC channels.

Note that some species such as the rat do not exhibit the plateau phase of the action potential because of a significantly greater expression of the transient outward K^+ channel in these species. It is important to note that this difference in I_{to} in the rat compared to other species was important in dissecting the role of early versus late "repolarization reserve" in the dynamical mechanism of EADs detailed in Chapter 3.

2.2 Excitation-Contraction Coupling

Excitation-contraction coupling[11] is a process where electrical excitation of a myocyte triggers a contractile response. In other words, it is the electrical activity of the heart that allows the heart to function effectively as a pump. The molecular mechanism by which this occurs is as follows. When an action potential is initiated, the LTCCs open resulting in an influx of Ca^{2+} into the myocyte. This influx of Ca^{2+} on its own is insufficient to trigger a significant contractile response described below. Fortunately, the heart has evolved a positive feedback system that allows this "miniscule" LTCC-mediated influx of Ca^{2+} to trigger a much larger release of Ca^{2+} from large Ca^{2+} stores within the myocyte known as the sarcoplasmic reticulum (SR).

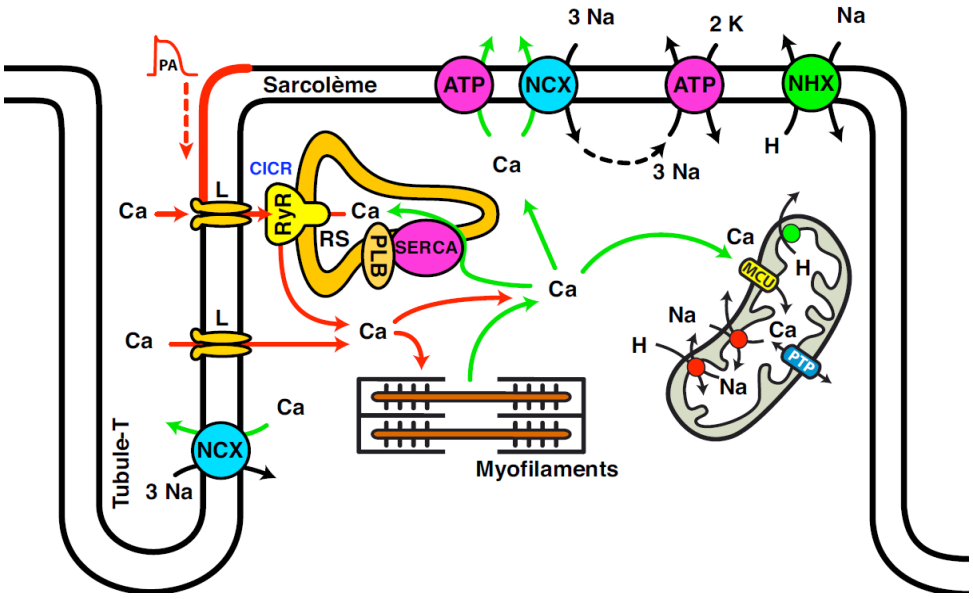

Figure 2-2. Excitation Contraction Coupling. Action potential results in opening of L-type Ca^{2+} channels (LTCC). Ca^{2+} influx via LTCC induces a greater release of Ca^{2+} from the sarcoplasmic reticulum (SR) in a process called Ca^{2+}-induced Ca^{2+}-release process. This greater release of Ca^{2+} from the SR facilitates contraction during systole. During diastole, intracellular [Ca^{2+}] levels fall to allow the heart to relax via a number of Ca2+ reuptake (ie. sarcolemmal and SR Ca^{2+} ATPase pumps) and extrusion (ie. Na^{+}/Ca^{2+} exhcanger) mechanisms. Figure reprinted from [12] (adaptation of Figure from [11]).

This Ca^{2+}-induced Ca^{2+}-release (CICR) process is able to occur because the SR has Ca^{2+} release channels called ryranodine receptors (RyR) that are activated by Ca^{2+} (Fig. 2-2). Efflux of Ca^{2+} from the SR via RyRs occurs in a graded fashion such that the amount of Ca^{2+} that is released from the SR is commiserate with the magnitude of the LTCC-induced Ca^{2+} influx. In other words, a small amount of Ca^{2+} influx triggers the RyRs to release a smaller amount of Ca^{2+} from the SR than would a larger Ca^{2+} influx. CICR occurs robustly because of the close spatial association between the LTCC and SR within the diadic space of the t-tubules[13], which are

invaginations within the myocyte's membrane. It is important to note that while CICR is a positive feedback process, the Ca^{2+} system as a whole is stable because of a number of negative feedback processes such as Ca^{2+}-dependent inactivation (CDI) of the LTCC. CDI is a process by which the LTCC is inactivated by a rise in local cytosolic Ca^{2+} via the LTCC and SR Ca^{2+} release. It involves the ubiquitously expressed Ca^{2+} sensing molecule, calmodulin (CaM), and is the primary mechanism by which the LTCC is inactivated during the action potential. This is because CDI of the LTCC is very fast, on the order of milliseconds compared to that of voltage-dependent inactivation (VDI) which is on the order of seconds[14].

During systole, the myocyte is able to contract because the contractile machinery consisting of mainly actin and myosin filaments is heavily dependent on the significant increase in cytosolic Ca^{2+} provided by the CICR process[15]. Briefly, in order for force contraction to occur, myosin must cross-link with actin (Fig. 2-3). However, this cross-linking process cannot occur in the absence of Ca^{2+} because of a molecule called tropomyosin that "covers" the actin-myosin binding sites on actin. These actin-myosin binding sites on actin can only be "uncovered" when another molecule called troponin undergoes a conformational change that is induced by Ca^{2+}. This Ca^{2+}-induced conformational change gives troponin the ability to "slide" tropomyosin "out of the way," thereby exposing the actin-myosin binding sites to allow the cross-linking process that is necessary for force contraction to occur.

Following repolarization of the action potential, the heart must relax in order to allow it to adequately fill with blood during diastole. In order for the myocytes of the heart to relax, the cytosolic Ca^{2+} level must fall sufficiently so that actin is no longer able to interact with myosin. This fall in cytosolic Ca^{2+} is facilitated by a number of reuptake and extrusion mechanisms (Fig. 2-2). The SR via the Sarco/Endoplasmic Reticulum Ca^{2+}-ATPase (SERCA) pump resequesters the majority of excess cytosolic Ca^{2+}. The rest of the excess cytosolic Ca^{2+} is extruded via the Na^{+}/Ca^{2+} exchanger (NCX) and Ca^{2+} ATPase pumps present on the sarcolemmal membrane, the latter playing only a very limited role. NCX extrudes this excess Ca^{2+} by using the Ca^{2+} gradient to drive the efflux of 1 Ca^{2+} ion in exchange for 3 Na^{+} ions, producing a net inward NCX current[16]. It is important to note that under normal non-pathological conditions, this net inward NCX current is usually insufficient to cause any abnormalities in the AP. However, in conditions of significant Ca^{2+} overload and upregulated NCX (ie. heart failure), this inward NCX current is sufficient to cause abnormalities in electrical activity, and serves as the primary mechanism by which delayed afterdepolarzations (DADs)[17] occur. It has also been implicated in the mechanism of late phase-3 EADs[18-22] described below.

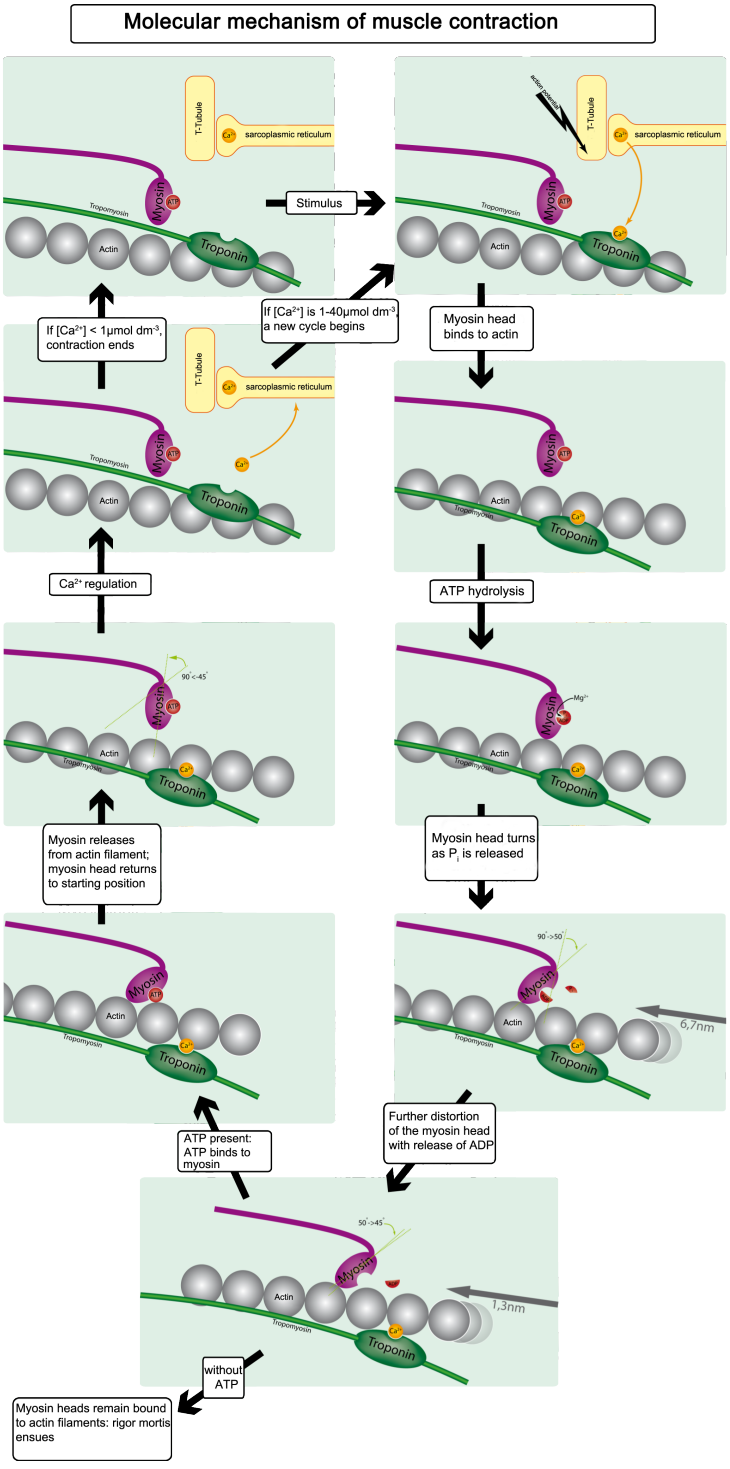

Figure 2-3. Molecular mechanism of muscle contraction. Figure reprinted from [23].

2.3 Cardiac Conduction in the Whole Heart

Cardiac myocytes are coupled to one another via gap junctions which allows an action potential to propagate from one cell to next, initiating a "wave" of excitation in tissue[24]. Because of the excitation-contract coupling process described above, this wave of excitation (ie. the action potential) initiates a similar wave of contraction of a similar directionality. The directionality of this wave of contraction is important because it determines the efficiency at which blood is propelled from the left ventricle into the aorta with each beat (ie. ejection fraction).

2.3.1 Normal Conduction in the Heart

During normal sinus rhythm, the heart contracts in the most optimal fashion. The path that the electrical activity takes occurs in sequential fashion from the sinoatrial node to the atrioventricular node, Bundle of His, His Purkinje System, the Apex of the Ventricle, and finally the Base of the Ventricle. The fact that electrical activity in the left ventricle occurs from Apex to Base, and so does its contraction, is of great importance because this allows the most amount of blood to exit the left ventricle through the aorta which is situated at the base of the heart. This process may be more intuitive when described in the context of a ketchup bottle. If one wanted to most effectively squeeze all of the ketchup out of a bottle (ie. left ventricle), how would they do so? They would squeeze from the bottom of the bottle

(ie. apex of left ventricle) towards its spout (ie. the aorta at the base of the ventricle). This process is analogous to the optimal contraction of the heart that occurs during normal sinus rhythm.

2.3.2 Abnormal Conduction and Sudden Cardiac Death

When arrhythmias occur, the normal pathway of electrical activity is disturbed. As a consequence, the normal pathway of contraction (SA node to ➔ AV node ➔ Bundle of His ➔ His-Purkinje System ➔ the Apex of the Ventricle ➔ Base of the Ventricle) is also disturbed such that contraction is no longer occurring in the most optimal fashion. Again, this is much more intuitive in the context of a ketchup bottle. If the ketchup (ie. blood) is simultaneously being squeezed out of the bottle (ie. left ventricle) from multiple sites (ie. top, sides, and bottom), the ketchup is unable to efficiently exit the bottle. This process is analogous to the non-optimal contraction that occurs during an arrhythmia. As a result, the resulting ejection fraction is insufficient to perfuse the body's vital organs. Of the organs that receive inadequate perfusion is the heart, leading to cardiac tissue death and sudden cardiac death.

2.4 Afterdepolarizations and Triggered Activity Arrhythmias

Afterdepolarizations [25] are abnormal oscillations of the membrane

potential that occur either before or after full repolarization of the action potential (Fig. 2-4). Abnormal oscillations occurring prior to AP repolarization are referred to as early afterdepolarization (EAD), whereas oscillations following repolarization of the action potential are referred to as a delayed afterdepolarization (DAD). When afterdepolarizations propagate in tissue as a wave of excitation, they are referred to as "triggered activity. "

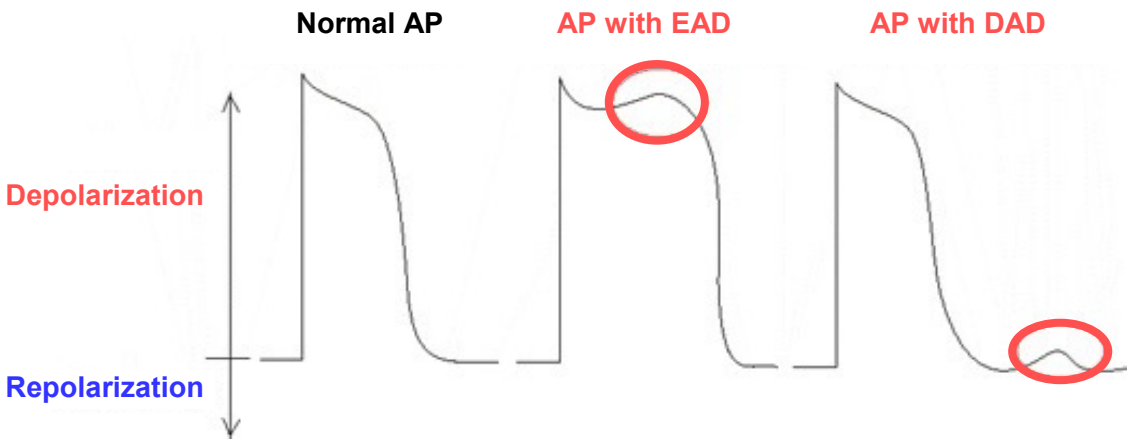

Figure 2-4. Afterdepolarizations. Abnormal oscillations that occur either during (EAD) or following repolarization (DAD) of the action potential. Figured adapted from [26].

2.4.1 Delayed Afterdepolarizations (DADs)

Even though DADs are outside the scope of this dissertation, it is worth discussing because the classical mechanism by which they occur, which is via *reverse excitation-contraction coupling*, has also been implicated in a subset of EADs, particularly the phase-3 EADs that occurs very late in repolarization via NCX[16]. *Reverse excitation-contraction coupling* is a process by which the Ca^{2+} transient

induces a voltage response. DADs (Fig. 2-5) occurs when the intracellular Ca^{2+} is sufficiently high to produce a significant enough NCX-mediated inward current to produce a "bump" in the membrane potential following repolarization. If this “bump” depolarizes with sufficient rate and magnitude to activate the Na^{+} channel, another “all or none” action potential is initiated that has the potential to propagate through the heart as an ectopic focus. In the case of phase-3 EADs, NCX may produce sufficient inward current late in repolarization and prior to full repolarization, to facilitate the reactivation of the Na^{+} channel and/or LTCC.

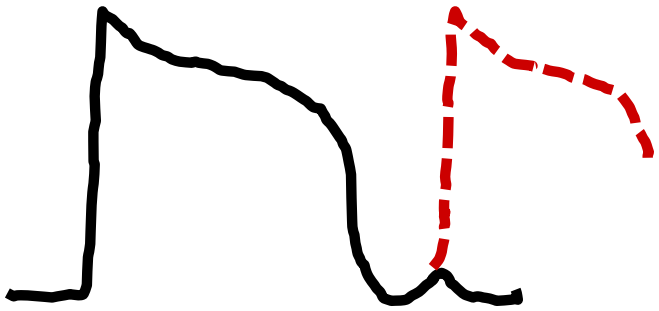

Figure 2-5. Delayed after depolarization (DAD). DADs that rise with sufficient rate and magnitude can trigger another action potential

2.4.2 Early Afterdepolarizations (EADS)

While the NCX-mediated mechanism described above has been implicated in phase-3 EADs, EADs have been classically described to occur via (1) an increase in the magnitude of inward currents over outward currents, (2) reactivation of LTCC via an increase of the LTCC “window current” (overlap of the activation and inactivation curves), and (3) a prolongation in the magnitude of the AP duration

(APD), also equivalent to the "QT interval" on EKG. While all these explanations for EADs may be true, they hinge on magnitude rather than timing, and thus are insufficient to explain the occurrence of EADs, especially those that exhibit multiple oscillations ("bumps") seen in Fig. 2-6.

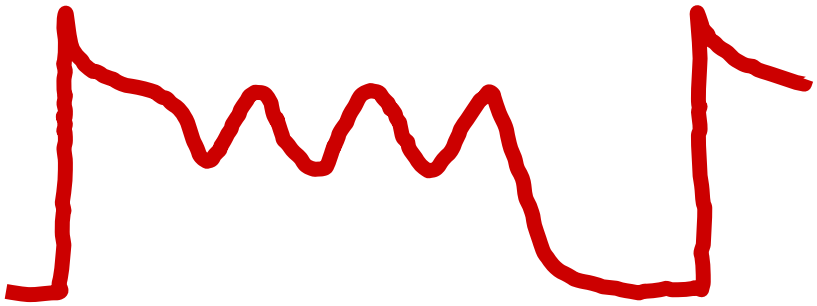

Figure 2-6. EAD with multiple oscillations. Conventional explanations based on magnitude are insufficient to explain oscillations that are by definition, dependent on time.

Our group has previously addressed this void by taking a non-linear dynamics approach to constructing a "unifying" theory for EADs that is both qualitative and quantitative in nature. The rationale for using a non-linear dynamics approach is presented in the subsequent section below. Briefly, our group revealed that EADs arise from a dynamical process called the Hopf bifurcation[1], whose occurrence can be predicted by the following mathematical formula (where d and f are the inactivation and inactivation gates of the LTCC):

$$\frac{1}{\tau_f}(\frac{1}{\tau_f}-a)(\frac{1}{\tau_d}-a+s_f c)+\frac{1}{\tau_d}(\frac{1}{\tau_d}-a)(\frac{1}{\tau_f}-a-s_d b)<0 \quad (1)$$

$$\Rightarrow h<0$$

where $a=\frac{dF}{dV}$

$b=\frac{dF}{dd}$

$c=\frac{dF}{df}$

$s_d=\frac{d_\infty}{dV}$

$s_f=\frac{-df_\infty}{dV}$

$b>0, c>0$ for $V<E_{Si}$;

$s_d>0$ and $s_f>0$ for any V

Note that this equation, which determines whether or not the system undergoes a Hopf bifurcation that is required for EAD induction, is solely dependent on 1) the maximum value of the LTCC "window current"; 2) the slopes of dV_m/dt with respect to voltage; 3) the slopes of the LTCC activation and inactivation curves with respect to voltage; and 4) the time constants of the LTCC activation and inactivation gates.

Once the Hopf bifurcation initiates EADs, these EADs are then terminated by another dynamical process called the Homoclinic bifurcation, detailed below in Section 2.5.2.

The role of both the Hopf and Homoclinic bifurcation in EADs was previously published[1] in the premiere physics journal, Physical Review Letters (PRL), and

offers the first and only, fully sufficient and complete, non-“hand-waving” theory for the initiation and termination of EADs. This work by Tran et al.[1] has been one of the major inspirations of my thesis, which attempts to experimentally validate this theory and give further insight into EAD-mediated arrhythmias such as *Torsades de Pointes*.

2.5 Non-linear Dynamics in Biology

The strengths of non-linear dynamics is that it offers both qualitative and quantitative insights into biological phenomena that are often times experimentally impossible to tease out. When does this approach become particularly useful? Take for example the case where multiple groups run the same experiment (ie. same perturbation), but each observe completely different phenomenon or no phenomenon at all. Or the case where many group's experiments suggest a mechanism for a particular phenomenon (ie. "steep SR Ca^{2+} load causes is required for Ca^{2+} alternans"), while another group's experiments reveal that this mechanism is not necessary for this phenomenon to occur (ie. "steep SR Ca^{2+} load is not required for Ca^{2+} alternans"). So who is right? Such discrepancies are often times the subject of many heated debates at scientific conferences that often times involve masterful showmanship and circuitous arguments that yield no consensus. In short, the observations of all differing groups may be true for a set of initial conditions

while their inferred mechanisms may be incorrect or incomplete. This will hopefully become more clear in the example below.

Non-linear dynamics can dissect the "true" mechanism by which the same perturbations can result in entirely different phenomena, or different perturbations can result in the same phenomena as follows. In non-linear dynamics, a bifurcation is a sudden change in the qualitative behavior of a system when parameters reach their critical values. Examples of bifurcations in biology include a sudden qualitative change in a myocyte's electrical activity from rest to pacemaking, or an epithelial cell's cell cycle phase from quiescent to proliferative. Bifurcation analysis of a system may reveal the quantitative parameter space in which different phenomenon occur. Take the parameter space seen in Fig. 2-7 as an example.

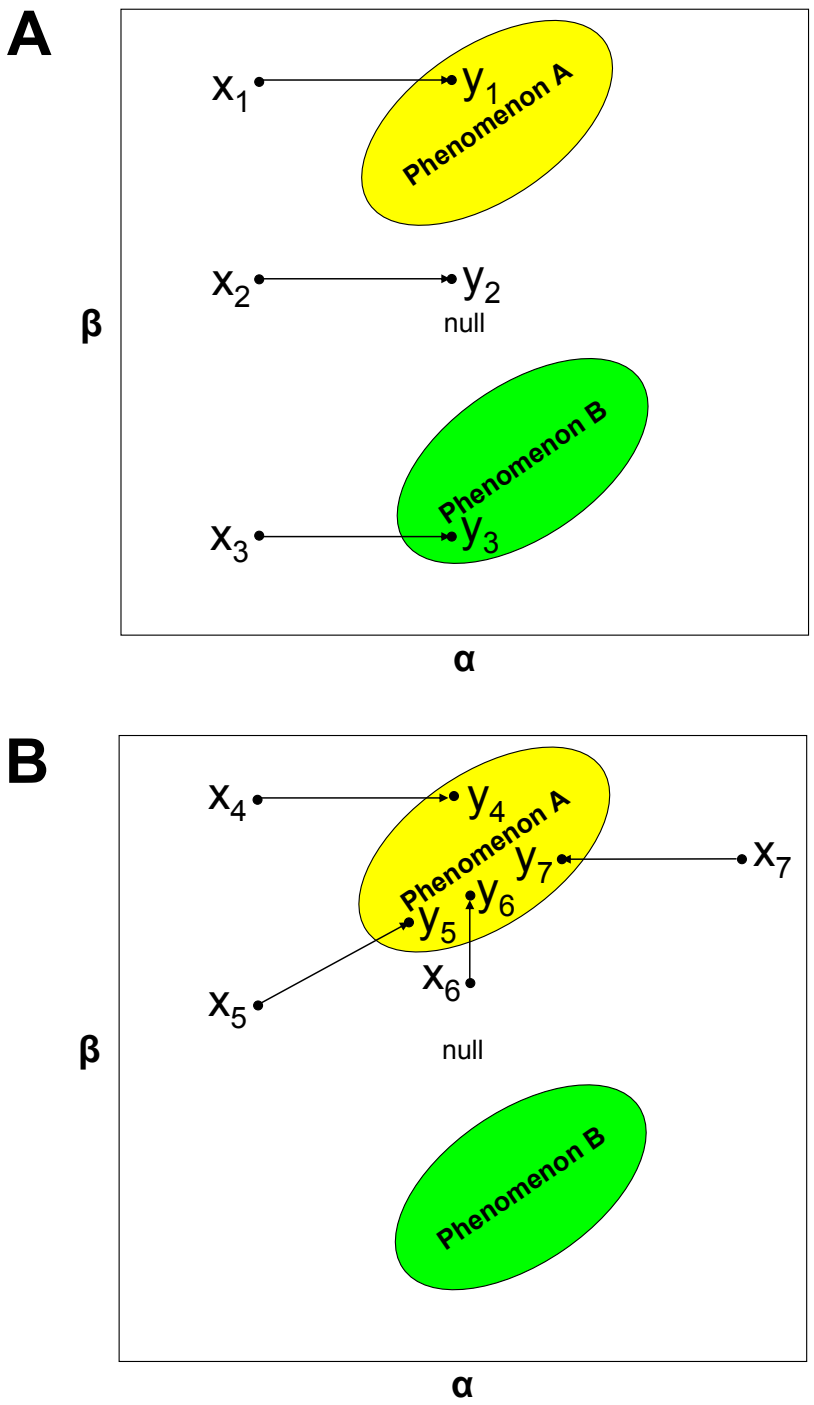

Figure 2-7 Nonlinear dynamics in dissecting both a qualitative and quantitative mechanism. (A) illustrates how the same perturbation (ie. increase in α) can result in different experimental observations (ie. null, Phenomenon A, or Phenomenon B). (B) illustrates how different perturbations (ie. increases and/or decreases in α and/or β) can result in the same phenomenon.

It is clear that same perturbation (ie. an increase in α) may result in different outcomes (null, Phenomenon A, Phenomenon B) depending on the initial conditions, or the initial point within the parameter space, as seen in Fig. 2-7A. It is also clear that two different perturbations (ie. an increase in x, an increase in y, or a combination of the two) may be able to produce the same phenomenon, as seen in Fig 2-7B. This illustrates the strength of taking a non-linear dynamics approach to efficiently dissect a unifying mechanism that would otherwise be very difficult, or impossible, to tease out experimentally. This approach is particularly powerful in studying biological systems, many of which are highly non-linear.

Below, I discuss two important bifurcations: the Hopf and Homoclinic bifurcations. This is because EADs, which is the focus of this thesis work, are "born by Hopf and die by Homoclinic"[1].

2.5.1 Poincare-Andronov-Hopf Bifurcation

The Poincare-Andronov-Hopf Bifurcation, otherwise known as the Hopf bifurcation, is a dynamical process by which oscillations may be initiated[4]. If a Hopf bifurcation occurs, this theory provides the mathematical criterion by which oscillations can occur. Specifically, a Hopf bifurcation is the birth of a limit cycle (ie. oscillations) when an equilibrium of a dynamical system defined by a set of differential equations loses stability via a pair of complex conjugate eigenvalues, and crosses the imaginary axis of a complex plane. While this definition of the Hopf

bifurcation is probably incomprehensible to most reading this thesis, it will hopefully become more clear in the example below of a simple 2D system.

2.5.1.1 Hopf Bifurcation in a Simple 2D System: Van der Pol Model

The Hopf bifurcation is best first understood in the context of simplest dynamical system in which oscillations can occur which is a system consisting of 2 differential equations (ie. 2D/planar system). Take for instance a simple model of a Van der Pol (VdP) oscillator, which has previously been used to model the electrical activity of the heart. This model is described by the following set of differential equations:

$$\begin{cases} \dot{x} = \dfrac{dx}{dt} = u(1-y^2)x - y & (2) \\ \dot{y} = \dfrac{dy}{dt} = x & (3) \end{cases}$$

To determine the Hopf bifurcation, the equilibrium point(s) must first be computed. The equilibrium point is the point in the system where none of the parameters change with time. In other words, it is the point in the system where all the differential equations are set to zero:

$$\begin{cases} \dfrac{dx}{dt} = u(1-y^2)x - y = 0 & (4) \\ \dfrac{dy}{dt} = x = 0 & (5) \end{cases}$$

It is easy to see that equation #4 is easily satisfied when x = 0. Equation #4 can easily be computed by setting x = 0 as follows:

$$\frac{dx}{dt} = u(1-y^2)x - y = 0 \text{ where } x = 0 \quad (6)$$
$$\Rightarrow u(1-y^2)(0) - y = 0$$
$$\Rightarrow -y = 0$$
$$\Rightarrow y = 0$$

Thus the equilibrium point of the Van der Pol oscillator model is

$$(x_{eq}, y_{eq}) = (0, 0) \ (7)$$

Next, the Jacobian matrix (J) at the equilibrium point must be computed as follows:

$$J = \left[\begin{array}{cc} \frac{d\dot{x}}{dx} & \frac{d\dot{y}}{dy} \\ \frac{d\dot{y}}{dx} & \frac{d\dot{y}}{dy} \end{array} \right] \Bigg|_{(x_{eq}, y_{eq})=0} \quad (8)$$
$$= \left[\begin{array}{cc} \frac{d}{dx}[u(1-y^2)x - y] & \frac{d}{dx}[u(1-y^2)x - y] \\ \frac{d}{dx}[x] & \frac{d}{dy}[x] \end{array} \right] \Bigg|_{(x_{eq}, y_{eq})=0}$$
$$= \left[\begin{array}{cc} u(1-y^2) & -1 \\ 1 & 0 \end{array} \right] \Bigg|_{(x_{eq}, y_{eq})=0}$$
$$= \left[\begin{array}{cc} u(1-0) & -1 \\ 1 & 0 \end{array} \right]$$
$$= \left[\begin{array}{cc} u & -1 \\ 1 & 0 \end{array} \right]$$

The eigenvalues (λ) can then be determined by satisfying the following expression, where I is the identity matrix and J is the Jacobian matrix at the equilibrium point:

$$
\begin{aligned}
& det \left| \; J_{eq} \; - \; \lambda I \; \right| \qquad (9) \\
=& det \left| \; \begin{bmatrix} u & -1 \\ 1 & 0 \end{bmatrix} \; - \; \lambda \begin{bmatrix} 1 & 0 \\ 0 & 1 \end{bmatrix} \; \right| \\
=& det \left| \; \begin{bmatrix} u & -1 \\ 1 & 0 \end{bmatrix} \; - \; \begin{bmatrix} \lambda & 0 \\ 0 & \lambda \end{bmatrix} \; \right| \\
=& det \left| \begin{bmatrix} u-\lambda & -1-0 \\ 1-0 & 0-\lambda \end{bmatrix} \right| \\
=& det \left| \begin{bmatrix} u-\lambda & -1 \\ 1 & -\lambda \end{bmatrix} \right| \\
\Rightarrow & (u-\lambda)(-\lambda) - (-1)(1) = 0 \\
\Rightarrow & -u\lambda + \lambda^2 + 1 = 0 \\
\Rightarrow & \lambda^2 - u\lambda + 1 = 0 \\
\Rightarrow & \lambda_{1,2} = \frac{-(-u) \pm \sqrt{(-u)^2 - 4(1)(1)}}{2(1)(1)} \\
\Rightarrow & \lambda_{1,2} = \frac{u \pm \sqrt{u^2 - 4}}{2}
\end{aligned}
$$

The Hopf bifurcation theorem states that a Hopf bifurcation can only occur when a pair of complex conjugate eigenvalues passes the imaginary axis, ie. when real component of λ is equal to zero, or Re(λ) = 0. It can determine whether or not our systems exhibits this criteria for the Hopf bifurcation as follows. First, the parameter range of μ in which the system exhibits complex conjugate eigenvalues, or a real component +/- an imaginary component, must be computed. Thus, the defining characteristic of a complex conjugate eigenvalue is the presence of an imaginary (*i*) component, or simply the presence of a negative square root component– ie. ω*i* where *i*= √(-1). The parameter range of μ for which complex

conjugate eigenvalues exist must occur when the square root component of the eigenvalue is negative, or less than zero:

$$\lambda_{1,2} = \frac{u}{2} \pm \frac{\sqrt{u^2 - 4}}{2} \qquad (10)$$
$$\Rightarrow \frac{\sqrt{u^2 - 4}}{2} = wi$$
$$\text{if } u^2 - 4 < 0$$
$$\Rightarrow u^2 < 4$$
$$\Rightarrow -2 < u < 2$$

Next, the value of the parameter u for which the Re(λ) = 0 must be determined.

$$\lambda_{1,2} = \frac{u}{2} \pm \frac{\sqrt{u^2 - 4}}{2} \qquad (11)$$
$$\text{if } \frac{\sqrt{u^2 - 4}}{2} = wi$$
$$\text{then } Re(\lambda) = \frac{u}{2}$$
$$\text{if } Re(\lambda) = 0,$$
$$\text{then } \frac{u}{2} = 0$$
$$\Rightarrow u = 0$$

Lastly, it must be determined whether the value calculated for the parameter u which Re(λ) = 0 falls within the range of parameter u that the eigenvalues are complex conjugates. If this is true, then the system is capable of exhibiting a Hopf bifurcation. If not, the Hopf criteria is not fulfilled and the system is incapable of undergoing a Hopf bifurcation. In the case of the VdP model, there exists a Hopf

bifurcation because the value of the parameter u which Re(λ) = 0 was computed to be (μ = 0), and falls within the computed range of the complex eigenvalues (-2 < μ < 2).

Following the Hopf bifurcation, oscillations occur as long as the real component of λ is positive, Re(λ) > 0. This is because each of the differential equations of the system, when solved are an exponential function of the eigenvalue as follows.

$$\dot{x} \Rightarrow x(t) = x_0 \cdot e^{\lambda_1, t} \qquad (12)$$
$$\dot{y} \Rightarrow y(t) = y_0 \cdot e^{\lambda_2, t}$$

From these equations, it can be seen that the solved differential equations diverge to infinity when Re(λ) > 0. This divergence makes the system unstable, and allows it to "spiral" into a stable limit cycle. When Re(λ) < 0, the solved differential equations converge to zero so that the system is "stable", and unable to oscillate.

$$\begin{aligned} &\text{if } \lambda \to \infty, && x(t) \to \infty \qquad (13)\\ & && y(t) \to \infty \\ &\text{if } \lambda \to -\infty, && x(t) \to 0 \\ & && y(t) \to 0 \end{aligned}$$

Thus, in the case of the VdP model, oscillations must occur when h > 0 following a Hopf bifurcation (h=0).

2.5.1.2 Hopf bifurcation in the Luo-Rudy I Model

The above example of the VdP model can be extrapolated to the Luo-Rudy I cardiac myocyte model that was used to dissect the criteria for the Hopf bifurcation. The Luo-Rudy I myocyte model consists of four differential equations: the change in voltage, LTCC activation gate, LTCC inactivation gate, and K activation gate with respect to time.

$$C_m \frac{dv}{dt} = -[I_{Na} + I_{Si} + I_K + I_0(V)] + I_{sti} \tag{14}$$
$$I_{Si} = \overline{G_{Si}} df (V - E_{Si})$$
$$I_K = \overline{G_K} x x_1 (V - E_K)$$
$$\frac{d}{dt} d = \frac{d_\infty(V) - d}{\tau_d(V)}$$
$$\frac{d}{dt} f = \frac{f_\infty(V) - f}{\tau_f(V)}$$
$$\frac{d}{dt} x = \frac{x_\infty(V) - x}{\tau_x(V)}$$
Since I_{Na} is inactive during plateau,
$$C_m \frac{dv}{dt} = -[0 + I_{Si} + I_K + I_0(V)] + I_{sti}$$
$$= -[\overline{G_{Si}} df (V - E_{Si}) + \overline{G_K} x x_1 (V - E_K) + I_0(V)] + I_{sti}$$

Because the dx/dt is relatively slow compared to the other differential equations, it was neglected in the Hopf bifurcation condition formulation. Thus, only the following three differential equations were used to formulate the Hopf bifurcation: the change in voltage, LTCC activation gate, and LTCC inactivation gate with respect to time.

Since I_{Na} is inactive during plateau,

$$C_m \frac{dv}{dt} = -[\overline{G_{Si}} df (V - E_{Si}) + \overline{G_K} x x_1 (V - E_K) + I_0(V)] + I_{sti} \qquad (15)$$

$$\frac{d}{dt} d = \frac{d_\infty(V) - d}{\tau_d(V)}$$

$$\frac{d}{dt} f = \frac{f_\infty(V) - f}{\tau_f(V)}$$

Because of the complexities involved in this higher order system, the Hopf bifurcation criteria is not explicitly derived here but I overview again the same systematic theoretical approach presented above. Again, the equilibrium point is derived by setting the differential equations to zero, and solving for (V,d,f).

The formulation of the Jacobian at the equlibrium point was found to be:

$$J = \begin{pmatrix} a & b & c \\ s_d/\tau_d & -1/\tau_d & 0 \\ -s_f/\tau_f & 0 & -1/\tau_f \end{pmatrix} \qquad (16)$$

where $a = \dfrac{dF}{dV}$

$b = \dfrac{dF}{dd}$

$c = \dfrac{dF}{df}$

$s_d = \dfrac{d_\infty}{dV}$

$s_f = \dfrac{-df_\infty}{dV}$

$b > 0,\ c > 0$ for $V < E_{Si}$;

$s_d > 0$ and $s_f > 0$ for any V

As in the VdP example above, the det|J-Iλ|=0 is then calculated to determine the eigenvalue expression. Note that the determinant of a 3x3 matrix is calculated as follows.

$$\begin{vmatrix} a & b & c \\ d & e & f \\ g & h & i \end{vmatrix} = aei + bfg + cdh - afh - bdi - ceg \qquad (17)$$

The square root component of the eigenvalue expression is set to negative, to derive the parameters for which there exists an imaginary component, ωi. The eigenvalues ($\lambda_{1,2}$) were then computed to be complex conjugates ($\pm i\omega$) when,

$$\omega^2 = \frac{1}{\tau_d \tau_f} - \frac{a}{\tau_d} - \frac{a}{\tau_f} - \frac{s_d b}{\tau_d} + \frac{s_f c}{\tau_f} > 0 \qquad (18)$$

The values of the parameters V, d, and f that allow a pair of complex conjugate eigenvalues to cross the imaginary axis were computed by determining the values or formulaic expression that the parameters V, d, and f must satisfy for Re(λ) = 0. This formulaic expression that satisfies Re(λ) = 0 was found to be the following.

$$h = \frac{1}{\tau_f}(\frac{1}{\tau_f} - a)(\frac{1}{\tau_d} - a + s_f c) + \frac{1}{\tau_d}(\frac{1}{\tau_d} - a)(\frac{1}{\tau_f} - a - s_d b) = 0 \qquad (19)$$

Thus, the Hopf bifurcation occurs when the following are satisfied:

$$\omega^2 = \frac{1}{\tau_d \tau_f} - \frac{a}{\tau_d} - \frac{a}{\tau_f} - \frac{s_d b}{\tau_d} + \frac{s_f c}{\tau_f} > 0 \qquad (20)$$
$$h = \frac{1}{\tau_f}(\frac{1}{\tau_f} - a)(\frac{1}{\tau_d} - a + s_f c) + \frac{1}{\tau_d}(\frac{1}{\tau_d} - a)(\frac{1}{\tau_f} - a - s_d b) = 0$$

Oscillations occur when the Re(λ) > 0 and was computed to occur when:

$$\frac{1}{\tau_f}(\frac{1}{\tau_f}-a)(\frac{1}{\tau_d}-a+s_f c)+\frac{1}{\tau_d}(\frac{1}{\tau_d}-a)(\frac{1}{\tau_f}-a-s_d b)<0 \quad (21)$$

$$\Rightarrow h<0$$

where $a=\frac{dF}{dV}$

$b=\frac{dF}{dd}$

$c=\frac{dF}{df}$

$s_d=\frac{d_\infty}{dV}$

$s_f=\frac{-df_\infty}{dV}$

$b>0,\ c>0$ for $V<E_{Si}$;

$s_d>0$ and $s_f>0$ for any V

It is important to note that this expression is the unifying mechanism by which all EADs must occur. In other words, EADs may occur via a number of "mechanisms", but they must through this "master" mechanism where the above expression h<0 is satisfied. Inspection of this expression h<0 reveals that EADs are dependent on the following:

(1) the maximum value of the LTCC “window current”,

(2) slopes of dV_m/dt with respect to voltage,

(3) the slopes of the LTCC activation and inactivation curves with respect to voltage, and

(4) the time constants of the LTCC activation and inactivation gates.

This unifying mechanism highlights the importance of these slopes and time constants in the genesis of EADs -- ie. oscillations. It also offers the tantalizing possibility of targeting the kinetics of ion channels to prevent EADs in a fashion that does not disrupt or impair normal excitation-contraction coupling.

2.5.2 Homoclinic Bifurcation

The homoclinic bifurcation is one of the dynamical processes that can cause a limit cycle (ie. oscillation) to disappear[4]. Our group previously dissected the mechanism of EAD termination to be due to the homoclinic bifurcation. A homoclinic bifurcation occurs when the periodic orbit collides with a saddle point. A saddle point is an equilibrium point that has both unstable and stable directions, ie. orbits are attracted to it from one direction, and repelled away from another direction (Fig. 2-8). The saddle point can be visualized at the coordinate (0,0,0) in the topological graph of $z = x^2 - y^2$ seen in Fig. 2-8.

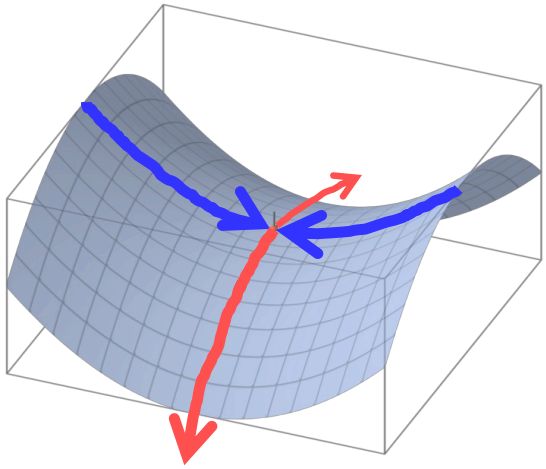

Figure 2-8 Saddle Node. Topographically resembles a "horse saddle" with two perpendicular vectors, one pointing towards and the other away from the saddle node.

The homoclinic bifurcation has also been referred to as an infinite period bifurcation, because the period of the limit cycle (ie. oscillations) increases with time as it approaches the saddle point (ie. the equilibrium point). Thus, the characteristic signature of a Homoclinic bifurcation is a gradual increase in the period (or a decrease in the frequency) of oscillations. In fact, this signature of a gradual increasing period is such a strong indicator of a homoclinic bifurcation that it is the defining criteria used by the automatic bifurcation analysis software AUTO[27].

The increase in the period of the oscillations occurs as follows. The equilibrium point is defined as the point where all parameters with respect to time are equal to zero. Thus, as the limit cycle approaches the equilibrium point, the system becomes slower. In other words, the closer the system is to the equilibrium point, the slower the system will be. Once the limit cycle comes into contact with the

saddle point (Fig. 2-9), which is an equilibrium point, all activity must cease by the very definition of an equilibrium point.

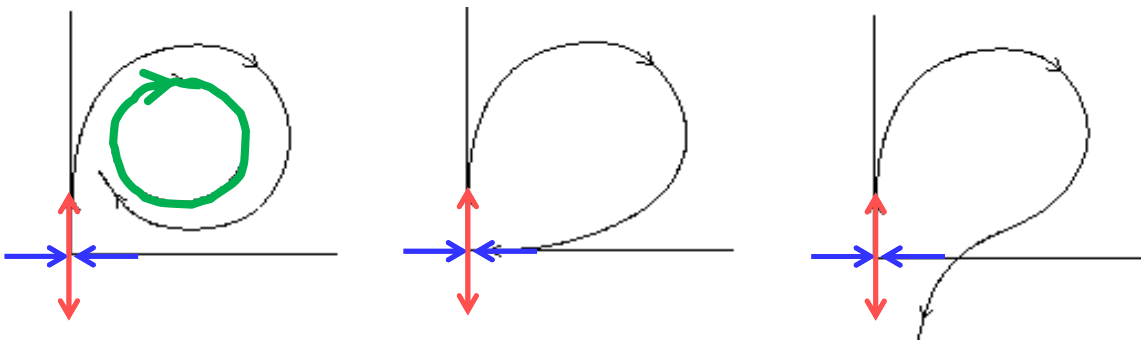

Figure 2-9 Hopf-Homoclinic bifurcation mechanism. As the periodic orbit (green) created by the Hopf bifurcation approaches the equilbrium point (ie. the saddle node) of the Homoclinic bifurcation, the period increases. When the periodic orbit comes into contact with the saddle node, the periodic orbit is destroyed and all activity ceases.

As part of my thesis work, I was able to experimentally demonstrate that EAD bursts in cardiac monolayers exhibit the dynamical signature of the homoclinic bifurcation described above. Furthermore, I was able to dissect the physiological mechanism of the homoclinic bifurcation using the UCLA myocyte model that has complex intracellular Ca^{2+} handling and intracellular Ca^{2+} and Na^{+} fluxes.

2.6 Experimental dissection of tissue level arrhythmias

Evaluation of EADs at the tissue level (with optical mapping, microelectrode array, etc.) as opposed to the cellular level (via patch clamping, confocal, etc.) is

important because arrhythmias at the cellular level do not always manifest at the tissue level. In fact, most of times they do not. Recent theoretical work[28] by our group revealed that a large number of contiguous cells must be synchronized and all exhibit EADs for an EAD to propagate in tissue and produce a clinically relevant arrhythmia (1D cable: 70 myocytes, 2D tissue: 6940 myocytes, 3D tissue: 696,910 myocytes), ie. one that produces an electrical signature on EKG in the form of a PVC, Torsades de Pointes, etc. This emphasizes the importance of studying arrhythmias at the tissue level.

2.6.1 Optical Mapping

Optical mapping (Fig. 2-10) is a powerful tool that allows evaluation of arrhythmias at the tissue by recording the relative membrane potential and/or intracellular Ca^{2+} of the tissue using voltage (ie. RH237, Di-4-ANNEPPS) and/or Ca^{2+} (ie. Rhod-2) sensitive dyes, respectively. Each specific dye has its own characteristic excitation and emission wavelength. When the dye is excited at its characteristic wavelength, it emits light at a particular wavelength whose intensity is inversely related and relative to the membrane potential in the case of voltage sensitive dyes, and directly related and relative to the intracellular Ca^{2+} in the case of Ca^{2+} sensitive dyes. These intensity values are recorded with highly sensitive instruments such as CCD cameras or photodiode arrays. Most commercially available setups are able to record with sufficiently high temporal (>200fps) and spatial (<1mm) resolution.

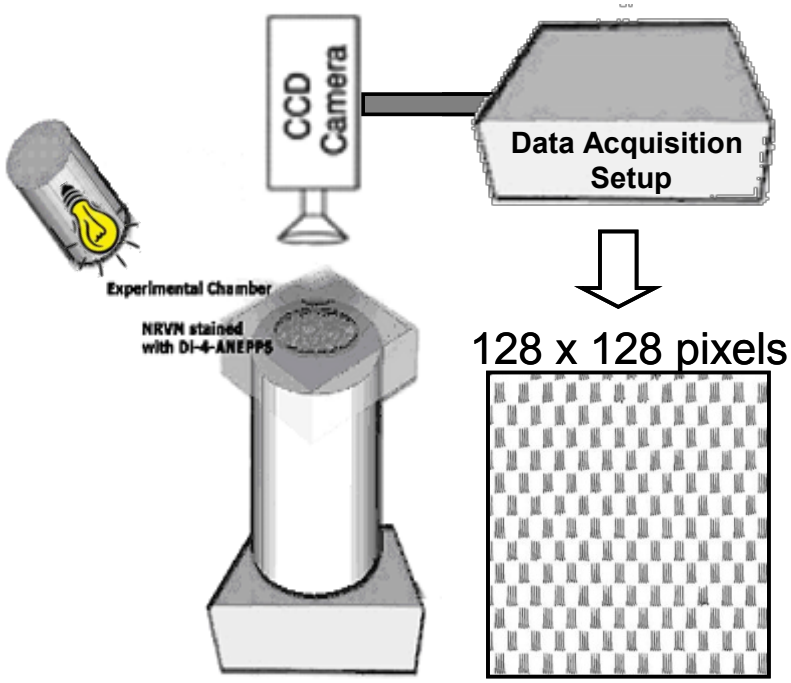

Figure 2-10 Optical mapping setup. Optical action potentials and Ca^{2+} transients can be recorded from cardiac tissue with high spatial and temporal resolution using this technique.

The data can be interpolated across the recording channels to yield voltage activation maps seen in Fig. 2-11.

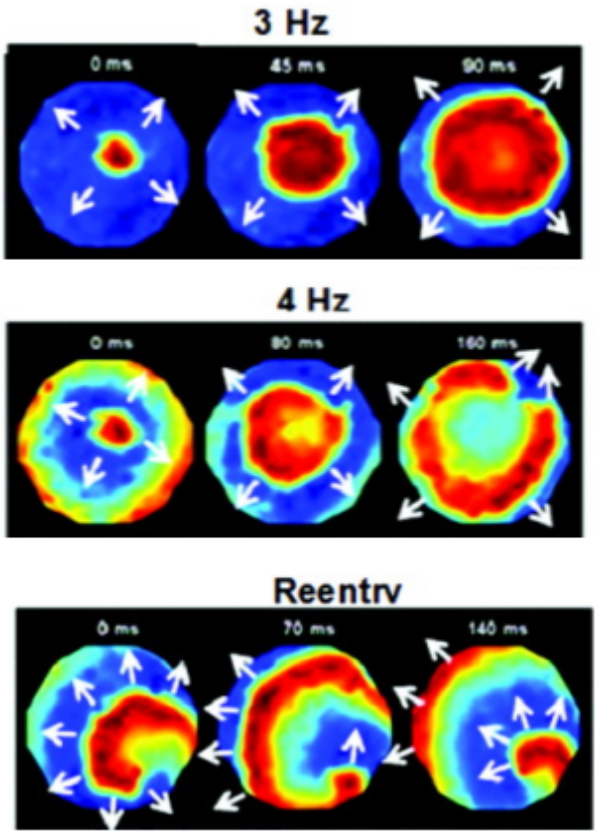

Figure 2-11 Voltage maps of electrical wave propagation in a cardiac monolayer. Optical mapping allows sufficient spatial and temporal resolution to study "arrhythmias in a dish." Here, rapid pacing (4Hz) in an *in vitro* model of the infarct border zone results in wavebreak that initiates a reentrant arrhythmia (ie. a single spiral wave). Figure reprinted from [6].

Note that while today's CCD and photodiode arrays can record with a spatial resolution better than 1mm, the scattering of the emission signal for all dyes is significant enough that the upperbound of actual achievable spatial resolution is on the order of a millimeter. Also note that while the intensity values of the voltage images are inversely related to the membrane potential, all recordings here have been "flipped" to represent relative membrane potential recordings (F_v).

2.6.2 Neonatal Rat Ventricular Myocyte (NRVM) Monolayers

Neonatal rat ventricular myocytes (NRVM) when isolated and plated at the appropriate density are able to form gap junctions with each other after a couple days in culture, and beat as a syncytium. Rats are the only species whose myocytes are able to create a confluent monolayer (Fig. 2-12) after being isolated in culture. Note that this is only the case with neonatal rats, and not adults. While the electrophysiology of NRVMs differs from that of humans and other species, the use of NRVM monolayers in optical mapping studies has provided a wealth of knowledge related to the basic mechanisms of cardiac impulse propagation and arrhythmias[16, 29-46]. After 9-11 days in culture, NRVMs exhibit mature Ca^{2+} handling[47] (Fig. 2-13), and striations that resemble those observed in adult myocytes (Fig. 2-14).

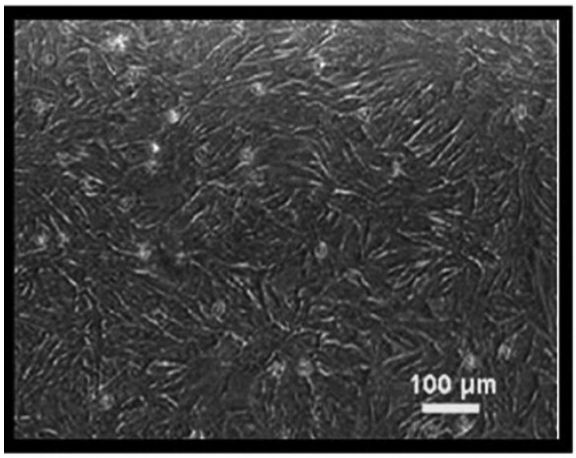

Figure 2-12. Confluent NRVM monolayer

Figure 2-13. Cultured NRVMs exhibit robust Ca^{2+}-induced Ca^{2+}-release. Large Ca^{2+} transients are observed via optical mapping following stimulation during superfusion with normal Tyrode (1.8mM Ca2+) (top trace). Ca^{2+} transients are abolished after disabling the SR with 10mM caffeine (bottom trace) consistent with mature Ca^{2+} handling.

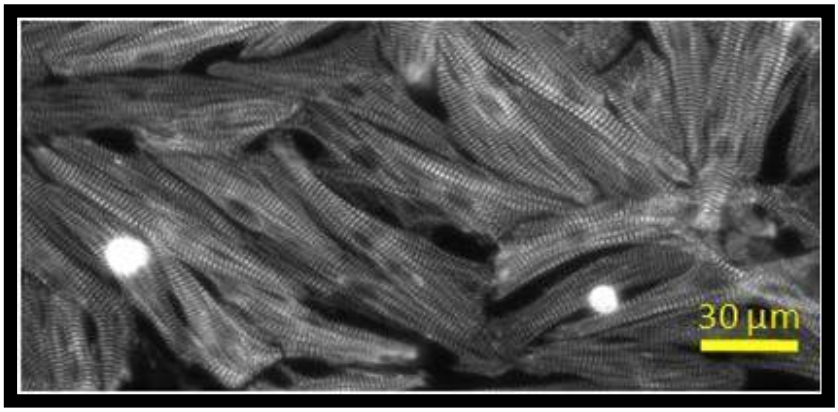

Figure 2-14 Cultured NRVMs resemble adult myocytes. Fluorescent microscopy image of a day 11 NRVM-only monolayer stained for α-actinin. The α-actinin staining resembles that observed in adult myocytes.

Using 2D preparations such as NRVMs are ideal because the electrical activity is confined to a plane so that many of the technical obstacles associated with whole heart mapping are overcome. In whole heart mapping, only the outer portion of the

heart, the epicardium, can be imaged. As a result, it is often times impossible to determine whether the electrical activity on the epicardium is originating from the epicardium itself or transmurally from beneath the epicardium (ie. endocardium, mid-myocardium). For example, transmural reentry may present as focal activity on the epicardium. Because of optical scattering, there are also significantly greater artifacts in the optical recordings when imaging the whole heart compared to monolayers because of the extra dimension (ie. depth) involved[48, 49].

Also, the whole heart itself is extremely heterogeneous in nature, both structurally and electrophysiologically. This makes it impossible to dissect fundamental mechanisms in any sort of well controlled manner. In the case of monolayers, homogeneous monolayers can be readily created to exclude any structural factors. The substrate can also be manipulated by employing microfabrication techniques previously developed in the semiconductor industry, to pattern cells in a highly controlled fashion. This has given considerable insights into both physiological and pathological conditions[16, 29-46]. Additionally, NRVMs are very amenable to genetic modification and are useful in proof of principle gene therapy studies[50-53]. Furthermore, co-cultures can be easily created to assess the electrophysiological consequences of stem cell transplantation[50, 54] and altered cell-to-cell coupling[6, 51, 55-58] in substrates such as the infarct border zone.

3. The Dynamics Underlying Early Afterdepolarization-Mediated Triggered Activity in Cardiac Monolayers

3.1 Abstract

Early afterdepolarizations (EADs) are voltage oscillations during the repolarizing phase of the cardiac action potential, which cause cardiac arrhythmias in a variety of clinical settings. EADs occur in the setting of "reduced repolarization reserve" and "increased inward over outward currents," which explains intuitively repolarization delay, but does not mechanistically explain the time-dependent voltage oscillations characteristic of EADs. In a recent theoretical study, we identified a dual Hopf-homoclinic bifurcation as a dynamical mechanism causing voltage oscillations during EADs, dependent jointly on the amplitude and kinetics of the L-type Ca^{2+} channel (LTCC) current relative to repolarizing K^{+} currents. Here we demonstrate this mechanism experimentally. We show that cardiac monolayers exposed to the LTCC agonists BayK8644 and isoproterenol produce EAD bursts which are suppressed by the LTCC blocker nitrendipine, but not by the Na^{+} current blocker tetrodoxin, depletion of intracellular Ca^{2+} stores with thapsigargin and caffeine, or buffering intracellular Ca with BAPTA-AM. These EAD bursts exhibited a key dynamical signature of the dual Hopf-homoclinic bifurcation mechanism, namely a gradual slowing in the frequency of oscillations prior to burst termination. A detailed cardiac action potential model reproduced the experimental observations,

and identified intracellular Na^+ accumulation as the likely mechanism terminating EAD bursts. Our findings in cardiac monolayers provide direct support for the Hopf-homoclinic bifurcation mechanism of EAD-mediated triggered activity, and raise the possibility that this mechanism could also contribute to EAD formation in clinical settings such as long QT syndromes, heart failure, and increased sympathetic output, providing new therapeutic targets and expanding the current concept of reduced repolarization reserve.

3.2 Introduction

Early afterdepolarizations (EADs) can cause lethal arrhythmias in cardiac conditions such as congenital and acquired long QT (LQT) syndromes and heart failure, which are often potentiated by increased sympathetic output [59, 60]. EADs have been classically attributed to reactivation of the L-type Ca^{2+} channel (LTCC) as membrane voltage passes through the LTCC "window" voltage region (approximately 0 to -40 mV, where steady state activation and inactivation curves overlap) [22, 61-64]. If the rate of repolarization is not sufficiently rapid through this voltage range, then LTCC can reactivate, reversing repolarization to produce the EAD upstroke. This scenario typically occurs when repolarization reserve is reduced [65-68]. In this setting, it is intuitively obvious that the increase in the magnitude of inward currents relative to outward currents will cause an increase in the action potential (AP) duration (APD) (or its ECG analogue, the QT interval); an increase in APD is often held to be by itself a marker for pro-arrhythmia. However, EADs are characterized by voltage oscillations, implying that time-dependent factors, such as the time constants of the steady state activation, inactivation and recovery from inactivation of the LTCC relative to those of K^+ channels, are also critical. Specifically, in order for voltage to oscillate, the time constants of these currents have to be in the resonance with each other.

To explore how time- and voltage-dependent factors interact to cause EAD voltage oscillations, we adopted a nonlinear dynamics approach to analyze EAD

formation in the Luo-Rudy I (LR1) ventricular action potential (AP) model [1]. Based on this analysis, we theorized that EADs are generated by a *Hopf bifurcation* and terminated by a *homoclinic bifurcation*. The Hopf bifurcation is a dynamical process by which an equilibrium (in this case, the plateau voltage) becomes unstable and begins to oscillate [4], which occurs as the slopes of feedback relations are increased in the presence of an appropriate time delay. For example, the change from the non-oscillatory mode to the oscillatory mode of the sino-atrial nodal pacemaker cell has been modeled as a Hopf bifurcation [69]. Hopf bifurcations are thought to underlie many other biological oscillations, such as the cell cycle [70], glycolytic oscillations [71] and circadian rhythms [72]. In the LR1 model, we found that the Hopf bifurcation-mediated voltage oscillations at the plateau potential (i.e., EADs) can occur when the slopes of the LTCC activation and inactivation curves are steep, with properly matched time constants and window LTCC current [1]. The homoclinic bifurcation is a parameter point at which the oscillatory orbit collides with the saddle point, resulting in an infinite-period orbit. After the bifurcation point, no oscillatory orbit exists. The Hopf bifurcation initiates the membrane oscillations, causing single or multiple EADs, and as the outward currents activate slowly, the system gradually approaches and passes the homoclinic bifurcation, at which the voltage fully repolarizes, terminating the EADs. The defining feature of this process is frequency slowing, i.e., as the oscillatory orbit approaches the infinite period orbit, the period of the oscillations increases.

In this study, we performed optical mapping experiments of cultured neonatal rat ventricular myocyte (NRVM) monolayers to determine whether EAD-mediated triggered activity in this preparation exhibited features that corroborate the theoretical mechanism described above. We induced EADs by exposing monolayers to the LTCC agonists BayK8644 and isoproterenol. In cardiac monolayers, we find that EADs exhibit the key dynamical signature of the Hopf-homoclinic bifurcation mechanism [1], namely gradual slowing of the frequency response prior to burst termination. Bursts were resistant to Na^+ channel blockade (with TTX), depletion of SR Ca^{2+} (with caffeine and thapsigargin), and suppressed by Ca^{2+} channel blockade (with nitrendipine), consistent with the predicted central role of LTCC. Moreover, interventions that delayed entry into the LTCC "window" region, such as blocking the transient outward K^+ channel (I_{to}) and other K^+ currents with 4-aminopyridine(4-AP), or overexpressing a Ca^{2+}-insensitive mutant calmodulin (CaM_{1234}) to suppress LTCC inactivation, also suppressed EAD bursts, despite further prolonging APD. These experimental findings were reproduced in a detailed cardiac AP model, which revealed that the frequency slowing and burst termination were due to a slow accumulation of intracellular Na^+. These results provide strong experimental evidence that the Hopf-homoclinic bifurcation mechanism of EAD-mediated triggered activity can occur in a real cardiac tissue.

3.3 Materials and Methods

All protocols used conform to the standard set forth by the National Institutes of Health in the *Guide for the Care and Use of Animals* (NIH publication No. 85-23, Revised 1996).

Cell culture. We created monolayers of neonatal rat ventricular myocytes (NRVMs) by plating $1x10^6$ cells on 21mm fibronectin-coated plastic coverslips, as previously described [50]. Representative appearance of myocytes after 11 days in culture is shown in the Supplement (Supplemental Fig. S3-1). We confirmed maturation of SR Ca^{2+} handling in NRVM cultures by recording Ca^{2+} transients during pacing in Tyrodes solution before and after exposure to 10mM caffeine which depletes SR Ca^{2+} stores. Ca^{2+} transients were abolished by the addition of caffeine (Supplemental Fig. S3-2), consistent with a mature SR Ca^{2+} handling phenotype, as described previously for NRVM monolayers after several days in culture [73-75].

Optical mapping. Arrhythmias were imaged by optical mapping performed after 11-14 days in culture. Coverslips were visually inspected under a microscope and monolayers with obvious gaps in confluence and non-beating cultures were rejected (after 7d in culture, most NRVMs are quiescent and a dominant pacemaker is responsible for electrical activity in monolayers). The coverslips were then transferred to a custom-designed chamber, stained with 5 μmol/L di-4-ANEPPS, a voltage-sensitive dye for 5 min or 5μmol/L Rhod-2 AM, a Ca^{2+}-sensitive dye for 30

min, and then continuously superfused with warm (36.5°C) oxygenated (normal) Tyrode solution containing (in mM) 135 NaCl, 5.4 KCl, 1.8 CaCl2, 1 MgCl2, 0.33 NaH2PO4, 5 HEPES, and 5 glucose. A unipolar point electrode was used to stimulate the cells.

Action potentials were recorded using either a custom-built contact fluorescence imaging system with 253 recording sites as previously described [50] (Supplemental Fig.S3-3), or a CCD-based optical imaging system (Photometrics Cascade 128+, Tucson, AZ) , with 128 x 128 spatial resolution at 0.6- to 5-ms per frame. Voltage and Ca^{2+} signals were acquired continuously over 2-15 minutes either in the absence of pacing or during pacing at <0.5 Hz. Data were stored, displayed, and analyzed using custom software written in Visual C++ (Microsoft), Laboratory VIEW (National Instruments), and MATLAB (Math Works).

Experimental protocols. Mode-2 gating of LTCC was induced by adding the LTCC agonist BayK8644 (2.5μM) and the beta adrenergic receptor agonist isoproterenol (1μM) to the perfusate. In some experiments, Na^{+} channels and LTCC were blocked by adding 10μM Tetrodotoxin (TTX) or 5 μM nitrendipine, respectively, directly to the superfusate. To deplete SR Ca^{2+}, some monolayers were pre-treated with10 mM caffeine and 5μM thapsigargin for 30 min [76-79]. To buffer intracellular Ca^{2+}, some monolayers were incubated with 100μM BAPTA-AM for 7 min. The relative Ca concentrations under these conditions are shown in supplemental Fig.S3-4. To create intracellular Ca^{2+} overload without inducing mode-

2 gating of LTCC, some monolayers were superfused with Tyrode's solution containing 100μM ouabain and 3.6 mM Ca^{2+}. To block the outward transient K+ current and other K^+ currents, some monolayers were superfused with 4-aminopyridine (4-AP, 10 mM). To ablate Ca^{2+}-dependent inactivation of the LTCC, some monolayers were pre-infected with the adenoviral adenoviral construct Ad-CaM_{1234} to overexpress the mutant Ca^{2+}-insensitive calmodulin CaM_{1234}, as previously described [80].

Data analysis. The baseline drift due to photobleaching of the potentiometric dye was reduced by subtracting a third order polynomial best fit curve of the optical signals. To reduce noise in the optical signals, a seven point moving median filter was applied to the de-trended data. Animations of electrical propagation were generated from signals that were low-pass filtered between 0 and 100 Hz. The activation time was defined as the instant of maximum positive slope. Burst frequency plots were computed by determining the inverse of time between upstrokes. Pseudo ECGs were computed (using the concept of the lead field) from the potential difference determined between two virtual electrodes positioned 5mm above diametrically opposite points on the monolayer, and located parallel to the horizontal edge of the recording hexagonal area [81].

Statistics. Data were expressed as mean ± SD and analyzed using a paired Student's t-test. *P* values <0.05 were considered to be significant.

Computer simulations. Computer simulations used the ventricular action potential model by Mahajan et al.[82] with further modifications described in [83]. In addition, two linear background currents: I_{Cab} and I_{Nab}, were added, with the corresponding conductances chosen as $g_{B,Ca}$ = 0.0002513 mS/μF and $g_{B,Na}$ = 0.0004 mS/μF and the maximum rate of electrogenic Na^+-K^+ pump was decreased to g_{NaK} = 0.8 mS/μF to give a steady state intracellular sodium concentration of $[Na]_i$ = 10 mM. To generate the bursting behavior, we started from the EAD model in [83] and increased the maximum Ca flux of the LTCC by 41% and the maximum conductance of the fast I_{to} by 45%. Although we did attempt to reproduce the effects of BayK8644 and isoproterenol in a quantitatively exact manner, our modifications are qualitatively in line with their effects on the LTCC current. Accordingly, to induce EADs in the control model [82], we increased the LTCC current and sped up its kinetics [83]. Here we further increased LTCC to result in EAD burst. In addition, increasing I_{to} to potentiate burst agrees with our experiments that blocking the transient outward current suppressed the bursting behavior. A nonlinear instantaneous BAPTA buffer with K_{BAPTA}=215 μM was added to simulate the presence of BAPTA-AM. See the supplemental material for the detailed parameter changes and a study of the sensitivity and dependence of the burst duration and frequency on parameter values (Supplemental Fig.S3-5). All simulations were performed using the CVODE time-adaptive solver for stiff equations from the SUNDIALS package [84]. The time-adaptive solver guarantees a maximum local

error on all state variables, which was set to be smaller than 10^{-5} in relative value and 10^{-6} in absolute value.

3.4 Results

3.4.1 BayK8644 and isoproterenol induce bursts of EAD-mediated triggered activity

Cultured NVRM monolayers superfused with BayK8644 (2.5μM) and isoproterenol (1μM) developed robust synchronized bursts of electrical activity that arose abruptly during slow pacing (<0.04 Hz), as detected by either voltage or Ca^{2+} imaging (Fig. 3-1 A & B, Supplemental Fig. S3-2). Bursts were characterized by incomplete repolarization between beats, consistent with EAD-mediated triggered activity. Also consistent with EAD-mediated triggered activity, bursts were focal, originating at one or more distinct sites and propagating throughout the monolayer (Fig. 3-2 A & B), resulting in a pseudo-electrocardiogram resembling polymorphic VT (Fig. 3-2C). Burst episodes were self-limited and recurrent, with burst duration averaging 34 [standard deviation (SD) 23] seconds and the frequency of triggered activity during the burst averaging 2.6 (SD 0.3) Hz (n=9 monolayers). During individual bursts, the frequency of triggered activity decreased gradually to 45 (SD 5) % of the initial frequency (n=9) (Fig. 3-1A), a classic dynamical signature of the dual Hopf-homoclinic bifurcation mechanism. Ca^{2+} imaging of EAD bursts exhibited frequency plots (Fig. 3-1B) similar to those recorded by voltage imaging.

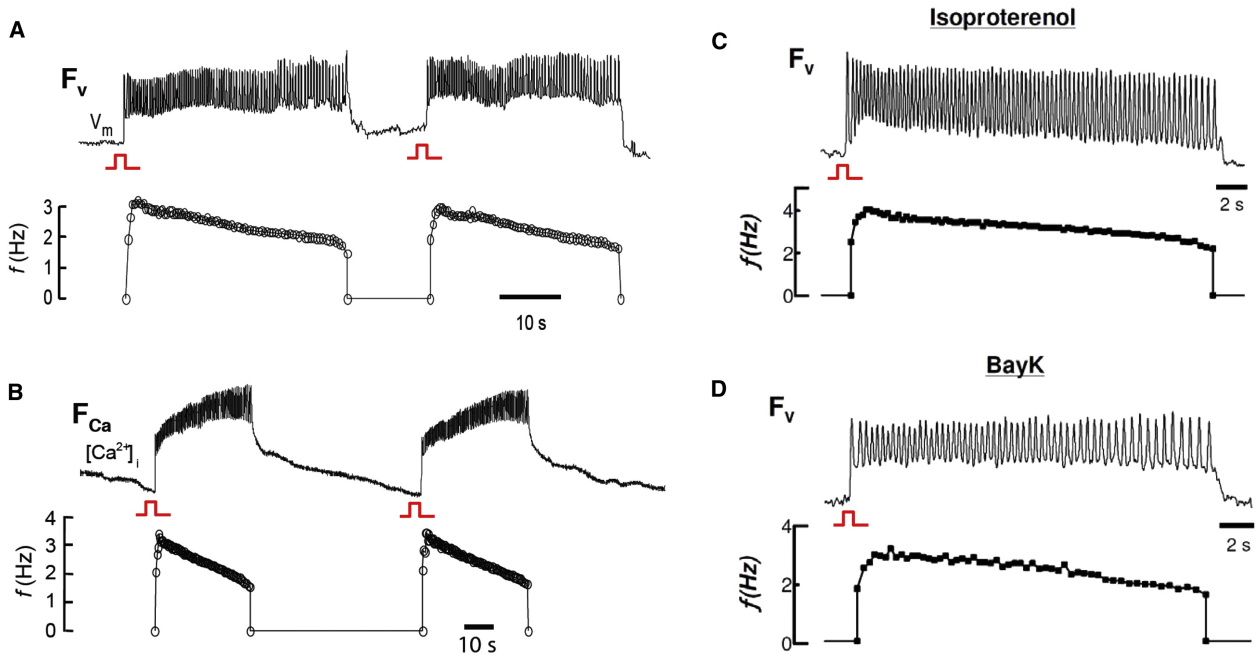

Figure 3-1. Voltage and Ca^{2+} bursts induced by BayK8644 and isoproterenol. Voltage and calcium bursts (top panels of panels A and B, respectively) recorded by voltage (F_V) or Ca^{2+} (F_{Ca}) optical mapping in two different monolayers, and their corresponding frequency response plots (lower panels). (C) and (D) Perfusing with solely isoproterenol (Panel C) or solely BayK8644 (Panel D) induced bursts.

Since BayK8644 and isoproterenol directly or indirectly affect other ionic currents besides LTCC, we also tested both drugs separately. EAD bursts were observed with isoproterenol alone (Fig. 3-1C) in 3 of 8 monolayers, and with BayK8644 alone in 7 of 7 monolayers (Fig. 3-1D). In both cases, bursting frequencies gradually declined prior to burst termination. Thus, unless BayK8644 and isoproterenol have overlapping off-target effects, these findings implicate altered LTCC gating properties as the common factor by which these drugs induce EAD bursting.

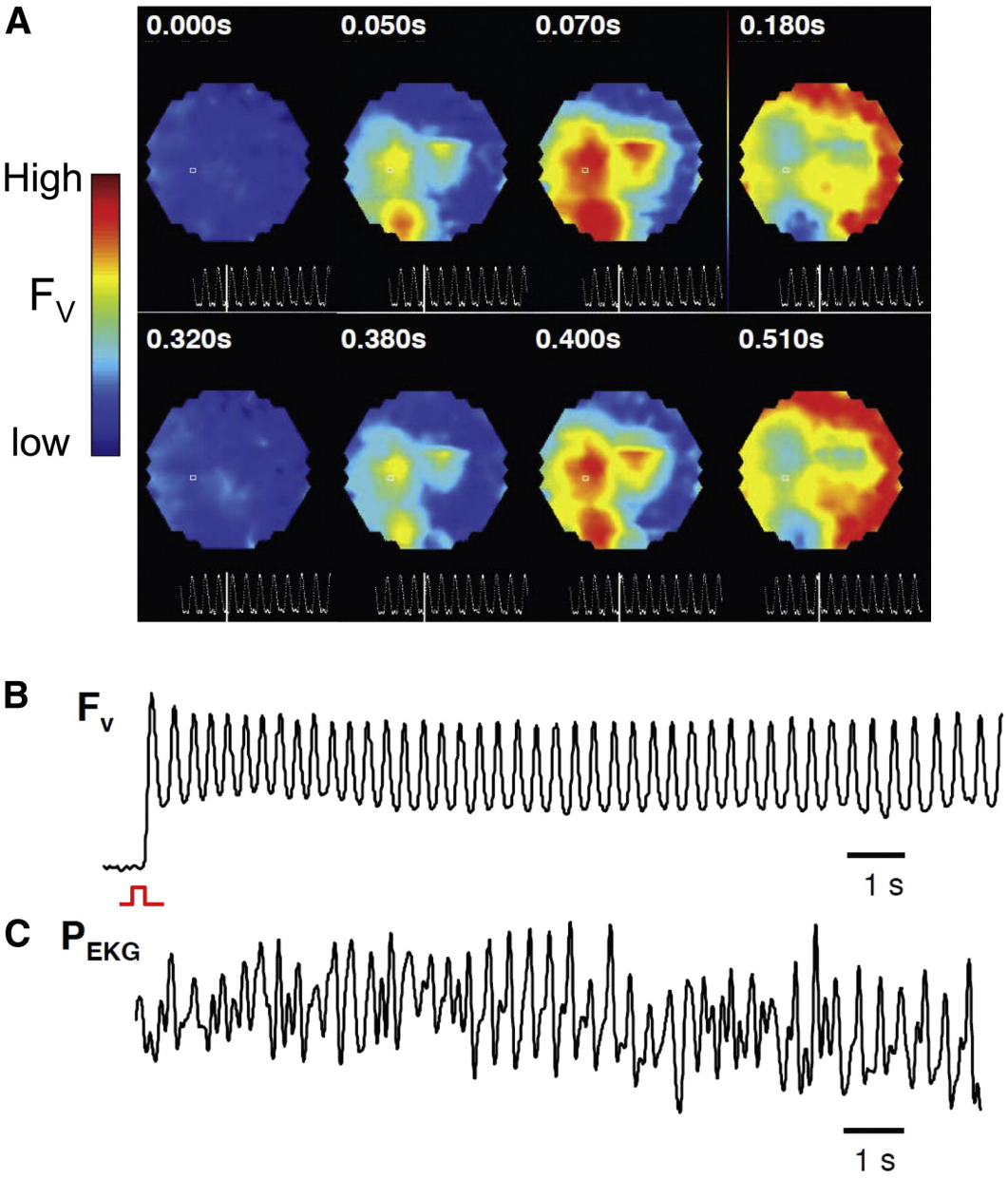

Figure 3-2. BayK8644 and isoproterenol induces bursts of focal activity resembling polymorphic VT. (A) Voltage maps of bursting activity revealed repetitive firing of focal activity. Color bar corresponds to the normalized voltage level, with blue being the minimum voltage level that occur following the initial upstroke of the burst and red the peak of activity observed during bursts. (B) A close-up of the initial voltage activity observed in the first burst shown in Fig 3-1, panel A, showing burst of EADs. (C) Pseudo-ECG showing polymorphic ventricular tachycardia corresponding to burst in Panel B underlie by multiple focal activity (Panel A).

3.4.2 EAD bursts depend on LTCC, but not on Na^+ channels, SR Ca^{2+} cycling, or Ca^{2+} overload per se

Following a single stimulated AP, EAD bursts induced by BayK8644 and isoproterenol were completely suppressed by the LTCC channel blocker nitrendipine (5 μM) (Fig. 3-3A; n=7). Neither Na^+ channel blockade with 50 μM TTX (Fig. 3-3B; n=5 monolayers) nor suppressing SR Ca^{2+} cycling with caffeine and thapsigargin (Fig. 3-3C) had any significant effect. In contrast, when monolayers were pre-treated with BAPTA-AM to buffer intracellular Ca^{2+}, burst duration prolonged, from 34 (SD 23) seconds to 61 (SD 27) seconds (n=9), without significantly affecting bursting frequency (Fig. 3-4). With BAPTA-AM present, bursting frequency declined more slowly during the burst, so that the frequency just prior to burst termination was similar to non-BAPTA-treated monolayers.

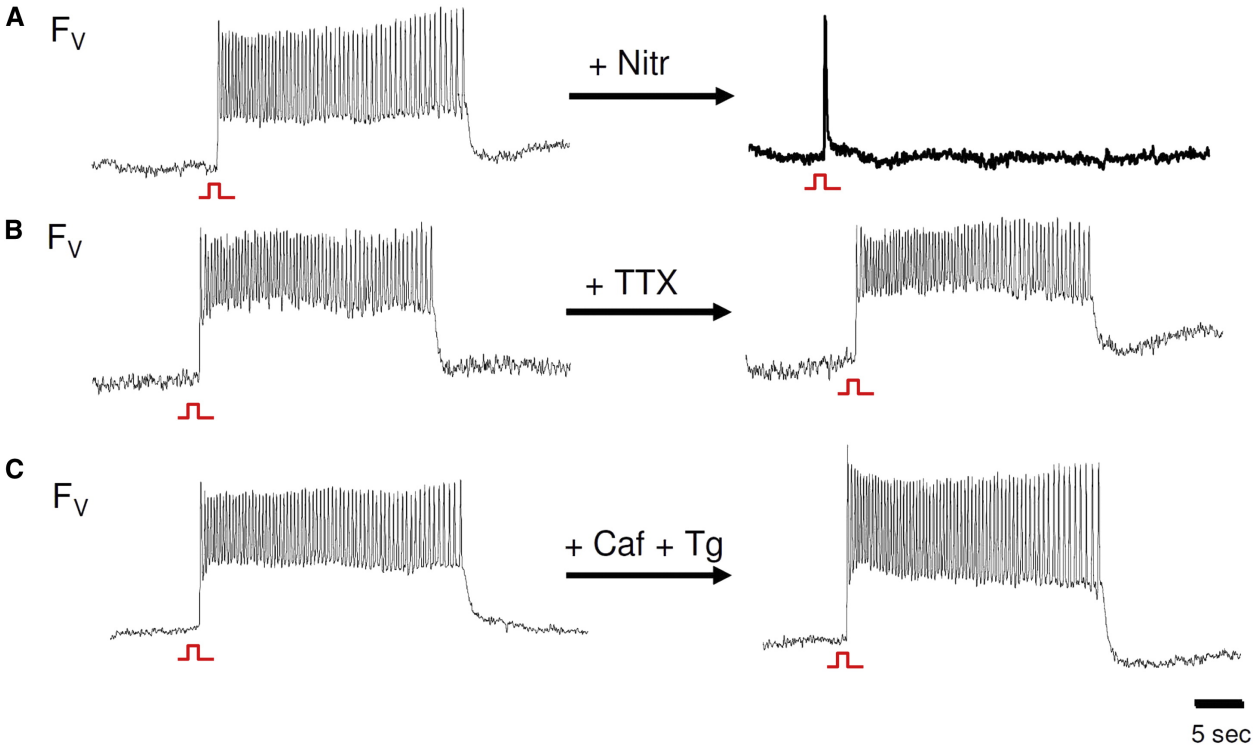

Figure 3-3. EAD bursts are abolished by Ca^{2+} channel blockade but occur independently of SR Ca^{2+} cycling and Na^{+} channel blockade. (A) Bursts were not observed following blockade of the L-type Ca^{2+} channel with 5μM nitrendipine. (B and C) Bursts continued to occur following Na^{+} channel blockade with TTX (Panel B) and disabling SR Ca^{2+} cycling with 10 mM caffeine and 5μM thapsigargin (Panel C).

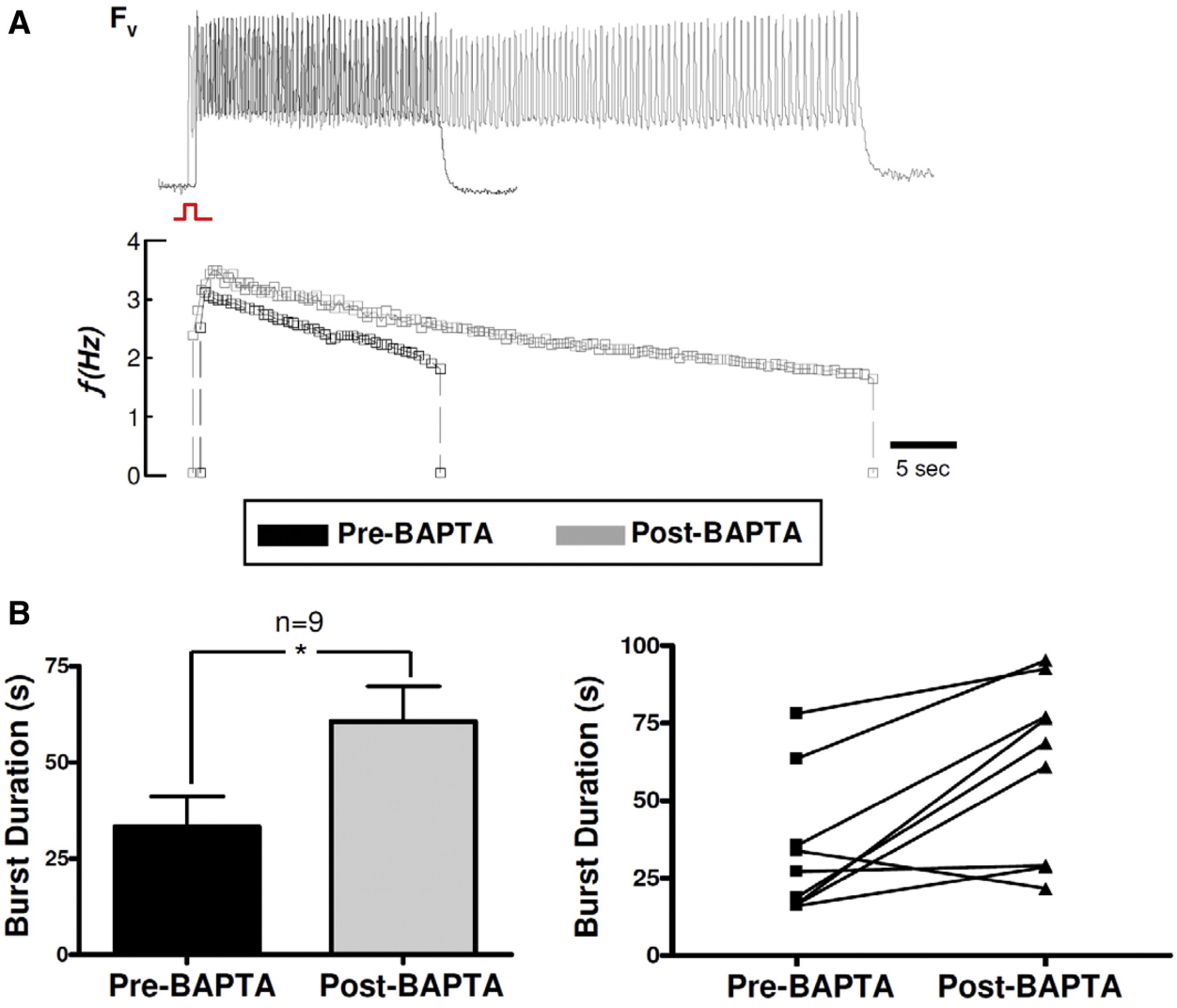

Figure 3-4. EAD bursts are prolonged following chelation of intracellular Ca^{2+}. (A) Representative bursts observed by voltage optical mapping prior to (top panel) and following incubation (bottom panel) with BAPTA-AM for 7 minutes. (B) Bar graph (left) and the corresponding individual plots of the average burst duration from n=9 monolayers (right) prior to and following incubation with BAPTA-AM (error bars represent SDs).

To evaluate whether EAD bursts were a nonspecific consequence of intracellular Ca^{2+} overload, we exposed monolayers to the Na^{+}-K^{+}-ATPase inhibitor ouabain (100 μM) in the presence of elevated extracellular Ca^{2+} (3.6 mM, n=5). In

this setting, Ca^{2+} overload results primarily from reduced Ca^{2+} efflux via Na^{+}-Ca^{2+} exchange, although Ca^{2+} entry via LTCC is also modestly potentiated by the elevated extracellular Ca^{2+}. Under these conditions, we observed runs of focal activity that increased, rather than decreased, in frequency, but no EAD bursts (Fig. 3-5).

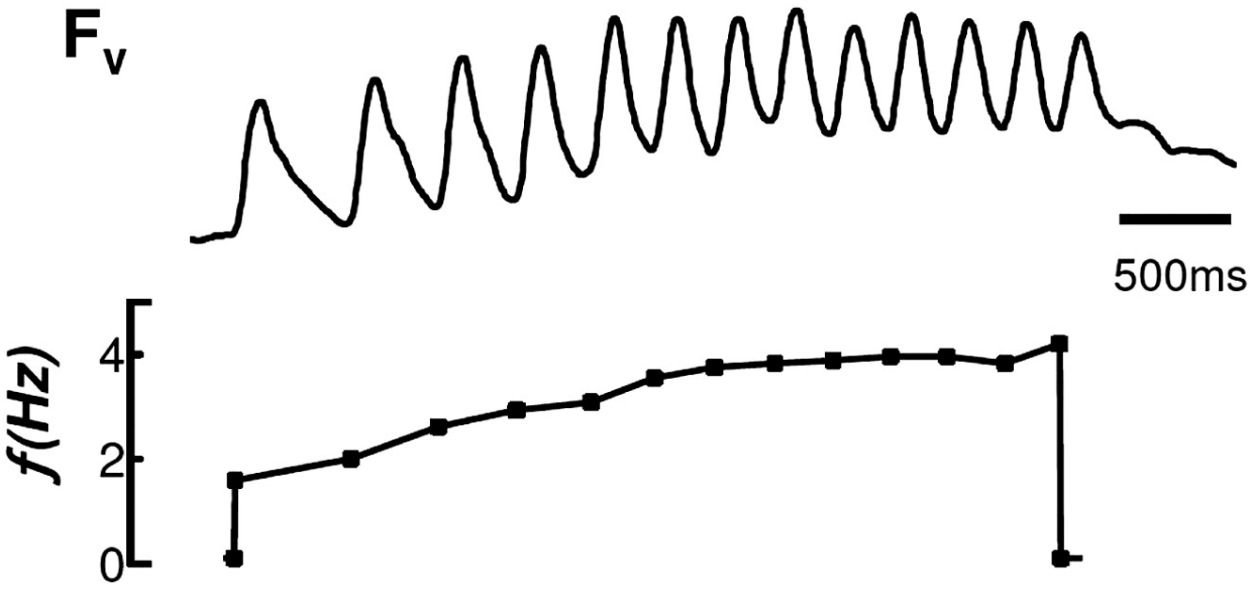

Figure 3-5. EAD Bursts depend on LTCC and not Ca^{2+} Overload Per Se. Ouabain and high Ca^{2+} (3.6mM) produced repetitive focal activity but not bursts. Frequency response plots revealed a gradual increase in bursting frequency that is inconsistent with the dual Hopf-homoclinic bifurcation mechanism. Before the drugs were administered, no spontaneous bursts were occurred.

3.4.3 Excessively decreased repolarization reserve suppresses EADs

Another prediction of the dual Hopf-homoclinic bifurcation mechanism is that EADs occur only when the balance between the reactivation kinetics of LTCC and the kinetics of repolarizing K^{+} currents fall within a critical range[1], irrespective of repolarization reserve per se. This leads to the prediction that when EADs are

present, further reduction in repolarization reserve may suppress, rather than exacerbate, EADs. To test this prediction, we examined the effects of two interventions designed to further reduce repolarization reserve in the presence of BayK8644 and isoproterenol. In the first case, we blocked the K^+ currents using 4-AP (10 mM). BayK8644 and isoproterenol-induced EAD bursts were consistently terminated by 4-AP despite the drug further prolonging AP duration (Fig. 3-6A) (n=7). This also agrees with a recent study in which H_2O_2-induced EADs in adult rabbit ventricular myocytes were suppressed by blocking I_{to} [85]. In the second case, we pre-infected monolayers with the adenoviral construct Ad-CaM_{1234} to overexpress the mutant Ca^{2+}-insensitive calmodulin CaM_{1234} [14, 80]. By displacing endogenous CaM, CaM_{1234} blocks Ca^{2+}-CaM-dependent inactivation of LTCC, thereby further reducing repolarization reserve and prolonging APD. Ad-CaM_{1234}-treated monolayers all exhibited marked AP prolongation, which increased further after exposure to BayK8644 and isoproterenol. However, no EAD bursts occurred either before or after BayK8644 and isoproterenol in 7 monolayers (Fig. 3-6B). These findings indicate that when EAD bursts were induced by BayK8644 and isoproterenol, further reduction in repolarization reserve by two different methods suppressed, rather than facilitated EAD bursts, in line with theoretical predictions.

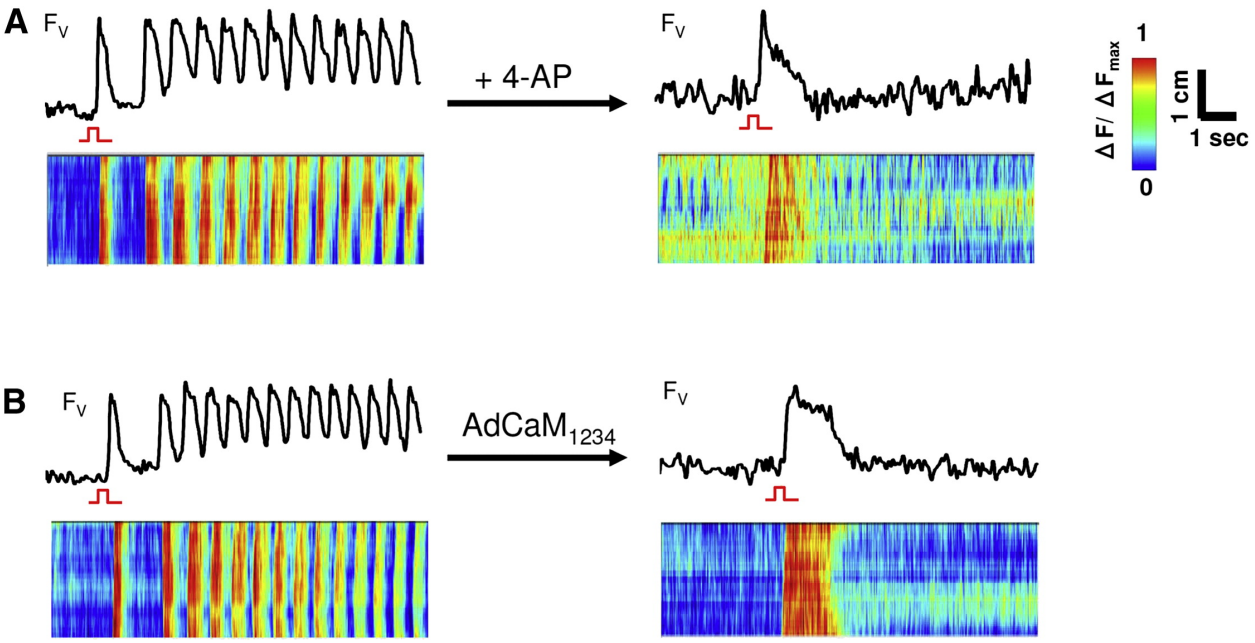

Figure 3-6. EAD bursts abolished by reducing repolarization reserve. Either blocking the K^+ currents with 4-AP (10mM) (Panel A), or overexpressing the mutant Ca-insensitive calmodulin CaM_{1234} with $AdCaM_{1234}$ (Panel B) abolished bursts (top panels). Line scans (bottom panels) show that following either 4-AP or $AdCaM_{1234}$, only focal activity due to the stimulus (orange arrow) was observed.

3.4.4 EAD bursting in a detailed action potential model

To provide insight into the ionic mechanisms underlying EAD bursting behavior, we carried out computer simulations using the UCLA rabbit ventricular AP model [86], which includes detailed Ca^{2+} cycling and ionic fluxes. The model reproduced the behavior of EAD bursts as observed in the experiments (Fig. 3-7A): 1) the frequency of voltage oscillations gradually declined prior to termination; 2) EAD bursts were unaffected by Na^+ channel blockade and by disabling of SR Ca^{2+} cycling. Bursts were also significantly prolonged in duration when intracellular Ca^{2+} was buffered (Fig. 3-7A, gray trace). The model revealed that intracellular Na^+

accumulated progressively during the EAD burst, suggesting that this parameter may play a role in burst termination. This was confirmed by clamping intracellular Na^+ in the model to 10 mmol/L (Fig. 3-7B, gray trace), which caused bursting to continue indefinitely. The mechanism by which intracellular Na^+ accumulation caused burst termination was related to stimulation of the electrogenic Na^+-K^+ pump, whose outward current eventually increased repolarization reserve sufficiently to allow full repolarization. This finding correlated with the prolongation of EAD burst duration when intracellular Ca^{2+} was buffered, which elevated the threshold value of intracellular Na^+ accumulation required to induce full repolarization (Fig. 3-7A). The dependence of the burst duration and frequency on BAPTA-AM concentration, I_{to} conductance, and LTCC conductance is shown in supplemental Fig. S3-5.

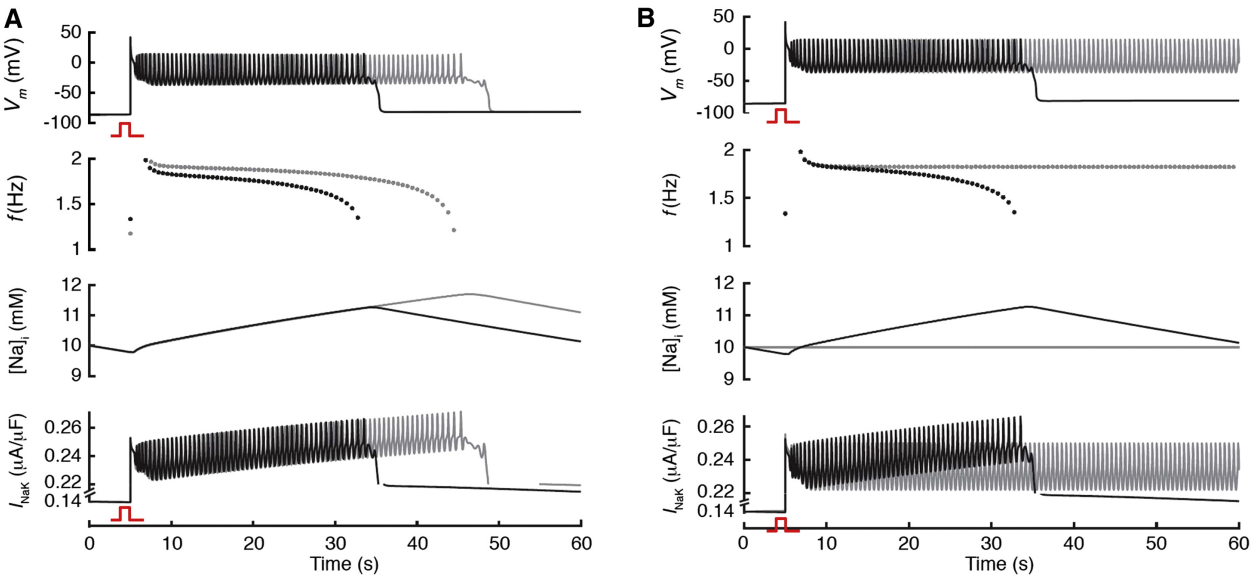

Figure 3-7. Computer simulation of EAD bursts in a detailed AP model. (A) Voltage, bursting frequency (f), Na^+ concentration, and I_{NaK} versus time for control (black traces) and when intracellular Ca^{2+} buffer was increased (grey traces). Consistent with experiments, intracellular Ca^{2+} buffering significantly prolonged burst duration and decreased the rate of frequency decline. During bursts, there is a slow rise in intracellular Na^+ that peaks with burst termination, and a gradual increase in the peak Na^+-K^+ outward current. (B) Same as A but the gray traces are when intracellular [Na^+] was clamped to 10 mM, at which bursts failed to terminate since the Na^+-K^+ current failed to accumulate as in the control.

3.5 Discussion

In this study, we provide experimental support for the previous theoretically proposed mechanism of EAD formation involving a dual Hopf-homoclinic bifurcation[1]. Specifically, we demonstrated that in NRVM monolayers exposed to BayK8644 and isoproterenol, bursts of EAD-mediated triggered activity exhibited the predicted dynamical signatures of the dual Hopf-homoclinic bifurcation mechanism. If this mechanism proves to be important in real, as well as cultured,

cardiac tissues, it may shed new light on the dynamical mechanism of how EADs arise and self-terminate, and suggest new avenues for arrhythmia treatment and risk assessment.

3.5.1 Hopf bifurcation mechanism of EAD formation

In nonlinear dynamics, a bifurcation is a change in the qualitative behavior of a system as one or more of its parameters pass a critical value (such as the change from a stable equilibrium to an oscillating behavior). Hopf bifurcation is the classic dynamical mechanism that many systems undergo when they begin to oscillate, ranging from cardiac pacemaking [87] to the fatal oscillations of the Tacoma Narrows Bridge, a wind-induced Hopf bifurcation [88].

A previous theoretical analysis using the LR1 AP model revealed that EADs were initiated by a Hopf bifurcation and terminated by a homoclinic bifurcation [1]. The Hopf bifurcation initiating the EADs requires not only a fine balance between the inward and outward currents to maintain the voltage in the LTCC "window" voltage range, but also places strict requirements on the timing and kinetics of these currents, which must be balanced in the right range to cause the voltage oscillations during the EAD.

To induce EADs in cardiac monolayers, we used BayK8644 and isoproterenol, which have complex effects on LTCC properties. In addition to increasing LTCC amplitude by promoting mode 2 gating and recruiting quiescent channels,

BayK8644 and isoproterenol also affect many other parameters, including the voltage dependence and steepness of steady state LTCC activation and inactivation curves, the kinetics of activation, inactivation and recovery from inactivation, and the late (non-inactivating) LTCC current component [89-91]. Moreover, these agents also influence other ionic currents, either directly (e.g. I_{Ks} regulation by isoproterenol) or indirectly through increasing intracellular Ca^{2+} (e.g. Na^{+}- Ca^{2+} exchange, activating Ca^{2+}-CaM kinase II, etc). Although it is difficult to pinpoint the exact role of each of these factors, the general effect is to increase the maximal value of the LTCC window current [62]. This makes more inward current available when the membrane voltage repolarizes into the LTCC "window" voltage range, which can reverse repolarization if sufficiently large. Supporting the critical and essential role of the LTCC in EAD bursts induced by BayK4688 and isoproterenol, bursts were abolished by the Ca^{2+} channel blocker nitrendipine, but not the Na^{+} channel blocker TTX, excluding an important role of Na^{+} currents (including late Na^{+} current). Also, EAD bursts still occurred when SR Ca^{2+} cycling was disabled with caffeine/thapsigargin or BAPTA-AM, thereby excluding spontaneous SR Ca^{2+} release as the cause of EADs in our experimental system. Thus, our findings provide direct experimental support for the prediction that the interaction of the LTCC with repolarizing currents is sufficient to explain EAD formation and bursting by the Hopf-homoclinic bifurcation mechanism [1], without requiring other factors such as intracellular Ca^{2+} cycling. However, this does not exclude that possibility that EADs

can also be caused by other mechanisms, such as spontaneous SR Ca^{2+} release, under different conditions or in different tissues.

A key prediction of the Hopf-homoclinic bifurcation mechanism [1] is that the repolarization speed has to be appropriate during the early repolarization phase to bring the voltage into the LTCC "window" region to facilitate the Hopf bifurcation and EAD burst. This was demonstrated in the experiments with 4-AP and CaM_{1234} shown in Fig. 3-6. Since I_{to} is a transient current that mainly occurs during the early repolarization phase of the action potential, blocking I_{to} reduces the repolarization speed in the early repolarization phase, delaying the time it takes for the voltage to enter the "window" region. Similarly, overexpression of CaM_{1234} slows the inactivation of LTCC, which also delays the time it takes for voltage to enter the "window" region. According to our previous study [85], EADs were promoted only in a certain range of I_{to} conductance, since too much I_{to} causes a too fast repolarization, which also prevents EADs. Therefore, in addition to reduced repolarization reserve in the later repolarization phase of the action potential, a proper repolarization reserve in the early repolarization phase is needed for EADs to occur.

3.5.2 Spontaneous termination of EAD bursts

Analysis of the physiologically-detailed rabbit ventricular AP model showed that the termination of EAD bursting was due to Na^+ accumulation, which gradually

increased outward Na^+-K^+ pump current until it became sufficiently large to promote full repolarization. The model reproduced the observed pharmacologic responses that buffering intracellular Ca^{2+} prolonged burst duration by shifting the homoclinic bifurcation point to occur at a higher intracellular Na^+ concentration. This is different from the previous theoretical analysis using the simpler LR1 model, in which the termination of the EADs was caused by the slow activation of the slow component of the delayed rectifier K^+ current. However, the underlying dynamical mechanism remained the same, i.e., the oscillations are terminated by the homoclinic bifurcation. Thus, in both cases, the bursting frequency gradually decreases prior to EAD termination. In addition, full activation of the delayed rectifier K^+ current only takes several seconds, while accumulation of Na^+ takes much longer, up to minutes [92], agreeing with the long duration of EAD bursts observed in our experiments. Our study demonstrates that while the specific current responsible for EAD termination may be different under different conditions, the underlying dynamical mechanisms may be still the same, which is important for a unified understanding of the EAD dynamics in different cardiac diseases.

3.5.3 Limitations and Conclusions

Important limitations of the present study include the potential off-target effects of pharmacological agents used in this study. In addition, the NRVM

monolayer preparation, despite its advantages for optical mapping, has important electrophysiological differences with human myocardium. Optical mapping also has limited spatial and temporal resolution, but permits genuine tissue level arrhythmias to be characterized and distinguished from non-propagating EADs. An important caveat is that the experimental model and computer models represented different species. On the other hand, the observation that the experimental model (NRVM) and two different mathematical models (the LR1 guinea pig ventricular model and the UCLA rabbit ventricular model representing different species and level of physiological detail) yielded consistent results increases our confidence that these findings are generally relevant to EAD-mediated arrhythmias. Whether they will ultimately prove to be clinically relevant is unclear, but the certain similarities are intriguing. For example, the optical mapping of NRVM monolayers revealed that EAD bursts originated from one or more distinct focal sites and produced a pseudo-ECG resembling polymorphic VT, which is the most common form of clinically-observed VT observed in heart failure, LQT syndromes such as Timothy syndrome (LQT8), and increased catecholamines. Finally, the dynamical understanding of EADs may suggest a new paradigm for antiarrhythmic drug development to prevent cardiac arrhythmias by targeting the kinetics, rather than the amplitudes, of ion channels such as LTCC, as determinants of EAD formation.

3.6 Supplemental Materials

3.6.1 Supplemental methods

We modified the ventricular action potential model from [86] as in [83] with the following changes:

1. Addition of two linear background currents as in [93]: I_{Ca} and I_{Na}. The respective conductances were chosen as $g_{B,Ca}$ = 0.0002513 mS/μF and $g_{B,Na}$ = 0.0004 mS/μF to give a steady state intracellular sodium concentration of $[Na]_i$ = 10 mM.
2. Addition of a nonlinear instantaneous Ca buffer to model the effect of BAPTA-AM, with K_{BAPTA} = 215 μM, activated to simulate the presence of BAPTA.
3. g_{Ca} = 770 mmol/cm/C.
4. $g_{to,f}$ = 0.08 mS/μF.
5. g_{NaK} = 0.8 mS/μF.

These parameter changes induced a long bursting behavior with a duration of the burst of about 37 seconds. Increasing the Ca buffer increases the burst duration in a linear fashion (see Fig. S3-5). The Ca current conductance has a similar effect on the burst duration. Decreasing g_{Ca} decreases the burst duration with the burst turning into a normal AP for g_{Ca} < 620 mmol/(cm C). The maximum conductance of

fast transient outward current, $g_{\mathrm{to,f}}$, has a strong influence on the burst duration. A decrease in $g_{\mathrm{to,f}}$ can increase the burst duration by a factor up to 3.

In general, an increase in the burst duration is accompanied by an increase in the bursting frequencies. The discontinuities in the traces in Fig. S3-5 can be explained by the all or nothing nature of the homoclinic bifurcation that terminates the burst; if by chance a parameter value is close to the point in which a peak is added to the burst, that peak may remain close to the "infinite period" trajectory of the bifurcation, thus lasting much longer and decreasing the frequency, while increasing the burst duration (cf. the right two panels in Fig. S3-5).

3.6.2 Supplemental figures

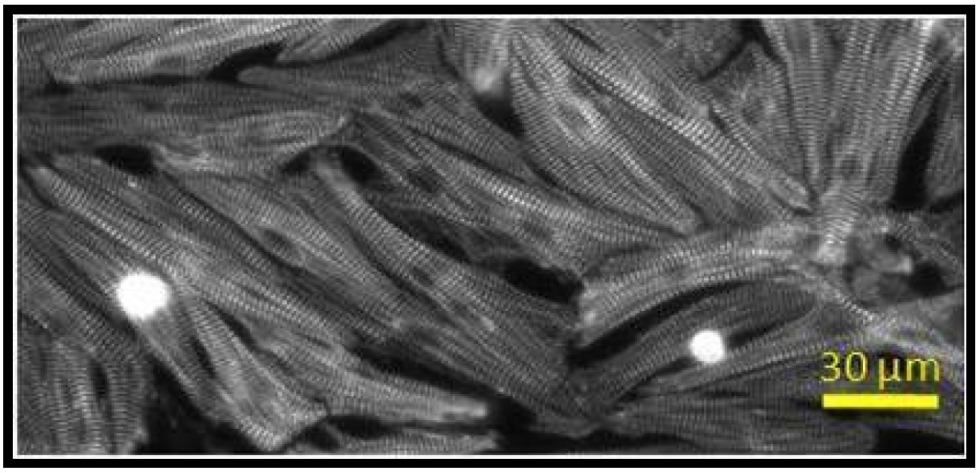

Figure S3-1. Fluorescent microscopy image of a day 11 NRVM-only monolayer stained for α-actinin. The α-actinin staining resembles that observed in adult myocytes.

Figure S3-2. Large Ca^{2+} transients are observed (via optical mapping) following stimulation during superfusion with normal Tyrode (1.8 mM Ca^{2+}) that are abolished after disabling the SR with 10 mM caffeine.

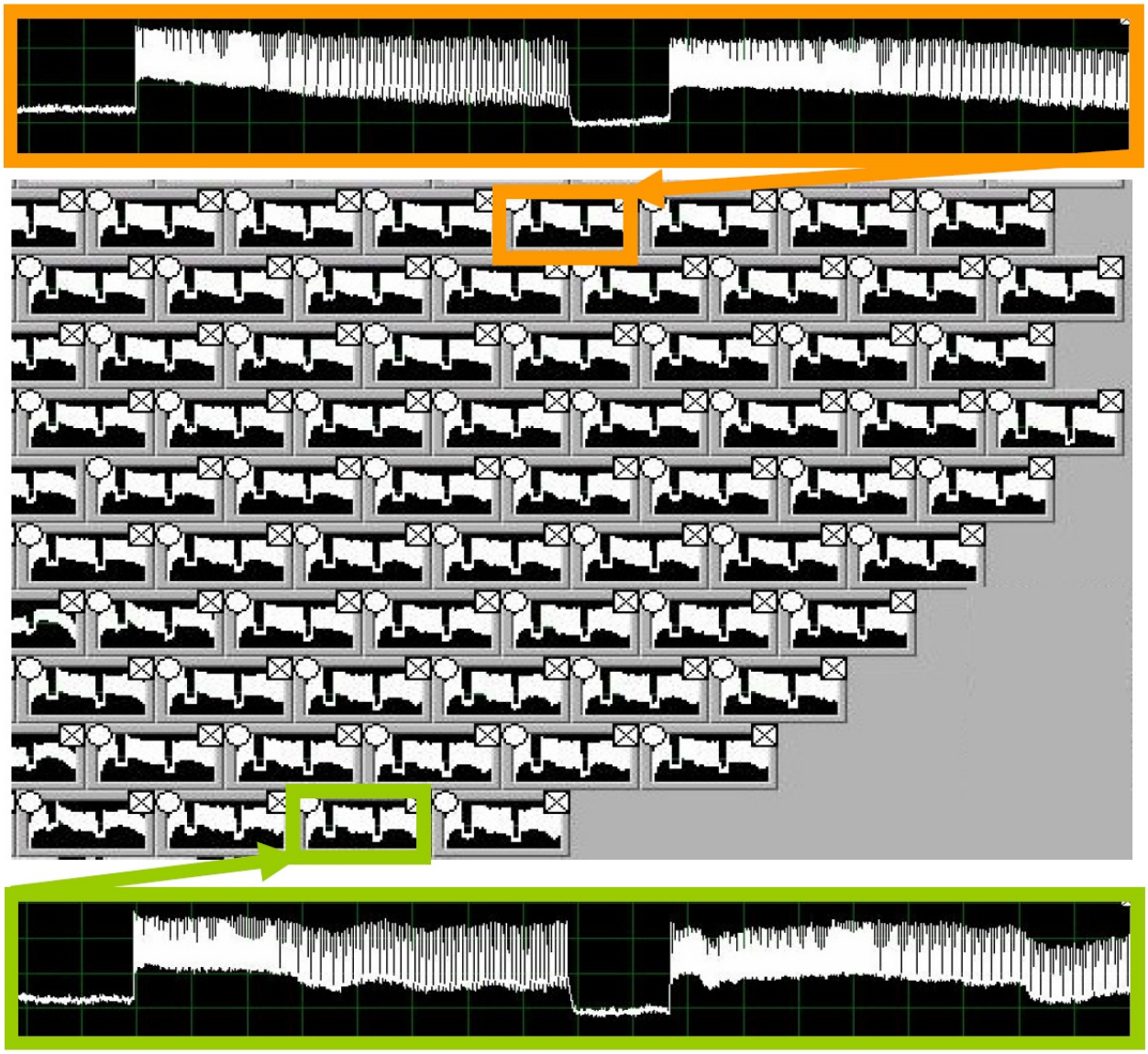

Figure S3-3. Tableau of recording channels (spaced 1 mm apart) from right lower quadrant of optical mapping photodiode array illustrating that voltage bursts occur on a macroscopic scale (>1 mm) and are synchronized.

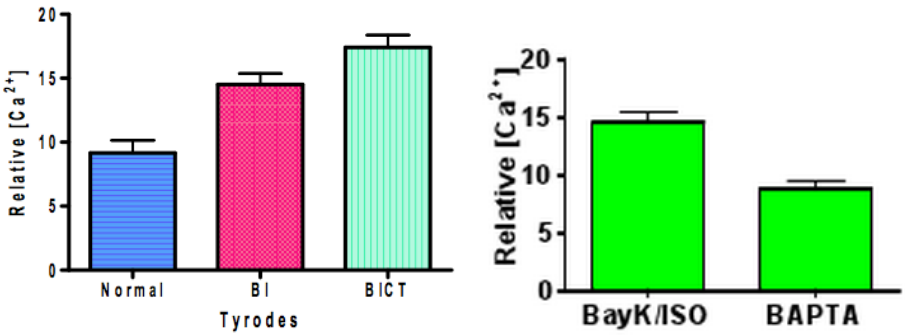

Figure S3-4. Relative intracellular Ca^{2+} concentration, ΔF, under different conditions. ΔF was obtained by computing ΔF = F - F_{min}. F_{min} was obtained by first rendering the cells Ca^{2+}-permeant with a Ca^{2+} ionophore, ionomycin (8 μM) for 6 min and then superfusing cells with Ca^{2+} free Tyrode containing EGTA (1 mM). Tyrode containing 4 mM $CaCl_2$ was then superfused for 7 min to confirm that photobleaching had not occurred and that our measurements are applicable. Lastly, the monolayer was superfused with 5 mM MnCl2 (which quenches the cytoplasmic Ca^{2+} signal) containing Tyrode solution for 7 minutes to obtain the autofluorescence intensity.

BI: BayK8644+ISO; BICT: BayK8644+ISO+Caffeine+Thapsigargin.

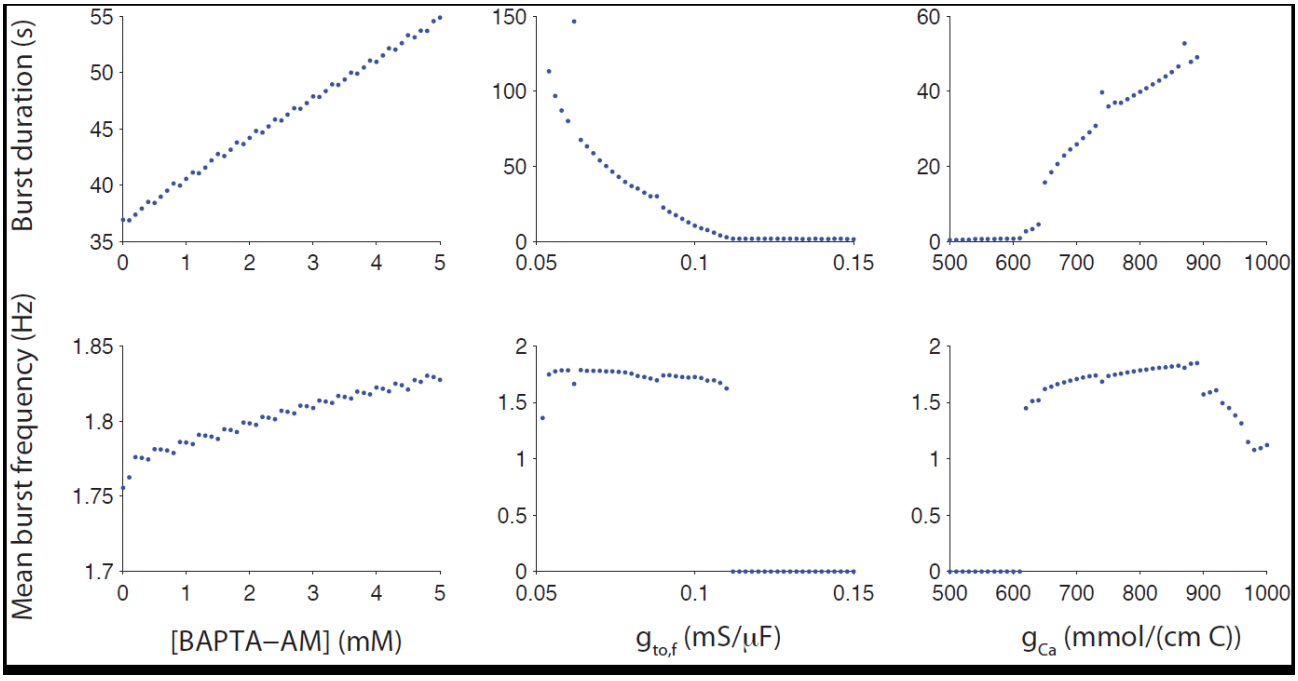

Figure S3-5. The influence of parameter values on the duration and frequency of bursting. A zero frequency means that the model exhibits a normal AP and no EADs.

4. Bistable Wave Propagation and EAD-Mediated Cardiac Arrhythmias

4.1 Abstract

BACKGROUND In normal atrial and ventricular tissue, the electrical wavefronts are mediated by the fast sodium current (I_{Na}), while in sino-atrial and atrioventricular nodal tissue, conduction is mediated by the slow L-type calcium current ($I_{Ca,L}$). However, it has not been shown whether the same tissue can exhibit both the I_{Na}-mediated and the $I_{Ca,L}$-mediated conduction.

OBJECTIVE To test the hypothesis that bistable cardiac wave conduction, mediated by I_{Na} and $I_{Ca,L}$, respectively, can occur in the same tissue under conditions promoting early afterdepolarizations (EADs), and to study how this novel wave dynamics is related to the mechanisms of EAD-mediated arrhythmias.

METHODS: Computer models of two-dimensional (2D) tissue with a physiologically-detailed action potential model were used to study the bistable wave dynamics. Theoretical predictions were tested experimentally by optical mapping in neonatal rat ventricular myocyte monolayers.

RESULTS: In the same 2D homogeneous tissue, we could induce spiral waves that are mediated by either I_{Na} or $I_{Ca,L}$ under conditions in which the action potential model exhibited EADs. This bistable wave propagation behavior was similar to bistability shown in many other nonlinear systems. Since the bistable states are also

excitable, we call this novel behavior bi-excitability. In a 2D heterogeneous tissue, the $I_{Ca,L}$-mediated spiral wave meanders, giving rise to a twisting electrocardiographic QRS axis, resembling Torsade de Pointes, while the co-existence and interplay between the I_{Na}-mediated wavefronts and $I_{Ca,L}$-mediated wavefronts give rise to polymorphic ventricular tachycardia. We also present experimental evidence for bi-excitability under EAD-promoting conditions in neonatal rat ventricular myocyte monolayers exposed to BayK8644 and isoproterenol.

CONCLUSIONS: Under EAD-prone conditions, both I_{Na}-mediated conduction and $I_{Ca,L}$-mediated conduction can occur in the same tissue. This novel wave dynamics may be responsible for certain EAD-mediated arrhythmias, such as Torsade de Pointes and polymorphic ventricular tachycardia.

4.2 Introduction

In normal ventricular and atrial tissue, the upstroke of the action potential is caused by the activation of the sodium (Na) current (I_{Na}), which mediates impulse conduction through both the atrium and the ventricles, with L-type calcium (Ca) current ($I_{Ca,L}$) playing a passive follower role. In the sinoatrial or atrioventricular nodal tissue, however, the upstroke of the action potential is caused by the activation of $I_{Ca,L}$ and thus impulse conduction is mediated by $I_{Ca,L}$. $I_{Ca,L}$-mediated conduction can also occur in ischemic ventricular muscle in which the resting potential is depolarized due to extracellular potassium (K) accumulation so that I_{Na} no longer contributes to the upstroke of the action potential [94], or when gap junction coupling is severely decreased [95, 96].

In this study, we show a novel wave propagation behavior which allows both I_{Na}-mediated conduction and $I_{Ca,L}$-mediated conduction to coexist in the same homogeneous tissue under identical conditions. In other words, in the same tissue, both I_{Na}-mediated wave and $I_{Ca,L}$-mediated waves propagate with distinct properties, and the two types of waves can switch from one to the other. This behavior is similar to a toggle switch in a typical bistable system [97], which has been demonstrated to regulate important physiological properties in many biological systems [98, 99]. Here we show that bistable wave behavior may occur in cardiac tissue when the tissue is prone to early afterdepolarizations (EADs). EADs are abnormal depolarizations in the repolarizing phase of the action potential, which

occur in many disease conditions [100-102], such as long QT syndromes (LQTS) and heart failure. EADs are thought to cause arrhythmias by promoting reentry through increasing dispersion of action potential duration (APD) and by causing premature ventricular complexes (PVCs) which induce reentry or triggered activity. It is widely accepted that EADs are associated with Torsade de Pointes (TdP) [100, 103-107], a type of polymorphic ventricular tachycardia (PVT) at rates ranging from 150 to 300 beats per minute. TdP has a distinctive electrocardiographic (ECG) appearance in which the QRS axis slowly undulates, and usually terminates spontaneously [104, 108, 109]. However, mechanisms linking EADs to TdP remain incompletely understood.

Using computer simulations of two-dimensional (2D) homogeneous tissue, we first document the presence of bistable wave behavior when EADs are present in the action potential. We then show that in a 2D heterogeneous tissue model, a meandering $I_{Ca,L}$-mediated spiral wave can give rise to the classic heart rate and ECG appearance of TdP. We also show that the dynamic interactions between $I_{Ca,L}$-mediated and I_{Na}-mediated wavefronts arising in the same tissue give rise to an ECG appearance of PVT. Finally, we present experimental evidence for bi-excitability in neonatal rat ventricular myocyte (NRVM) monolayers.

4.3 Material and Methods

Computer simulation. Computer simulations were carried out in models of isolated myocytes and 2D tissue. The voltage of the single cell is governed by an ordinary differential equation: $C_m dV/dt = -(I_{ion} + I_{sti})$, where C_m is the membrane capacitance of the myocyte, I_{ion} is the total ionic current, and I_{sti} the stimulation current. The 2D tissues were modeled using a mono-domain model with voltage described by the partial differential equation: $\partial V/\partial t = -I_{ion}/C_m + D(\partial^2 V/\partial x^2 + \partial^2 V/\partial y^2)$. The action potential models were modified from the rabbit ventricular model developed previously [86, 110], which are described in detail in the online supplemental materials. To generate large amplitude EADs that can propagate in tissue, we modified many of the parameters from the original rabbit ventricular model, such as increase in $I_{Ca,L}$ as well as I_{Ks}. Increasing in $I_{Ca,L}$ and I_{Ks} is consistent with the known effects of BayK8644 and isoproterenol. The detailed parameters are presented in the Table in the supplemental materials.

Cultured NRVM monolayers. NRVM monolayers were isolated by standard methods [111] and plated on 22-mm diameter circular cut polyvinyl chloride coverslips (PGC Scientifics, Frederick, Md). Briefly, hearts harvested from 2- to 3-day-old neonatal Sprague-Dawley rats were digested with collagenase (0.02%; Worthington Biochemical Corp, Lakewood, NJ) and pancreatin (0.06%; Sigma-Aldrich, St Louis, Mo). Myocytes were isolated with the use of a Percoll (Pharmacia

Biotech AB, Uppsala, Sweden) gradient and plated at a density of 10^6 cells/mm^3 per coverslip. Monolayers were cultured for 4 to 5 days to ensure full confluence (by phase contrast microscopy) and homogeneous electrical propagation before experimental use. Specimens were perfused with oxygenated Tyrode's solution at 37°C. NRVM monolayers were stained for optical voltage recording by immersion into oxygenated Tyrode's solution (in mmol/L: 136 NaCl, 5.4 KCl, 1.8 $CaCl_2$, 0.33 NaH_2PO_4, 1 $MgCl_2$, 10 HEPES, and 10 glucose; pH 7.3) containing the voltage dye RH-237 (5 μmol/L for 5 minutes) at room temperature [112]. We used electron-multiplying, back-illuminated, cooled charge-coupled device cameras (Photometrics Cascade 128+; 128 x 128 pixels), acquiring at 0.6 to 5 ms per frame. Signals were digitized with 16 bits of precision and processed offline as described previously [112]. Conduction velocity was obtained as described previously [112]. The use and care of the animals in these experiments were approved by the Chancellor's Animal Research Committee at the University of California, Los Angeles.

4.4 Results

4.4.1 Bistable wave conduction in a homogeneous tissue model

In normal ventricular tissue, the resting potential of a myocyte is around -80 mV. When a depolarizing stimulus rapidly elevates the voltage close to >-60 mV, the fast inward current I_{Na} is activated and depolarizes the myocyte to positive

potentials, after which I_{Na} quickly inactivates (Fig. 4-1A). Another inward current ($I_{Ca,L}$), with an activation threshold around -40 mV and slower inactivation, subsequently maintains the action potential plateau. The positive membrane voltage activates outward K currents on a still slower time scale, which then repolarize the myocyte back to the resting voltage. It is well-known that normal ventricular tissue can only support a single type of traveling wave or spiral wave, namely, conduction mediated by I_{Na} [94, 96]. If I_{Na} is blocked, $I_{Ca,L}$ is generally insufficient to support wave propagation in normal ventricular tissue unless other electrophysiological properties are also altered.

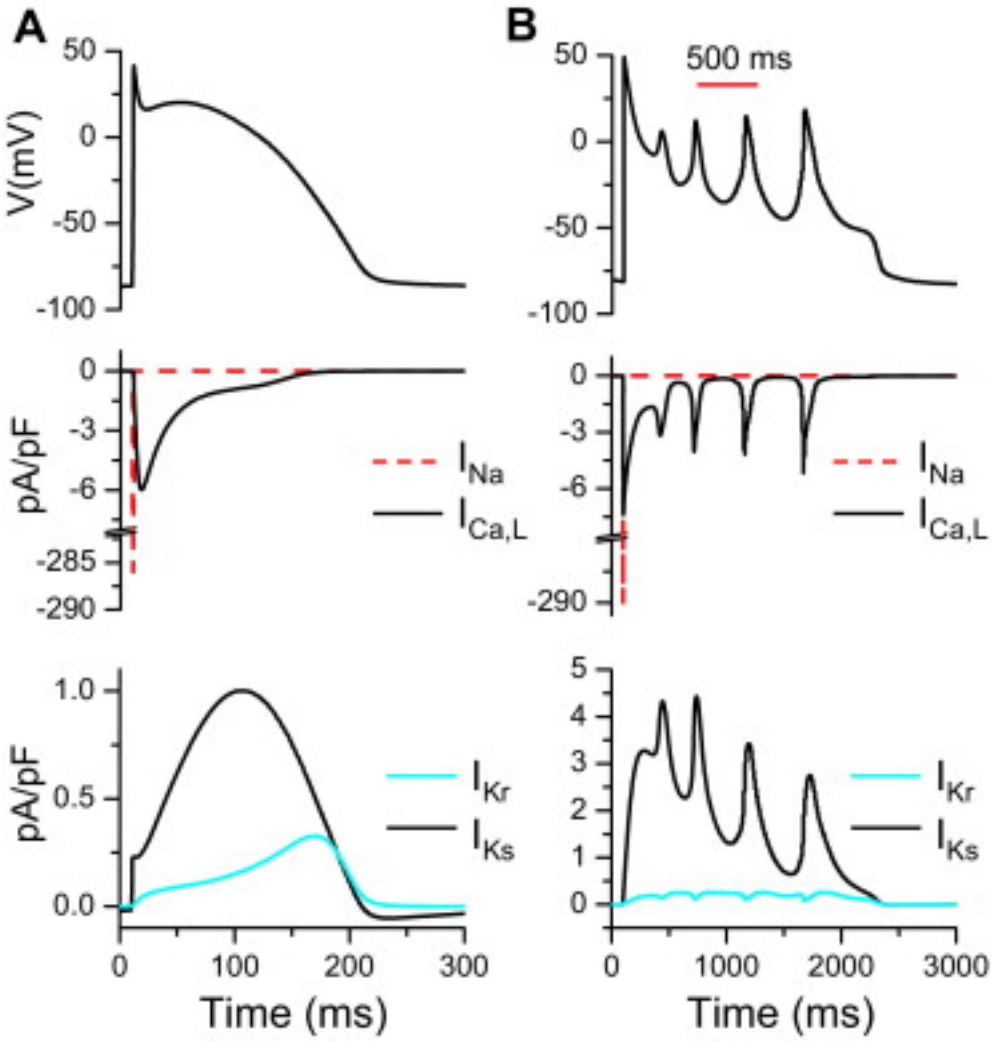

Figure 4-1. Normal and abnormal cardiac depolarizations of single-cell models. A. The voltage and major inward (I_{Na} and $I_{Ca,L}$) and outward (I_{Ks} and I_{Kr}) currents versus time in the normal action potential model [110], illustrating the depolarization and consequential activation and inactivation of different currents. The pacing cycle length is 500 ms. B. Same as A but from an action potential model generating EADs (the details of action potential model are shown in the online supplemental methods), showing that during EADs, I_{Na} maintains at zero while $I_{Ca,L}$ oscillates for depolarizations at the repolarizing phase. The pacing cycle length is 2743 ms.

Under diseased conditions [100-102], such as LQTS or heart failure, in which outward currents are reduced and/or inward currents are increased (and also have

their kinetics altered), EADs can occur during the repolarizing phases of the action potential, as shown in Fig. 4-1B. These membrane oscillations (EADs) are caused by $I_{Ca,L}$ reactivation competing with the slow component of the delayed rectifying K currents (I_{Ks}). Interestingly, when these same cells that exhibit EADs at the single cell level are coupled together to form a 2D homogeneous tissue, the tissue becomes capable of reentry mediated by either I_{Na} or $I_{Ca,L}$ depending on the initial conditions. This is unlike normal ventricular tissue or the AV node which can only support one type of propagation at a time, mediated either by I_{Na} (with $I_{Ca,L}$ following passively), or by $I_{Ca,L}$ (in absence of I_{Na}), irrespective of the initial conditions.

Figure 4-2 shows the two types of spiral waves in our simulation of a 2D homogeneous tissue composed cells modeled with the action potential shown in Fig. 4-1B. Figure 4-2A (Supplemental Movie 4-1) shows a spiral wave mediated by I_{Na}. This spiral wave was induced by a cross-field stimulation protocol in which an S1 stimulus was applied at the left edge of the tissue. When approximately half of the tissue repolarized to the resting potential, an S2 stimulus was applied at the left-lower quarter of the tissue (see Supplemental Movie 4-1), as typical for the induction of a spiral wave in a normal tissue. The cycle length of this I_{Na}-mediated spiral wave is short (<180 ms) and voltage repolarizes fully to ~-80 mV between beats. While both I_{Na} and $I_{Ca,L}$ are present in this case, the rotor and wavefront propagation is mediated by I_{Na}. Alternatively, an $I_{Ca,L}$-mediated spiral wave (Figure 4-2B and Supplemental Movie 4-2) can be induced in the same tissue. The cycle

length of this spiral wave is much longer (~560 ms) and voltage only repolarizes partially to a voltage between -50 mV and -40 mV between beats. Since the voltage remains above -50 mV in this case, I_{Na} remains fully inactivated and only $I_{Ca,L}$ is present to mediate the wave propagation. It should be noted that the induction of the $I_{Ca,L}$-mediated spiral wave in a homogeneous tissue is not as straightforward as the intiation of an I_{Na}-mediated spiral wave. Using the cross-field stimulation protocol, the spiral wave in Fig. 4-2B could only be induced after certain S1 beats, using a more premature and weaker S2 stimulus. The action potential in the S1 beat is long, and the S2 must be applied before the action potential repolarizes full and weak enough to avoid causing full repolarization (see Fig. 4-4). In contrast to homogeneous tissue, however, $I_{Ca,L}$-mediated reentry can be easily induced in heterogeneous tissue by the EADs with a single S1 stimulus (see Supplemental Fig. S4-1).

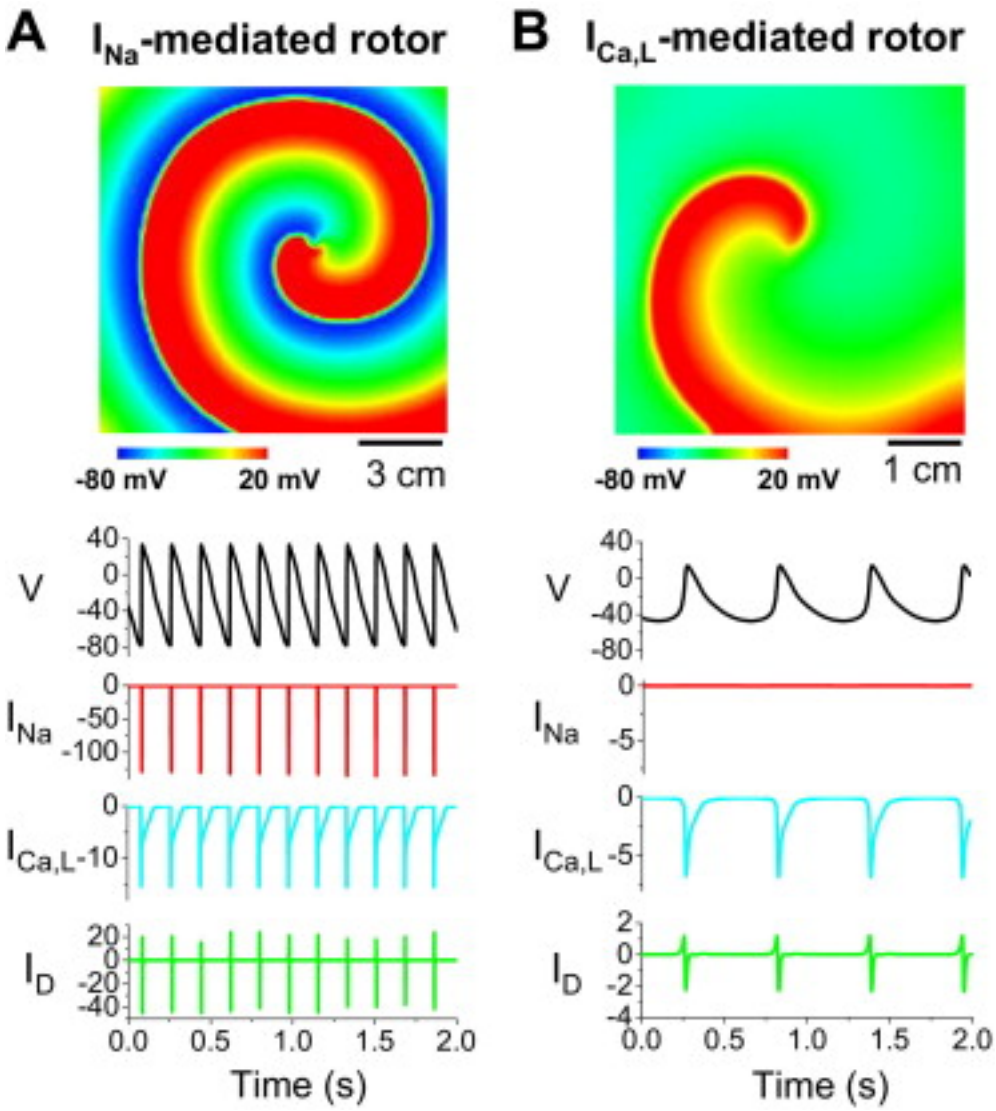

Figure 4-2. Bistable spiral waves in a homogeneous tissue model. A. An I_{Na}-mediated spiral wave in a homogeneous 2D tissue induced by cross-field stimulations (left), with traces of voltage, I_{Na}, and $I_{Ca,L}$ versus time at a representative location (right). B. An $I_{Ca,L}$-mediated spiral wave (left) induced by a different cross-field stimulation pattern in the same tissue, with traces of voltage, I_{Na}, and $I_{Ca,L}$ versus time from the same site as in A (right).

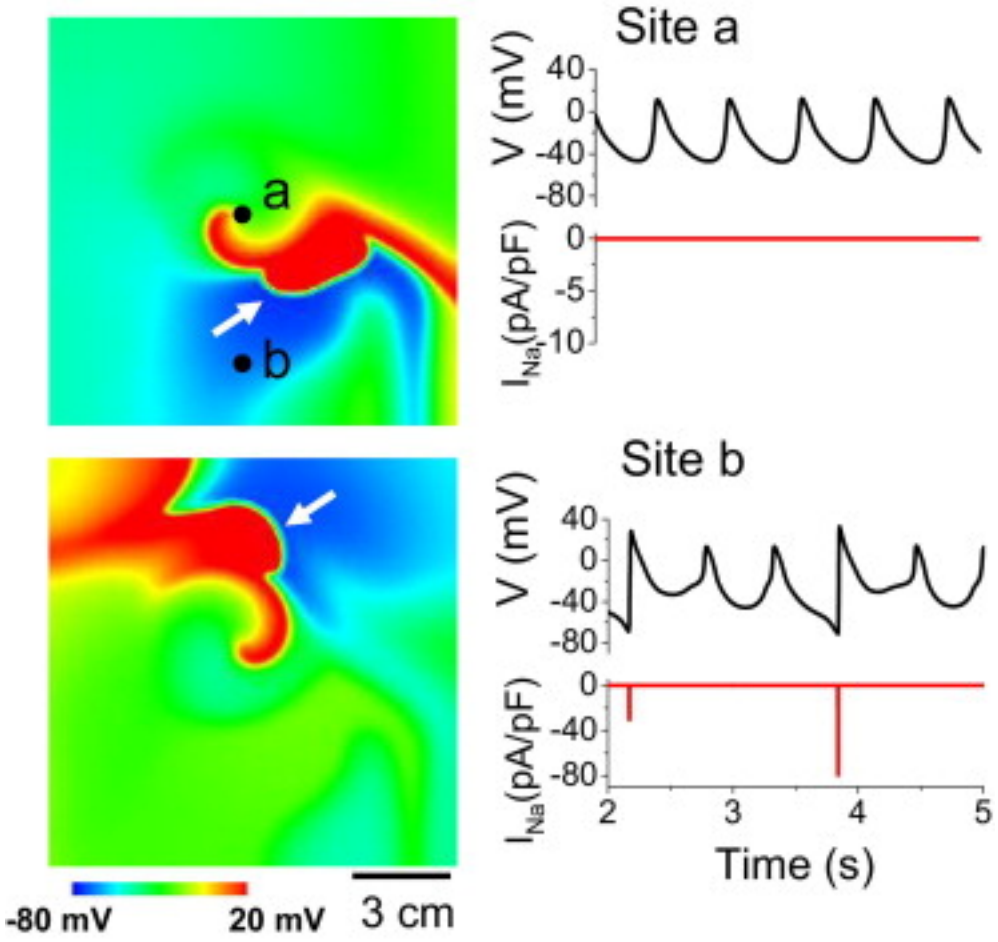

Figure 4-3. Co-existence of I_{Na}-mediated and $I_{Ca,L}$-mediated conductions. Voltage snapshots (left), and traces of voltage and I_{Na} versus time at two locations (right) during the spiral wave. Note intermittent full repolarization at site b, but not site a. Arrows indicate wavefronts mediated by I_{Na}. The action potential model was modified from that of Fig.2 by altering the Ca-activated nonselective cation current ($I_{ns(Ca)}$) (see supplemental materials).

Note that the two types of spiral waves occur in the *identical* homogeneous tissue, depending only on the different initial conditions (i.e. the specific stimulation protocol), unrelated to the tissue substrate itself. The property that the two stable steady states exist under the same parameter conditions of the tissue substrate is a well-known phenomenon called "bistability" in nonlinear dynamics [97], and has

been demonstrated in many biological systems [98, 99]. Since the bistable states in our model are also excitable states, we call this property *bi-excitability*.

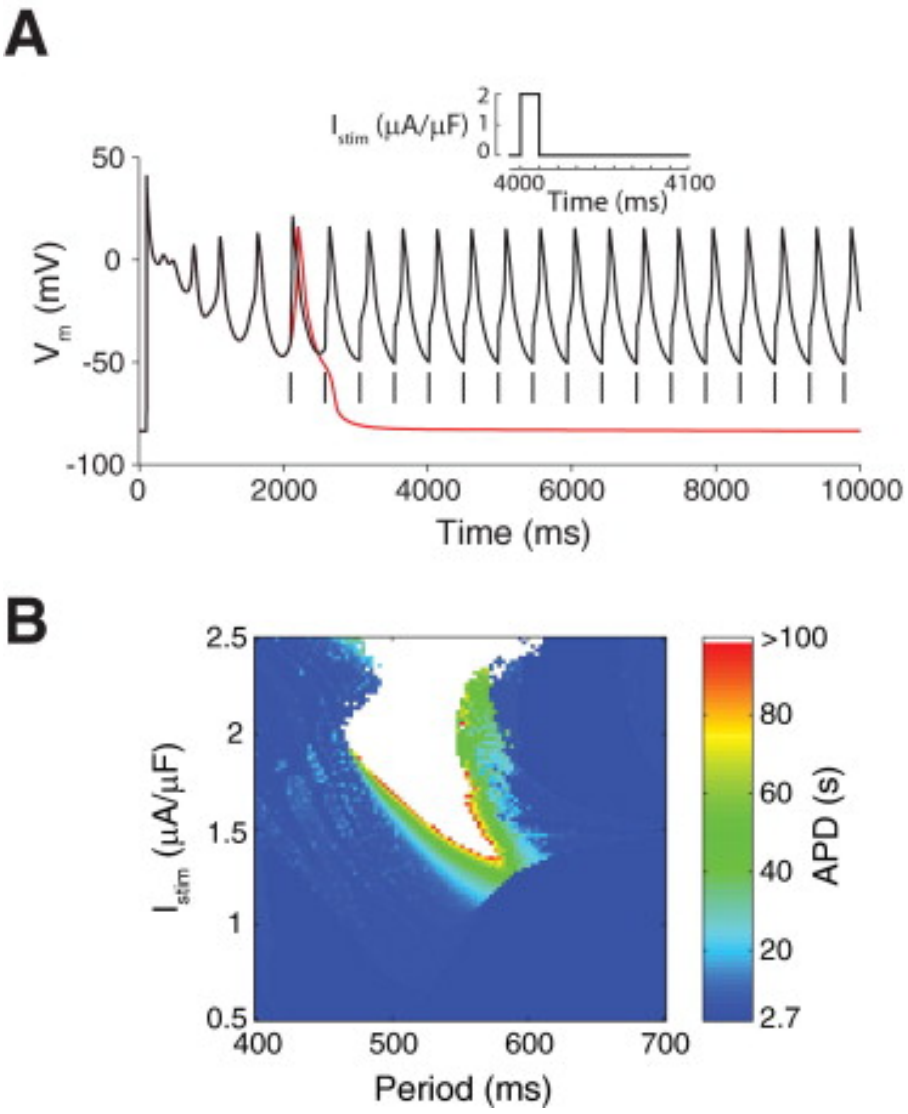

Figure 4-4. Prevention of full repolarization in a single cell by periodic simulation. A. Voltage versus time for periodic pacing (PCL=500 ms) with a weak stimulus (2 μA and 10 ms, as shown in the inset), the first beat was applied before full repolarization. For comparison, the red line is the voltage trace without the periodic pacing and black line the one with periodic pacing (pacing is marked by the short vertical lines). B. APD distribution (color scale) versus stimulation strength (y-axis) and pacing period (x-axis). White region is the region where the action potential does not recover to the resting potential during the 100 s simulation period.

4.4.2 Co-existence of I_{Na}-mediated and $I_{Ca,L}$-mediated conduction in the same homogeneous tissue

Bistable systems are able to toggle between one state and another in a switch-like manner, but generally do not exhibit both states at the same time. In our system, a mixture of the two types of conduction can co-exist in the same homogenous tissue if the refractoriness or the repolarization reserve of the cell is altered. Figure 4-3 (and Supplemental Movie 4-3) shows an example in which the central core region of the spiral wave is driven by $I_{Ca,L}$-mediated rotor (in which I_{Na} is inactivated). However, along the arm of the spiral wave, fast I_{Na}-mediated wavefronts (indicated by arrows) occur concomittently with slow $I_{Ca,L}$-mediated wavefronts.

4.4.3 TdP and PVT due to $I_{Ca,L}$-mediated and I_{Na}-mediated conductions in a heterogeneous tissue model

The $I_{Ca,L}$-mediated spiral wave shown in Fig. 4-2 was a stable spiral wave and thus periodic, which gave rise to monomorphic ventricular tachycardia on the simulated ECG. However, cardiac tissue is heterogeneous, exhibiting transmural K current and Ca transient gradients [113, 114]. Here we model heterogeneity by linearly increasing I_{Ks} from the center of the tissue to the tissue border (see Fig. 4-5 legend). In this heterogeneous tissue (Fig. 4-5A), the $I_{Ca,L}$-mediated spiral wave was

unstable and its core meandered, giving rise to the classic ECG appearance of TdP. While meandering I_{Na}-mediated spiral waves have been previously proposed as a mechanism of TdP [115], their frequency (5-15 Hz) is typically much faster than that of TdP (2-5 Hz). Since the frequency of a meandering $I_{Ca,L}$-mediated spiral wave is much slower, they may represent a better candidate for TdP.

In patients with LQTS [109], the classic TdP pattern is often observed in some surface ECG leads, and PVT in other leads. To explore the relationship of these different ECG patterns to bi-excitability, we simulated a larger heterogeneous tissue in which the outer region had greater repolarization reserve (achieved by increasing the conductance of I_{Ks}), as seen in the outer M-cell region of the heart. In this larger tissue, an $I_{Ca,L}$-mediated spiral wave formed in the central region while the outer region exhibited both $I_{Ca,L}$-mediated and I_{Na}-mediated wavefronts at varying locations at different times (Fig. 4-5B and Supplemental Movie 4-4). In this case, the position of the ECG electrode (Fig. 4-5C) relative to the $I_{Ca,L}$-mediated spiral wave determined whether a TdP-like or PVT-like ECG was observed. If the electrode was close to the central $I_{Ca,L}$-mediated spiral wave, TdP was recorded, but if the electrode was positioned either higher above the tissue, or in the periphery away from the central region, a PVT-like ECG was recorded due to the shifting contributions of the $I_{Ca,L}$-mediated and I_{Na}-mediated wavefronts. These results provide a novel explanation for the genesis of TdP on some ECG leads via a meandering $I_{Ca,L}$-

mediated spiral wave, and PVT on other ECG leads via the irregular appearance of the $I_{Ca,L}$-mediated and I_{Na}-mediated spiral wave wavefront in the surrounding tissue.

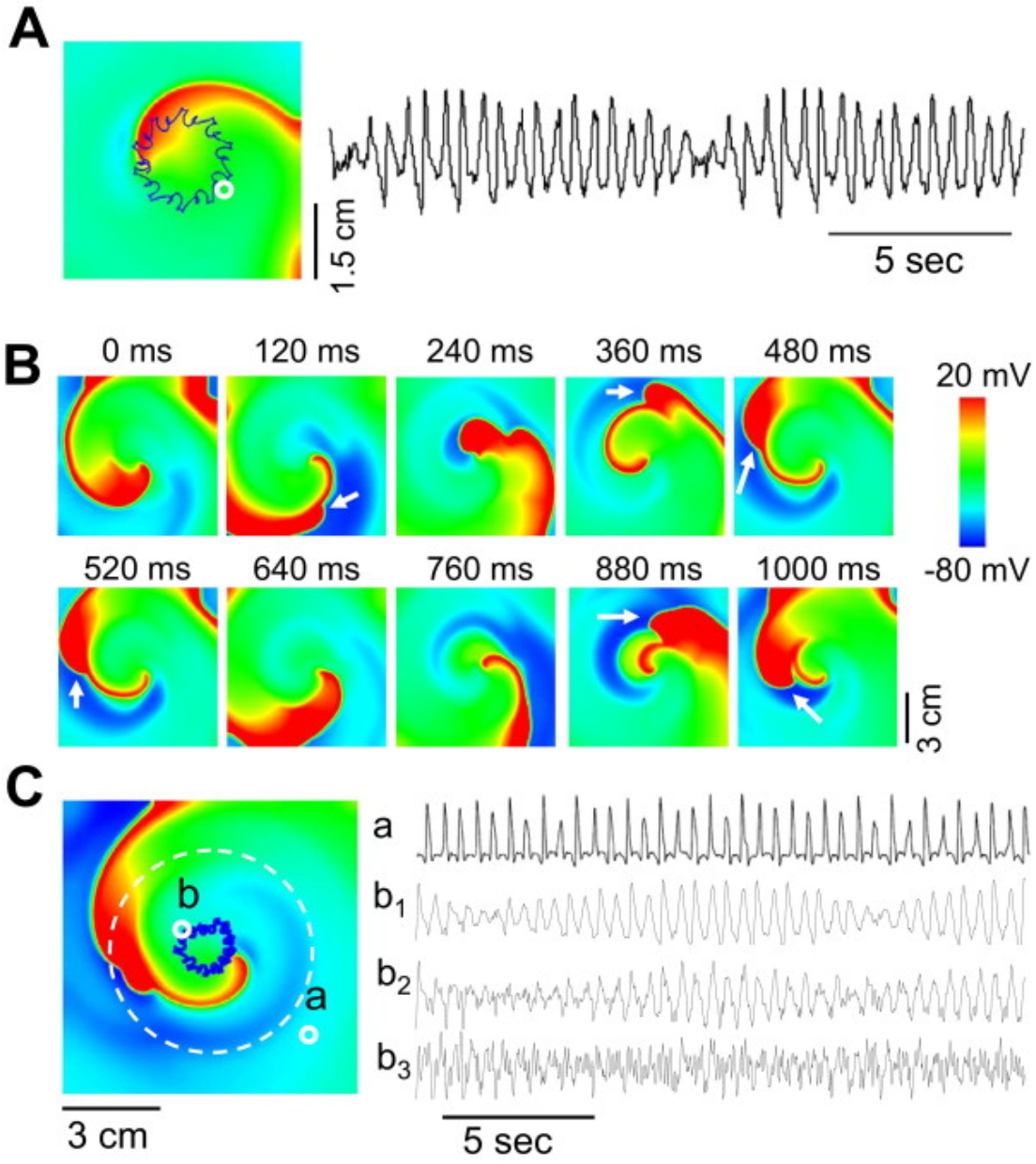

Figure 4-5. Bi-excitability causing TdP and PVT in heterogeneous tissue model. A. Left: Voltage snapshot showing a meandering $I_{Ca,L}$-mediated spiral wave (the spiral tip is shown by the blue trace) in a 4.5 x 4.5 cm heterogeneous tissue. Right: Pseudo-ECG showing a classic TdP pattern. The location of ECG electrode is

marked by white circle and is 1.8 cm above the tissue. B. Voltage snapshots in a larger 9 x 9 cm heterogeneous tissue showing an $I_{Ca,L}$-mediated spiral wave in the center, with co-existing I_{Na}-mediated fast wavefronts (white arrows) and $I_{Ca,L}$-mediated slow wavefronts in the outlying regions. C. Pseudo-ECG from electrodes at different locations and heights above the tissue. The white circles labeled as "a" and "b" in the left panel mark the locations in the x-y plane. The distances of "a" and "b1" are 0.9 cm above the tissue, "b2" is 1.8 cm above the tissue; and "b3" is 4.5 cm above the tissue. The action potential model is the same as in Fig.2 except that the maximum conductance of I_{Ks} was 0.5 times the value of Fig.2 in the tissue center and increased linearly from 0.5 to 2 times at the radius of 3 cm (dashed circle) and then was kept at 2 times in the outer region. The same action potential model and heterogeneity were used in A.

4.4.4 Experimental evidence of bi-excitability

To seek evidence of bi-excitability in real cardiac tissue, we carried out optical mapping studies in cultured NRVM monolayers. To facilitate the initiation of reentry, we placed an obstacle in the center of the monolayer (Figs. 4-6 A and B). Stable reentry (frequency ~5 Hz) was induced by a burst of rapid pacing during superfusion with normal Tyrode's condition. BayK8644 and isoproterenol were then added to the superfusate, and the reentry continued without a significant change in rotation period (Fig. 4-6A and Supplemental Movie 4-5). To perturb the system, a second burst of rapid pacing was then applied, which converted the original reentry into a new type of reentry (Fig. 4-6B and Supplemental Movie 4-6) with a much slower frequency (~2 Hz). This new type of reentry was insensitive to the Na channel blocker TTX, but was eliminated by the L-type Ca channel blocker nitrendipine (See Online Fig. S4-2). Since the new type of reentry was induced by pacing alone, without changing the intrinsic electrophysiological properties of the

monolayer (e.g. by adding a new drug), this behavior demonstrates that the same tissue can exhibit two distinct types of reentrant waves for different initial conditions (pre- and post the second episode of rapid burst pacing), as predicted by the computer simulations in Fig. 4-2. As in the computer simulations, we found that inducing both types of waves in the same tissue is nontrivial, and obtained only 3 episodes of such bi-stable waves out of 54 monolayers. However, when the BayK8644 and isoproterenol concentrations were increased, we could easily induce nitrendipine-sensitive reentry without I_{Na}-mediated reentry in the same monolayers, with the frequencies of rotation ranging from 1.5 Hz to 3 Hz in different monolayers. Presumably, the higher BayK8644 and isoproterenol concentrations impeded full repolarization to the resting potential under these conditions, preventing I_{Na}-mediated wavefronts formation.

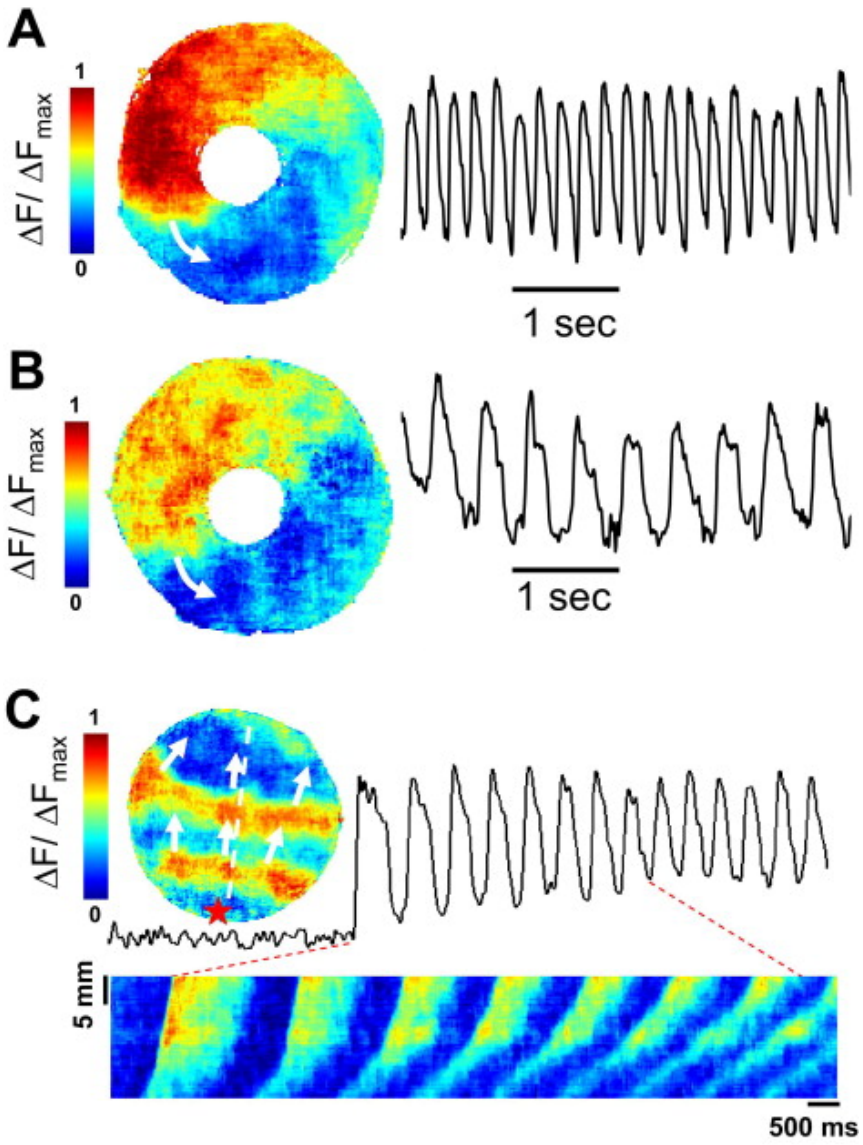

Figure 4-6. Bi-excitable wave propagation in experiments of NRVM monolayers superfused with BayK8644 and isoproterenol. A. Snapshot of reentry (left) around a central obstacle and a local trace of optical voltage (right) in a monolayer, in the presence of BayK8644 (5 nM) and isoproterenol (100 nM). B. Same monolayer, after rapid burst pacing induced a slower reentry. C. Voltage snapshot (left) and optical voltage trace (right) from a confluent monolayer after BayK8644 (50 nM) and isoproterenol (1 mM) showing focal excitations. A spontaneous action potential is followed by an EAD-mediated burst, which never fully repolarizes between beats. A line scan (along the white dashed line in the voltage snapshot above) of the first eight beats is shown below, illustrating the progressive slowing of conduction, due to a shift from I_{Na}- to $I_{Ca,L}$-mediated propagation.

In another NRVM monolayer, we observed $I_{Ca,L}$-mediated propagation arising from bursts of EAD-mediated focal activity that failed completely repolarize between beats (Fig. 4-6C and Supplemental Movie 4-7) following application of BayK8644 and isoproterenol. Note that the conduction velocity of the first wave, arising from fully repolarized tissue during the initial upstroke, was 30 cm/s, but progressively slowed to 4 cm/s during the subsequent waves mediated by $I_{Ca,L}$ during the EAD upstrokes, as seen in the space-time plot. This is consistent with a transition from I_{Na}-mediated propagation to $I_{Ca,L}$-mediated propagation, due to the progressive incomplete repolarization during successive beats during EAD bursts, as evident in the optical trace above.

4.5 Discussion and conclusions

Bistability is a widely-known behavior in nonlinear dynamics [97], and has been demonstrated in many biological systems [98, 99]. In this study, we show a novel bistable behavior of an excitable medium, in which cardiac tissue prone to EADs becomes capable of exhibiting two types of wave propagation with distinct conduction velocities and rotation frequencies, mediated either by I_{Na} or by $I_{Ca,L}$, respectively. The two types of waves can switch or co-exist simultaneously, even in completely homogeneous tissue. We also provided experimental evidence of bi-excitability in cultured NRVM monolayers exposed to BayK8644 and isoproterenol.

In the computer model, the $I_{Ca,L}$-mediated spiral wave is stable in homogeneous tissue, but in heterogeneous tissue, the $I_{Ca,L}$-mediated spiral wave meanders, which gives rise to both the heart rate and appearance of TdP on some ECG leads, while the interaction between the I_{Na}-mediated and $I_{Ca,L}$-mediated propagating wavefronts in the outer arm of the $I_{Ca,L}$-mediated spiral wave produce an appearance of PVT on other ECG leads.

4.5.1 EADs and bi-excitability

It is known that cardiac conduction can be mediated by either I_{Na} or $I_{Ca,L}$, depending on the characteristics of the tissue substrate. In general, to support I_{Na}-mediated conduction, cardiac tissue needs to have a resting potential more negative than -60 mV (as seen in normal atrial and ventricular myocardium). Conversely, to support $I_{Ca,L}$-mediated propagation, cardiac tissue requires a resting potential more depolarized than -60 mV, such as during ischemia or in the sinoatrial or atrioventricular nodes where the resting membrane potential is significantly elevated, and $I_{Ca,L}$ is solely responsible for the upstroke of the action potential. It is also important to note that $I_{Ca,L}$-mediated propagation may serve as the sole source of propagation in substrates with reduced gap junction coupling (such as the healed infarct border zone [95]) despite any change in the resting membrane potential. Thus, normal tissue can only support one type of propagation at a time, and that

changing from I_{Na}-mediated wave to $I_{Ca,L}$-mediated wave propagation requires changing the cellular or tissue properties.

The novel behavior identified in the present study, however, shows that when EADs are present, the same homogeneous tissue becomes capable of supporting both I_{Na}-mediated and $I_{Ca,L}$-mediated waves. The switching from one wave type to the other does not require a change in cellular or tissue properties. This is a typical bistable behavior [98, 99], and since the two states are also excitable, we call this behavior bi-excitability. Note that the conditions for bi-excitability to occur is not simply that the action potential exhibits EADs, but that the take-off potential of EADs be low enough and their amplitude large enough (as seen in Fig. 4-1B) to facilitate the propagation of EADs in tissue. If the takeoff potential of the EADs is too high and the amplitude too small (such as in the case of phase-2 EADs shown in many previous studies [86, 102, 116, 117]), the EAD is unable to propagate and the tissue is unable to exhibit bi-excitability. The take-off potential of EADs is multifactorial, and involves a complex interaction between amplitude and kinetics of $I_{Ca,L}$ properties and repolarizing currents such as I_{Ks}. Thus, $I_{Ca,L}$-mediated reentry in our model can be prevented if I_{Ks} is either too large (promoting full repolarization) or too small (such that the EAD take-off potential is too high to support propagation in tissue), relative to $I_{Ca,L}$.

4.5.2 Bi-excitability and cardiac arrhythmias

In this study, we show that a meandering $I_{Ca,L}$-mediated rotor is responsible for the appearance of TdP in some ECG leads. In addition, the rate of TdP, which typically ranges from 150 to 300 beats per minute (or 2.5 Hz to 5 Hz) in clinical settings [104, 109], is much more consistent with a meandering $I_{Ca,L}$-mediated spiral wave than an I_{Na}-mediated spiral wave. Our simulations of $I_{Ca,L}$-mediated spiral waves in Fig. 4-2B and Fig. 4-5 exhibit a frequency of 120 beats per minute (2 Hz), which is close to the lower end of the clinically observed rate of TdP. By enhancing $I_{Ca,L}$-mediated excitability in our model, the rate can be matched to the upper end as well. In contrast, the heart rate of I_{Na}-mediated reentry shown in Fig. 4-2A is 330 beats per minute (5.5 Hz), which is also consistent with I_{Na}-mediated reentry in human whole heart simulations [118], and other computational and experimental studies that show both I_{Na}-mediated reentry and VF (under conditions of normal excitability) occurring at frequencies ranging from 5 to 20 Hz [119-121]. However, the frequency of the $I_{Ca,L}$-mediated reentry strongly depends on the upstroke velocity (or the takeoff potential) of the EAD, which could be much faster than what we show in the present model if the $I_{Ca,L}$-mediated excitability is enhanced to exhibit very large amplitude EADs.

In addition to providing a novel explanation for the characteristic undulating QRS morphology observed on ECG that is consistent with its relatively slow rate (150-300 bpm) during episodes of TdP, bi-excitability may also explain the clinically

observed phenomenon of spontaneous termination of TdP and degeneration to VF. Most episodes of TdP terminate spontaneously, and only a small portion degenerates to VF to cause sudden cardiac death [104, 108, 109]. One possibility is that during TdP, hypotension-induced ischemia leads to opening the of ATP-sensitive K channels, which increases repolarization reserve, thereby suppressing the excitability of the $I_{Ca,L}$-mediated excitable state. This could lead to termination of the $I_{Ca,L}$-mediated spiral wave (or an $I_{Ca,L}$-mediated focus as shown in Fig. 4-6C), and thus the termination of TdP, or degeneration to VF if the repolarization pattern were sufficiently heterogeneous to initiate I_{Na}-mediated spiral waves.

4.5.3 Limitations

Although we believe that the general mechanisms outlined in this study can provide useful insight into the mechanisms of TdP and EAD-related arrhythmias in long QT syndrome and other diseased conditions, such as heart failure, further theoretical and experimental studies will be required to establish their physiological relevance. A condition required for bi-excitability to occur is EAD propagation, and to generate propagating EADs, a Ca-activated non-selective cation current ($I_{ns(Ca)}$) was added to the action potential model [86]. Although this current has been identified in different species [122, 123], its existence is controversial and its physiological or pathophysiological roles remain unclear. Nevertheless, EADs have been shown to be able to propagate in cardiac tissue [107], and large magnitude

EADs have been observed [124], therefore, no matter which ionic mechanism is responsible for EAD propagation, our observation of bi-excitability may still occur in cardiac tissue as long as the EADs can propagate.

4.6 Supplemental Material

4.6.1 Supplemental Methods

Single cell model. Voltage of single myocytes is described by the following differential equation:

$$dV/dt = (-I_{ion} + I_{sti})/C_m \qquad (1)$$

where V is the membrane voltage and $C_m = 1\ \mu F/cm^2$. I_{ion} is the total membrane ionic current, which is described below. I_{sti} is the stimulation current which was a 1 ms duration pulse of strength 40 μA/cm^2. Eq.1 was numerically solved using the Euler method with an adaptive time step varying from 0.01 ms to 0.1 ms.

2D tissue model. The partial differential equation to describe the membrane voltage V in the homogeneous 2D tissue is

$$\frac{\partial V}{\partial t} = -I_{ion}/C_m + D\left(\frac{\partial^2 V}{\partial x^2} + \frac{\partial^2 V}{\partial y^2}\right) \qquad (2)$$

No-flux boundary conditions were used. D=0.0005 cm^2/ms. Δx=Δy =0.15 mm. Eq.2 was numerically solved using the Euler method with an adaptive time step varying from 0.01 ms to 0.1 ms.

Calculation of Pseudo-ECG. Pseudo-ECG was calculated using the following equation [119, 125]:

$$\Phi_e(x', y', z') = D\iint_A (\nabla V)(\nabla(1/R))dxdy \qquad (3)$$

where $R = \sqrt{(x-x')^2 + (y-y')^2 + (z-z')^2}$, (x',y',z') is the location of the electrode and (x,y,z) is the location of electrical source in the tissue, and A is the total area of the tissue.

Initial conditions for tissue simulations. Due to Na^+ and Ca^{2+} equilibration, many pacing beats are required for the model to reach a stationary state at a specific pacing cycle length. To save computation time, especially for 2D tissue, we paced a single cell into its stationary state and used the values of the variables as initial conditions for all cells in the tissue.

Numerical and simulation methods. Partial differential equations were numerically solved using the operator splitting method [126] with a time step varying from 0.01 ms to 0.1 ms. Simulations of isolated myocytes, and 2D tissue were carried out on single processor computers. Simulations were carried out on a 32-node high performance computing cluster or using graphic processing units [127]. Each node has two dual-core AMD Opteron 2.0 GHz CPUs and 4GB RAM. The code was parallelized using the Message-Passing Interface (MPI) or OpenMP. All computer programs were coded in C++.

Action potential model. We modified the action potential model originally developed by our group [110] to obtain the desired AP properties. We were not able

to induce EADs in the original model simply by increasing the inward currents [by increasing the maximum conductance of the L-type Ca^{2+} current (I_{Ca}) or the Na^{+}-Ca^{2+} exchange current] or decreasing the outward K^{+} currents. To induce EADs, we modified the rate constant in the Markovian model of I_{Ca} to cause steeper activation and inactivation kinetics, and increased the maximum conductance of the L-type Ca^{2+} current. The major changes are summarized below.

In the action potential model used for **Figs. 4-1B** and **4-2**, the total ionic current was: $I_{ion} = I_{Na} + I_{to,f} + I_{to,s} + I_{Kr} + I_{Ks} + I_{K1} + I_{NaK} + I_{Ca} + I_{NaCa} + I_{ns(Ca)}$. The mathematical formulations of these currents were the same as in the paper by Mahajan *et al* [110], except that $I_{to,s}$ was changed and a nonspecific Ca^{2+}-activated current (I_{nsCa}) was added. The formulation of $I_{to,s}$ is:

$I_{to,s} = g_{to,s} X_{to,s} (0.5Y_{to,s} + 0.5R_s)(V - E_K)$ in which R_s is governed by $\frac{dR_s}{dt} = \frac{R_s^{\infty} - R_s}{\tau_{Rs}}$ with

$R_s^{\infty} = \frac{1}{1 + e^{(V+33.5)/10}}$ and $\tau_{Rs} = \frac{2300}{1 + e^{(V+60)/10}} + 720$. We also modified the rate constants of the Markovian formulation of the L-type Ca^{2+} channel as follows: $p_o^{\infty} = \frac{1}{1 + e^{-(V - vth)/ss}}$,

$s_1 = 0.367 f(c_p)$, $k_1 = 0.0298 f(c_p)$, $k_3 = \frac{e^{-(V+50)/10}}{3(1 + e^{-(V+50)/10})}$, $T_{Ca} = \frac{190}{1 + (c_p/\bar{c}_p)^4} + 10$,

$P_r = \frac{e^{-(V+30)/0.051}}{1 + e^{-(V+30)/0.051}}$, $P_s = \frac{1}{1 + e^{-(V+40)/10}}$, $k_2 = k_1 (s_2/s_1)(r_2/r_1)$, $k'_2 = k'_1 (s'_2/s'_1)(r_2/r_1)$, and

$g_{SR}(V) = \bar{g}_{SR}\, e^{-0.346(V+30)} / \left(1 + e^{-0.346(V+30)}\right)$. $I_{ns(Ca)}$ was adopted from the Luo and Rudy

model[128] with the following parameter changes: $P_{ns(Ca)} = 0.0000001137$ and $K_{m,ns(Ca)} = 0.15$ μM. The parameter changes are summarized in Table S4-I.

The parameters for **Fig. S4-3** were the same as those for Fig. 4-2 except $P_{ns(Ca)} = 0.0000001225$ and $K_{m,ns(Ca)} = 0.16$ μM.

Table S4-1. Parameters changed from the original model by Mahajan et al. [82]

Parameter	Definition	Value
P_{Ca}	Constant	0.00054 cm/s
g_{Ca}	Strength of Ca current flux	655 mmol/(cm C)
$\overline{g}_{Ca}$	Strength of local Ca flux due to L-type Ca channels	9998.6 mmol/(cm C)
$\overline{g}_{SR}$	Strength of local Ca flux due to RyR channels	23692 mmol/(cm C)
k_p^0	Threshold for Ca-induced inactivation	5.0117 μM
$\overline{c}_p$	Threshold for Ca dependence of transition rate k_6	4.0 μM
τ_{po}	Time constant of activation	0.35 ms
vth	Constant	4.36
ss	Constant	6.8
r_1	Opening rate	0.41 ms^{-1}

r_2	Closing rate	2.7 ms^{-1}
s_1'	Inactivation rate	0.00175 ms^{-1}
k_1'	Inactivation rate	0.00413 ms^{-1}
s_2	Inactivation rate	0.000377 ms^{-1}
s'_2	Inactivation rate	0.000687 ms^{-1}
T_{Ba}	Time constant	617.082 ms
g_{RyR}	Release current strength	3.0 sparks cm^2/mA
$g_{to,f}$	Maximum $I_{to,f}$ conductance	$0.055\ mS/\mu F$
$g_{to,s}$	Maximum $I_{to,s}$ conductance	$0.08 mS/\mu F$
g_{K1}	Maximum I_{K1} conductance	$0.36 mS/\mu F$
g_{Kr}	Maximum I_{Kr} conductance	$0.01 mS/\mu F$
g_{Ks}	Maximum I_{Ks} conductance	$0.512 mS/\mu F$
g_{naca}	Strength of exchange current	0.84μM/s
g_{NaK}	Maximum I_{NaK} conductance	$1.5 mS/\mu F$
v_{up}	Strength of Uptake	0.8 μM/ms
B_{ATP}	Total concentration of ATP binding sites	5000.0 μmol/l cytosol
K_{ATP}	Dissociation constant for ATP binding sites	200.0 μM

4.6.1 Supplemental Figures

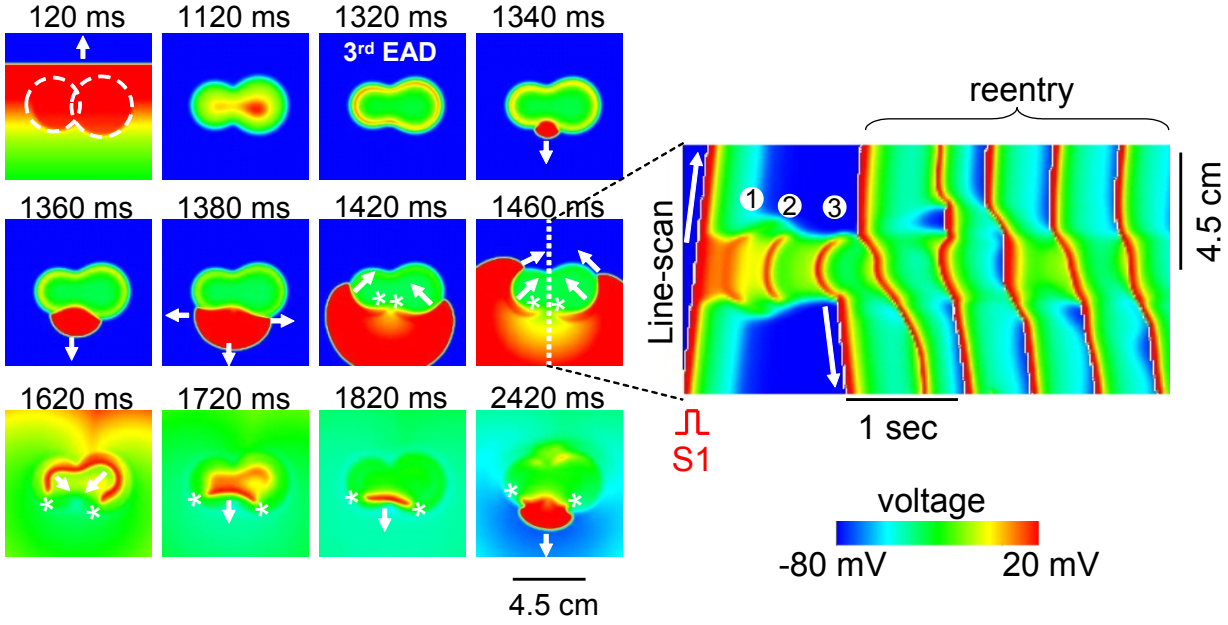

Figure S4-1. Induction of reentry by EADs in a 2D heterogeneous tissue model after a single S1 stimulus. The tissue model has a heterogeneous region composed of two circles (while dashed) in which EADs occur. A single S1 stimulus was applied at the bottom edge of the tissue to cause planar wave to propagate from bottom to top. Reentry occurred spontaneously due to the unidirectional conduction of an EAD in the heterogeneous region. The conduction in the heterogeneous region is mediated by $I_{Ca,L}$ but both I_{Na} and $I_{Ca,L}$ mediated conduction occur in other regions. Left: voltage snapshots showing that the third EAD after the pacing that failed to propagate out the positively curved regions successfully propagated out at the negatively curved region, forming unidirectional conduction block and inducing figure-of-eight reentry. Asterisks indicate the tips of the spiral wave reentry, while arrows indicate directions of propagation. Timing of each snapshot is marked on top of each panel. Right: the corresponding space-time plot of a line (white dotted line) for the same simulation showing that the first two EADs failed to propagate out the region but the 3rd one propagated unidirectionally to form reentry. The white arrows indicate directions of conduction. The diameters of the circular regions exhibiting EADs are 3 cm and 3.6 cm, respectively. The action potential model is the same as in Fig.2 in the main text except that the maximum conductance of I_{Ks} was increased by a factor of four in the outer region. The reason to use two circles is to create a negatively curved boundary at which the source-sink relation favors the EAD conduction to result in unidirectional conduction.

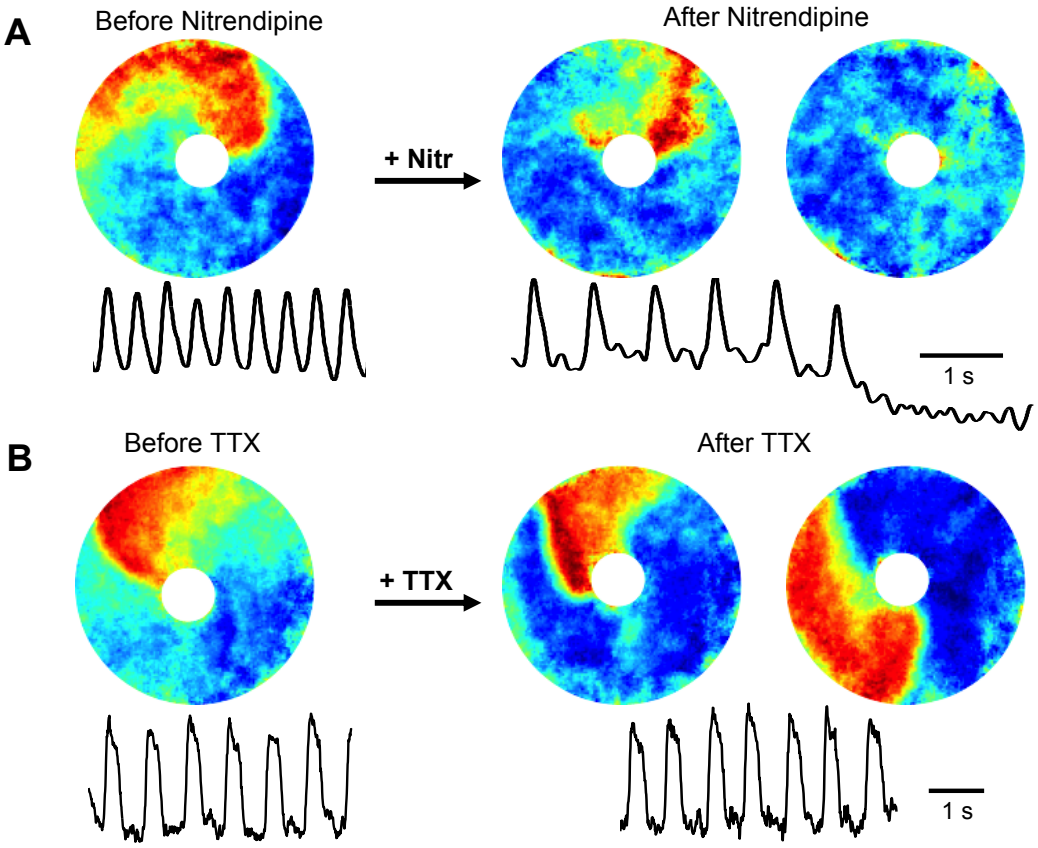

Figure S4-2. NRVM monolayer experiments showing termination of reentry by nitrendipine but not TTX. Reenrty were induced under BayK8644 (50nM) and iso (1μM). A. A reentry (~3 Hz, left) was terminated by nitrendipine (5 μM, right). B. A reentry (~1.5 Hz, left) remained after TTX (50 μM, right)

5 Flipping the Switch: K_{ATP} channel mediated conversion of I_{Ca}-mediated to I_{Na}-mediated Cardiac Conduction

5.1 Abstract

BACKGROUND: Under conditions promoting early afterdepolarizations (EADs), ventricular tissue can become bi-excitable, i.e. capable of wave propagation mediated by either the Na current (I_{Na}) or the L-type calcium current ($I_{Ca,L}$), raising the possibility that $I_{Ca,L}$-mediated reentry may contribute to polymorphic ventricular tachycardia (PVT) and Torsade de Pointes (TdP). ATP-sensitive K current (I_{KATP}) activation suppresses EADs, but the effects on $I_{Ca,L}$-mediated reentry are unknown.

OBJECTIVE AND METHODS: To investigate the effects of I_{KATP} activation on $I_{Ca,L}$-mediated reentry, we performed optical voltage mapping in cultured neonatal rat ventricular myocyte monolayers exposed to BayK4688 and isoproterenol. The effects of pharmacologically activating I_{KATP} with pinacidil were analyzed.

RESULTS: In 13 monolayers with anatomic $I_{Ca,L}$-mediated reentry around a central obstacle, pinacidil (50 mM) converted $I_{Ca,L}$-mediated reentry to I_{Na}-mediated reentry. In 33 monolayers with functional $I_{Ca,L}$-mediated reentry (spiral waves), pinacidil terminated reentry in 17, converted reentry into more complex I_{Na}-mediated reentry resembling fibrillation in 12, and had no effect in 4. In simulated 2D bi-excitable tissue in which $I_{Ca,L}$- and I_{Na}-mediated wavefronts coexisted, slow I_{KATP} activation (over minutes) reliably terminated rotors, but rapid I_{KATP} activation

(over seconds) often converted $I_{Ca,L}$-mediated reentry to I_{Na}-mediated reentry resembling fibrillation.

CONCLUSIONS: I_{KATP} activation can have pro-arrhythmic effects on EAD-mediated arrhythmias if $I_{Ca,L}$-mediated reentry.

5.2 Introduction

In normal ventricular and atrial tissue, wavefront propagation is driven by activation of the Na current (I_{Na}). Recently, we showed that under conditions promoting early afterdepolarizations (EADs), ventricular tissue can become bi-excitable, i.e. capable of wave propagation mediated by either the Na current (I_{Na}) or the L-type calcium current ($I_{Ca,L}$), separately or simultaneously, in the same tissue [129]. This raises the possibility that, in addition to focal activations, $I_{Ca,L}$-mediated reentry may contribute to EAD-mediated arrhythmias such as polymorphic ventricular tachycardia (PVT) and Torsade de Pointes (TdP). Consistent with this possibility, $I_{Ca,L}$-mediated rotors exhibit a much slower frequency than I_{Na}-mediated rotors, more compatible with the typical rates of PVT and TdP, and their core meandering reproduces characteristic electrocardiographic features of PVT and TdP[129].

Many experimental and clinical studies [130-137] have shown that pharmacological activation of sarcolemmal ATP-sensitive K (K_{ATP}) channels shortens action potential (AP) duration and abolishes EADs, preventing EAD-mediated triggered activity and suppressing PVT and TdP [130-137]. Since hypotension is a common consequence of PVT and TdP, the resulting ischemia-related K_{ATP} channel activation may be a factor contributing to spontaneous termination of PVT and TdP and restoration of sinus rhythm by abolishing EAD-mediated focal excitations. Occasionally, however, TdP or PVT degenerate into

ventricular fibrillation (VF), causing sudden cardiac death [108, 109, 138]. Why most episodes of TdP or PVT terminate spontaneously, but some degenerate into VF, is poorly understood. To explore these issues, we investigated the effects of K_{ATP} channel activation on $I_{Ca,L}$-mediated reentry, given its potential relevance to PVT and TdP. Using optical voltage mapping in neonatal rat ventricular myocyte (NRVM) monolayers, combined with computer simulations, we find that activation of K_{ATP} channels often terminates $I_{Ca,L}$-mediated reentry, but also has a significant probability of "flipping the switch" of bi-exctiable tissue converting $I_{Ca,L}$-mediated reentry into I_{Na}-mediated reentry, which can then degenerate into multi-wavelet VF, especially if I_{KATP} activation occurs rapidly.

5.3 Methods

All protocols used conform to the standard set forth by the National Institutes of Health in the *Guide for the Care and Use of Animals* (NIH publication No. 85-23, Revised 1996).

Monolayer preparation. We created monolayers of neonatal rat ventricular myocytes (NRVMs) by plating $1x10^6$ cells on 21 mm fibronectin-coated plastic coverslips, as previously described[50]. Briefly, the hearts harvested from 2- to 3-day-old neonatal Sprague-Dawley rats were digested with collagenase (0.02%; Worthington Biochemical Corp, Lakewood, NJ) and pancreatin (0.06%; Sigma-Aldrich, St Louis, Mo). Myocytes were isolated with the use of a Percoll (Pharmacia

Biotech AB, Uppsala, Sweden) gradient and plated at a density of 10^6 cells/mm^3 per coverslip.

Optical mapping. Arrhythmias were imaged by optical mapping performed after 11-14 days in culture. Coverslips were visually inspected under a microscope and monolayers with obvious gaps in confluence were discarded. Acceptable coverslips were then stained with the voltage-sensitive dye di-4-ANEPPS (5 μmol/L for 5 min), after which they were continuously superfused with warm (36°C) oxygenated (normal) Tyrode solution containing (in mM): 135 NaCl, 5.4 KCl, 1.8 $CaCl_2$, 1 $MgCl_2$, 0.33 NaH_2PO_4, 5 HEPES, and 5 glucose.

Action potentials were recorded using a CCD-based optical imaging system (Photometrics Cascade 128+; 128×128 pixels). Voltage signals were acquired continuously over 10 to 180 seconds at 0.6 to 5 ms per frame. Signals were digitized with 16 bits of precision and processed offline as described previously[112]. Data were stored, displayed, and analyzed using custom software written in Visual C++ (Microsoft) and MATLAB (MathWorks).

Experimental Protocols. Reentrant arrhythmias were initiated by either rapid pacing or incubating monolayers in the presence of the L-type Ca channel agonist BayK8644 (BayK, 2.5 μM) and the beta adrenergic receptor agonist isoproterenol (Iso, 1 μM) for > 2 hours. The dependence of wave propagation on I_{Na} versus I_{Ca} was tested in subset of monolayers exhibiting reentry (n=10) using the Na channel blocker tetrodotoxin (TTX, 50 μM) or the Ca channel blocker nitrendipine

(5 μM). K_{ATP} channels were activated by adding pinacidil (100 μM) to the superfusate.

Data Analysis. The baseline drift due to photobleaching of potentiometric dyes was reduced by subtracting a third order polynomial best fit curve of the optical signals. To reduce noise in the optical signals, a seven point median filter was applied to the de-trended data. Movies of electrical propagation were generated from signals that were low-pass filtered between 0 and 100 Hz. The activation time was defined as the instant of maximum positive slope. For each data set, the mean and accompanying 95% confidence intervals (CIs) are reported. The conventional percentile bootstrap-resampling approach with 10000 replications was used for estimating 95% CI [139]. A *P* value <0.05 was considered statistically significant. Conduction velocity was estimated as described previously [112, 129].

Computer simulations. Computer simulations used the ventricular action potential (AP) model by Mahajan et al.[82], modified to produce EADs and bi-excitability[129]. I_{KATP}, based on the formulation by Ferrero et al. [140], was added to the myocyte model with a density of 3.8 channels/mm^2. To simulate the effects of pinacidil, we increased the fraction of open K_{ATP} channels (f_{ATP}) from 0 to 0.0025 (over time periods of 50 ms, 10 s or 5 min). All simulations were performed in a monodomain 2D tissue of 300x300 cells (4.5 cm x 4.5 cm) as described previously [129]. A linear gradient in the maximum conductance of I_{Ks} from 0.512 to 2.048 mS/cm^2 was imposed from center-to-periphery in the tissue to facilitate the joint

appearance of both I_{Na} and $I_{Ca,L}$-mediated wavefronts as, described previously to mimic the electrocardiographic appearance of TdP [129]. Simulations were performed on NVIDA Tesla C2050 General Purpose Graphics Processing Units (GPGPUs).

5.4 Results

5.4.1 Effects of pinacidil on $I_{Ca,L}$-mediated reentry in NRVM monolayers

To generate $I_{Ca,L}$-mediated wave propagation and reentry, we used our previously characterized model of bi-excitability by superfusing NRVM monolayers with BayK + Iso[129, 141]. When exposed to BayK + Iso, monolayers developed bursts of EAD-mediated focal activity, typically arising from multiple sites, resulting in a complex mixture of focal activity and reentry, as illustrated in Fig. 5-1. The accompanying optical voltage trace recorded from a representative site in the monolayer during the initiation of a burst of focal activity illustrates the incomplete repolarization between beats, consistent with EAD-mediated triggered activity as described previously under these conditions [129].

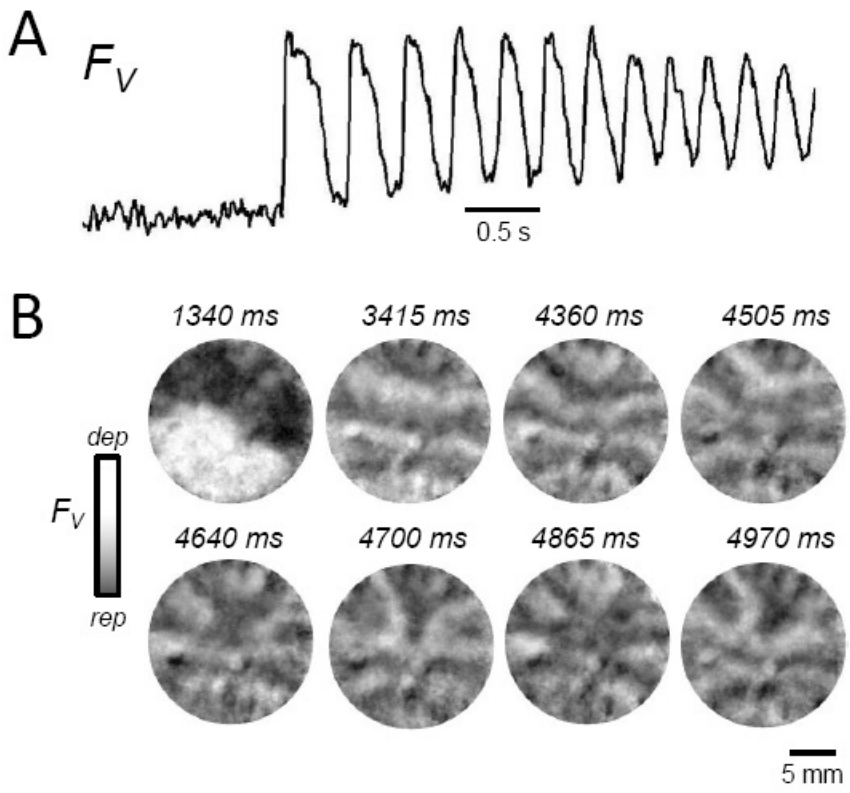

Figure 5-1. EAD-mediated arrhythmias induced by BayK4688 + isoproterenol in NRVM monolayers. (A) Optical voltage trace (F_V) illustrating a burst of EAD-mediated triggered activity following a paced beat. Note the incomplete repolarization between beats. (B) Snapshots of voltage fluorescence (F_V) on a gray scale (dep, depolarized; rep, repolarized) at the times indicated following the paced beat at 1340 ms, revealing a complex pattern of wavefronts due to a mixture of focal activity and reentry.

Since reentry during BayK + Iso-induced arrhythmias in NRVM monolayers tended to be complex and frequently interrupted by focal activations, we pre-fabricated monolayers with a hole in the center, which facilitated stable $I_{Ca,L}$-mediated reentry by anchoring reentry and also preventing spontaneous termination due to the core meandering and colliding with a tissue border. In these monolayers, incubation with BayK + Iso frequently resulted in sustained

arrhythmias, due to either sustained reentry around the central obstacle (Fig. 5-2), or more complex patterns in which rotors due to functional reentry were present (Figs. 5-3 and 5-4). Both forms of reentry were dependent on $I_{Ca,L}$-mediated wave propagation, since reentry was consistently abolished by the L-type Ca channel blocker nitrendipine (n=10), but not by the Na channel blocker TTX (n=13), as illustrated in the example of reentry around the central obstacle in Fig. 5-2.

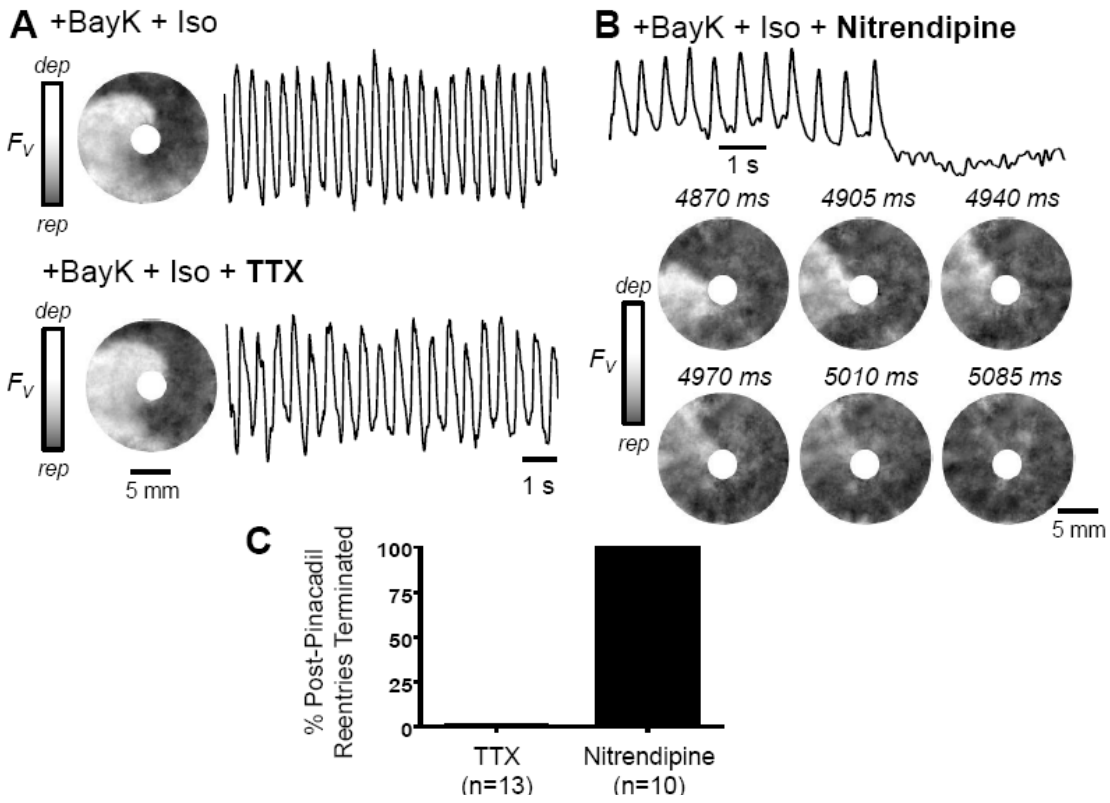

Figure 5-2. EAD-mediated reentry around a central obstacle in an NRVM monolayer. (A) Snapshot (left) and trace (right) of voltage fluorescence (F_V), illustrating that reentry around the central obstacle was unaffected by TTX (50 mM). (B) In contrast, nitrendipine (5μM) terminated reentry. (C) Bar graph summarizing incidence of termination of reentry by TTX vs nitrendipine in 23 monolayers.

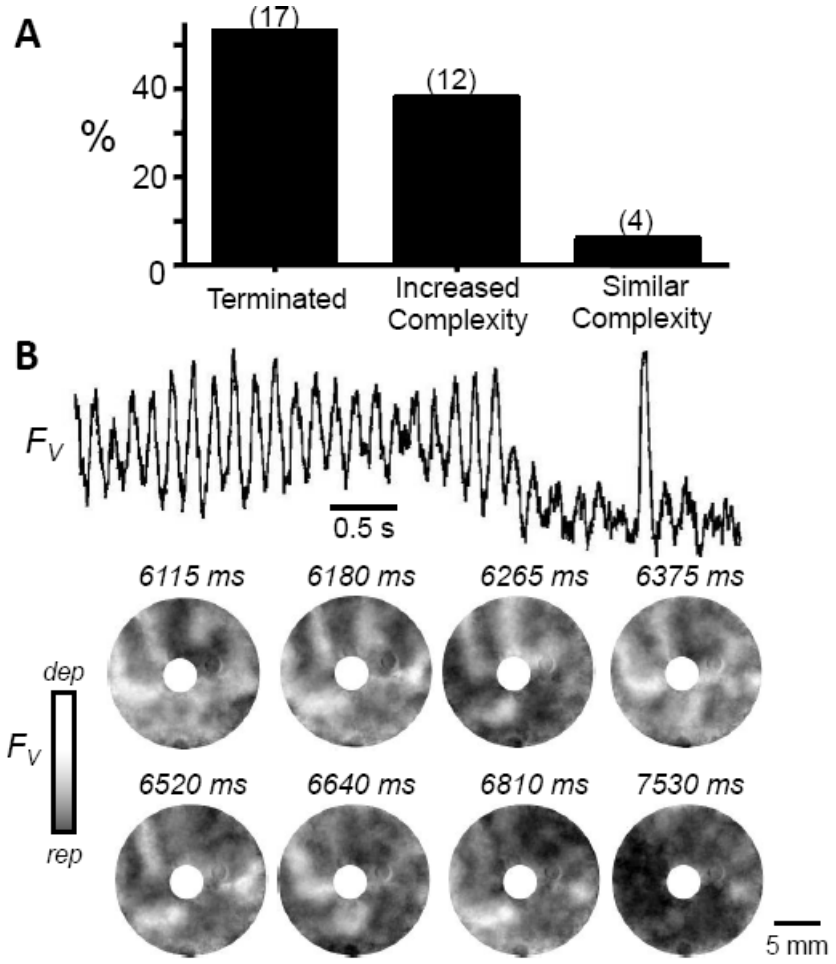

Figure 5-3. Effect of the K_{ATP} channel agonist pinacidil in NRVM monolayers with complex sustained EAD-mediated arrhythmias. (A) Histogram illustrating the outcomes of pinacidil (100 mM) treatment on complex EAD-mediated arrhythmias induced by BayK4688 + isoproterenol in 33 NRVM monolayers with a central obstacle. (B) Representative optical trace (top) and snapshots (below) of voltage fluorescence (F_V) at the times indicated, illustrated termination of a complex EAD-mediated arrhythmia by pinacidil. In this example, the arrhythmia was driven primarily by a functional rotor (spiral wave) at 1 o'clock.

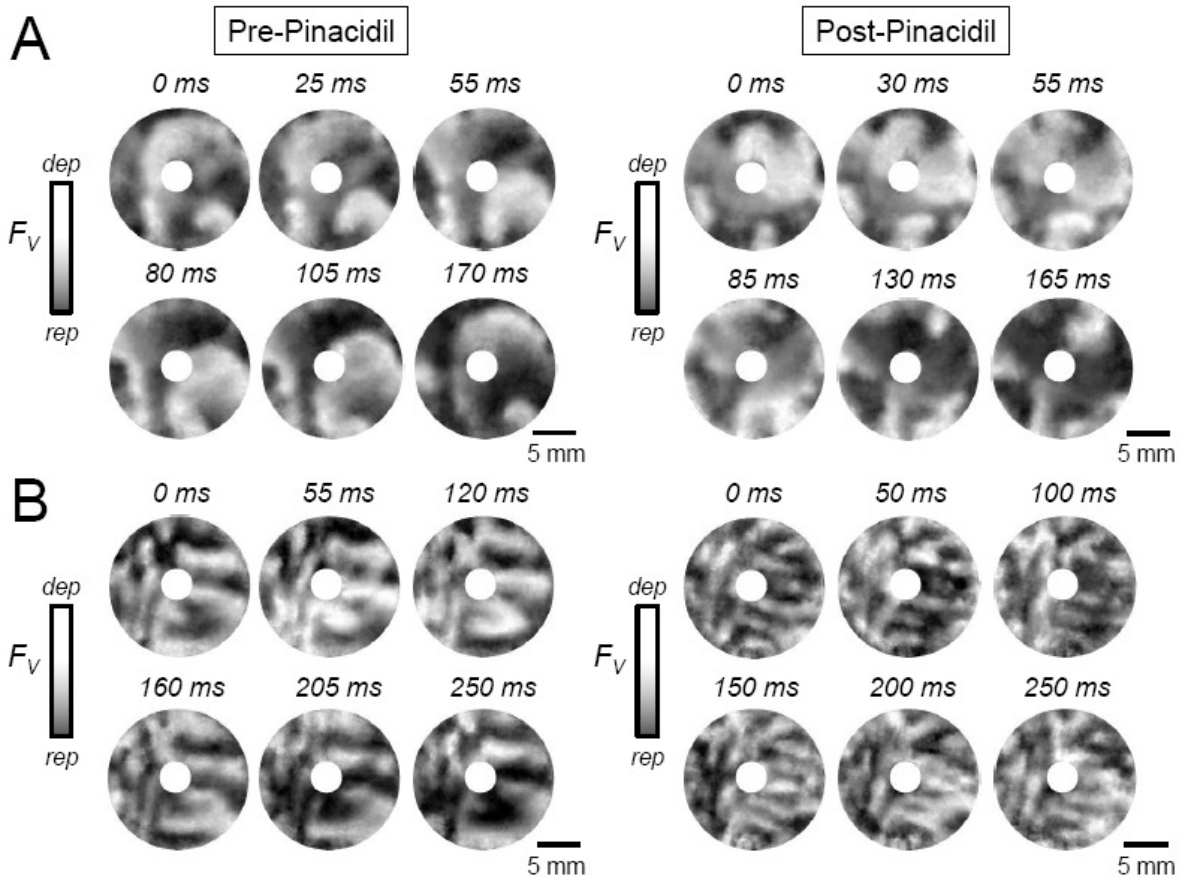

Figure 5-4. Effects of the K_{ATP} channel agonist pinacidil in NRVM monolayers with complex sustained EAD-mediated arrhythmias. (A) Snapshots of voltage fluorescence (F_V) at the times indicated in a monolayer with a central obstacle in which BayK4688 + isoproterenol induced an arrhythmia driven primarily by functional rotors (spiral waves) at 6 and 8 o'clock (left panels). Pinacidil (100 mM, right panels) did not significantly affect the complexity of the arrhythmia. (B) Voltage snapshots from another monolayer with a central obstacle, in which pinacidil (right panels) increased the complexity of the BayK4688 + isoproterenol-induced arrhythmia, as evident from the greater number of wavefronts.

We then examined the effects of K_{ATP} channel activation with 5 μM pinacidil in monolayers with sustained anatomic or functional $I_{Ca,L}$-mediated reentry for >10 min. In 13 monolayers with sustained anatomic reentry around the central obstacle, as in Fig. 5-2, pinacidil did not terminate reentry, but changed its pharmacological

profile. Before pinacidil, reentry was consistently terminated by nitrendipine (Fig. 5-2) but not by TTX. After pinacidil, however, the converse was true; reentry was terminated by TTX in all monolayers tested, whereas nitrendipine terminated reentry in only 2 of 10 monolayers tested (20%) (Fig 5-5 A & B). This result indicates that pinacidil converted $I_{Ca,L}$-mediated wave propagation to I_{Na}-mediated wave propagation. Consistent with this interpretation, conduction velocity after pinacidil increased by an average of 89 ± 82% (95% confidence interval, 46% to 141%) (Fig. 5-6A). This is illustrated by the increased spacing of the isochrone lines post-pinacidil in the example shown in Fig. 5-6B.

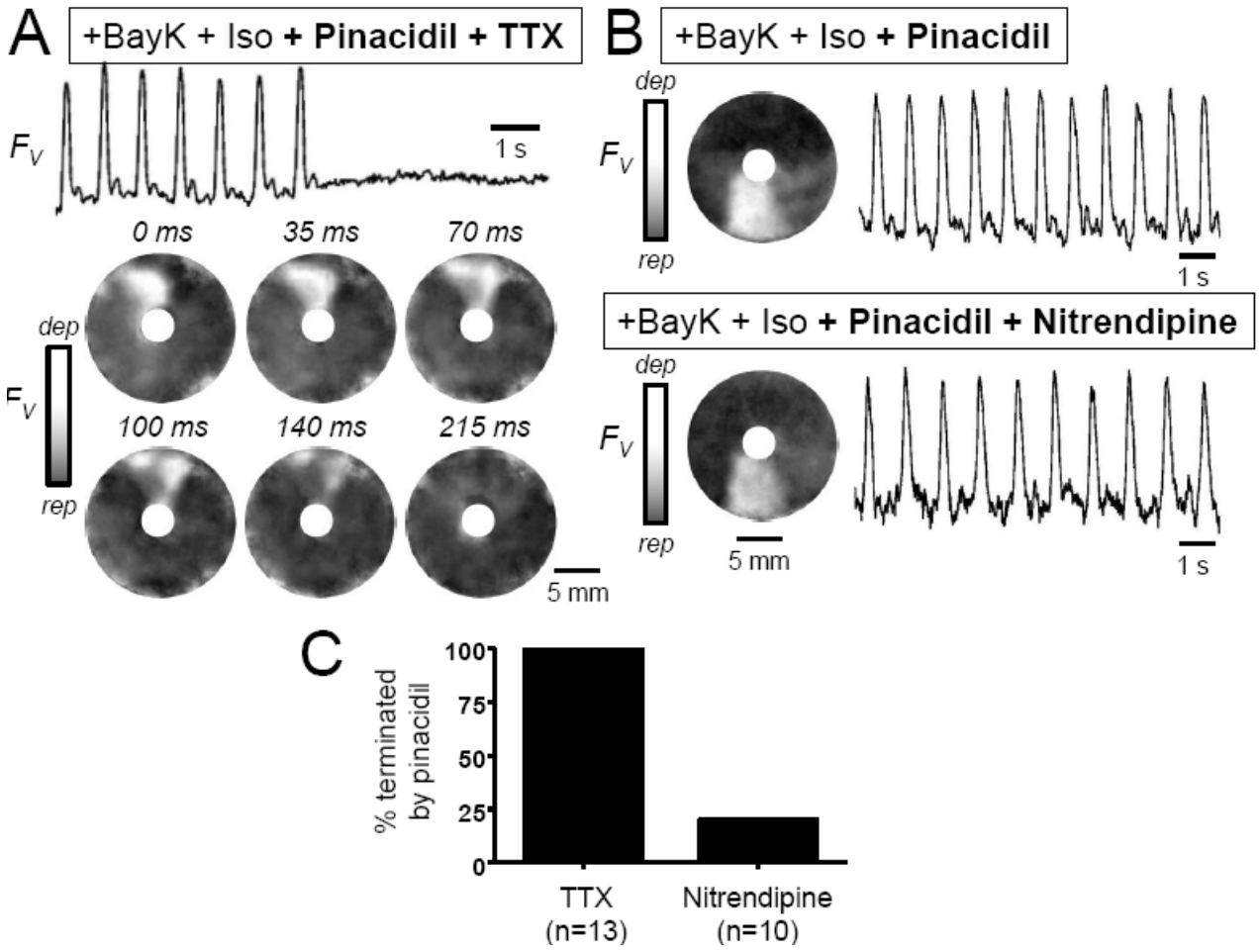

Figure 5-5. Effects of pinacidil on EAD-mediated reentry around a central obstacle in an NRVM monolayer. (A) Optical trace (above) and snapshots (below) of voltage fluorescence (F_V) in a monolayer in which BayK4688 + isoproterenol induced sustained reentry around a central obstacle. After pinacidil treatment, addition of TTX (50 μM) terminated reentry. (B) Same, but with nitrendipine (5 μM) added instead of TTX, showing that reentry persists. (C) Bar graph summarizing incidence of termination of reentry by TTX vs nitrendipine in 23 monolayers exposed to BayK4688 + isoproterenol + pinacidil.

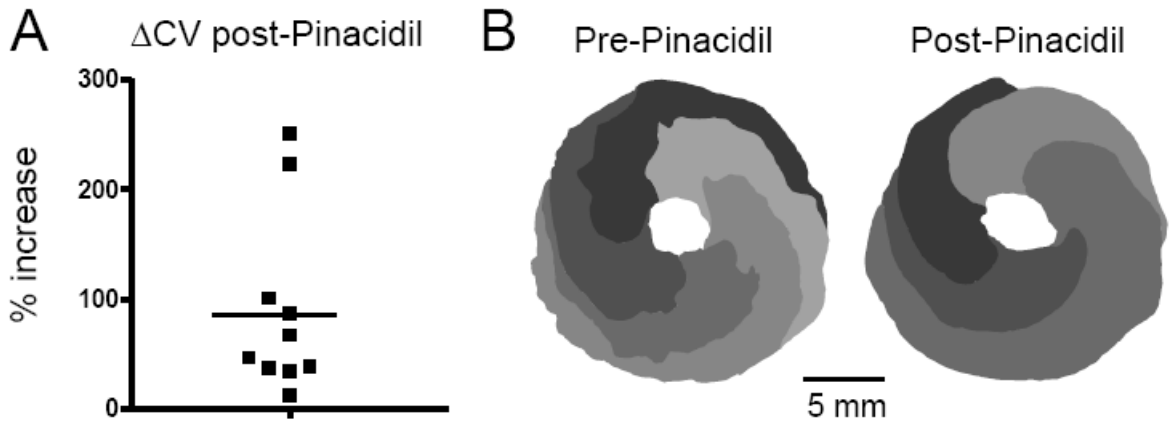

Figure 5-6. Effects of pinacidil on conduction velocity of EAD-mediated reentry around a central obstacle in NRVM monolayers. (A) The percent increase in conduction velocity after pinacidil in 10 monolayers (solid squares) in which BayK4688 + isoproterenol induced sustained reentry around a central obstacle. Mean increase is indicated by the horizontal bar. (B) Isochrome map during reentry in a representative monolayer, pre- and post-pinacidil treatment. Increased spacing between 80 ms isochrome lines post-pinacidil reflects increased conduction velocity.

In contrast, among 33 monolayers with more complex arrhythmia patterns involving functional $I_{Ca,L}$-mediated rotors as in Figs. 5-3 & 5-4 , application of pinacidil spontaneously terminated the arrhythmia in 17 (52%) (Fig 5-3). In 4 monolayers (12%), reentry was not significantly changed (Fig 5-4A), and in 12 (36%), reentry became more complex (Fig 5-4B).

5.4.2 Computer simulations in 2D tissue

To gain further insight into the experimental findings, we performed simulations using the Mahajan et al ventricular AP model [82], with parameters modified to produce EADs with bi-excitable wave propagation in tissue, as

described previously[129]. In homogeneous 2D tissue, either I_{Na}- or $I_{Ca,L}$-mediated reentry could be induced, depending on the stimulation protocol used to initiate reentry, indicative of bi-excitability [129]. To study the effects of I_{KATP} activation on functional reentry driven by an $I_{Ca,L}$-mediated rotor in which I_{Na}-mediated wavefronts were also intermittently present (as previously documented in bi-excitable monolayers[129]), we created a heterogeneous 2D tissue with a linearly increasing gradient in I_{Ks} from center-to-periphery, such that the center of the tissue had a longer AP duration than the periphery. When an $I_{Ca,L}$-mediated rotor was induced, the rotor meandered throughout the central region, with the arm of the rotor in the outer tissue containing a mixture of $I_{Ca,L}$- and I_{Na}-mediated wave propagation whose relative proportions varied in time (Fig. 5-7).

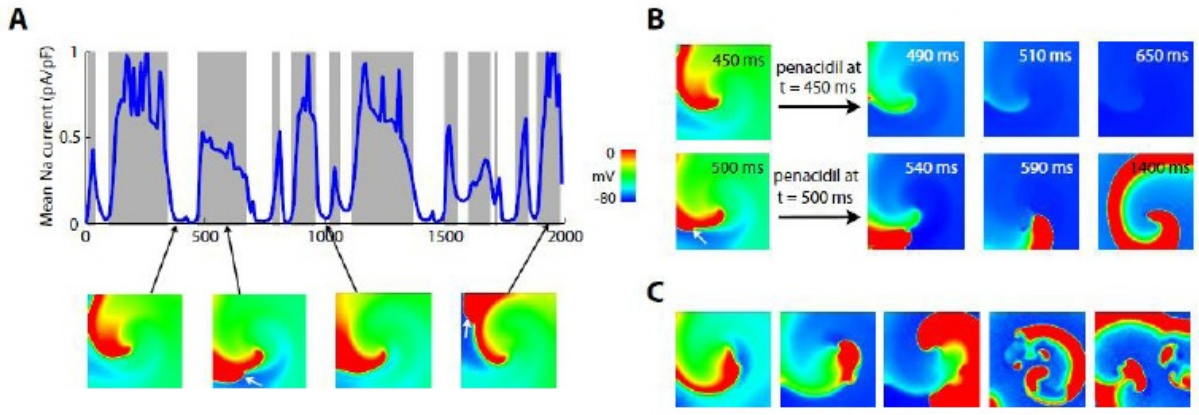

Figure 5-7. Effect of I_{KATP} activation on $I_{Ca,L}$-mediated reentry in simulated 2D heterogeneous cardiac tissue (300 x 300 myocytes). A. Outcomes of rapidly activating I_{KATP} at various time points during reentry driven by an $I_{Ca,L}$-mediated rotor in the center of the tissue. Grey zones indicate that $I_{Ca,L}$-mediated reentry converted to I_{Na}-mediated reentry after I_{KATP} activation, white zones that reentry terminated. The blue line shows I_{Na} amplitude averaged over all cells in the tissue over time. I_{KATP} activation terminated

reentry only if no significant I_{Na}-mediated wavefronts were present. Voltage snapshots (below) show the $I_{Ca,L}$-mediated rotor in the center of the tissue, with I_{Na}-mediated wavefronts intermittently present along the spiral arm (2nd and 4th panels, white arrows). B. Voltage snapshots showing termination of reentry by I_{KATP} activation at t=450 ms (top row), but conversion to I_{Na}-mediated reentry at t=500 ms (bottom row). C. When the number K_{ATP} channels was randomly varied from myocyte to myocyte (using a Gaussian distribution with mean 3.8 channels/mm^2 and standard deviation 2.0), I_{KATP} activation caused the stable $I_{Ca,L}$-mediated rotor to convert to an I_{Na}-mediated rotor, which then broke up into multi-wavelet VF.

To simulate the effects of pinacidil, we added a formulation of I_{KATP}[140] whose conductance throughout the tissue increased linearly to a maximum over a specified time period. Under these conditions, the outcome of I_{KATP} activation during the arrhythmia was probabilistic in nature, sensitive to both the timing and speed of I_{KATP} activation. When I_{KATP} was activated rapidly over 50 ms, reentry terminated and the tissue repolarized to a quiescent state in 41% of 201 trials. In the remaining 59% of trials, the $I_{Ca,L}$-mediated rotor was converted to an I_{Na}-mediated rotor (Fig. 5-7A). The specific outcome depended on whether I_{Na}-mediated wavefronts were present in the tissue when I_{KATP} was activated. If I_{KATP} was activated at a time when no I_{Na} wavefronts happened to be present in the arm of the rotor, reentry terminated (Fig 5-7A, unshaded areas) because no I_{Na} wavefronts were present to form a new rotor after the $I_{Ca,L}$-mediated rotor terminated. In contrast, if I_{KATP} was activated at a time when I_{Na} wavefronts were present in the arm of the rotor (Fig. 5-7A, shaded areas), these I_{Na} wavefronts were unaffected by I_{KATP} activation. Transformation from an $I_{Ca,L}$-mediated into an I_{Na}-mediated rotor was achieved by

the I_{Na}-mediated wavefronts whipping around the front end of the vanishing $I_{Ca,L}$-mediated rotor, reactivating the fully repolarized tissue previously occupied by the $I_{Ca,L}$-mediated wavefront (Fig. 5-7B).

In this scenario, the speed of I_{KATP} activation also played a critical role. When I_{KATP} was activated slowly, over 10 sec or 5 min, the incidence of termination increased to 54% (101 trials) and 100% (21 trials), respectively. This is because when I_{KATP} reached a sufficient amplitude to terminate all $I_{Ca,L}$-mediated wavefronts, the AP duration and wavelength were still too long to allow an I_{Na}-mediated rotor to become sustained. That is, if an I_{Na}-mediated rotor formed at this point, it meandered to the tissue border and self-terminated (Supplemental Movie 5-1, supplemental material). Only if I_{KATP} continued to activate rapidly did the AP duration and wavelength shorten sufficiently to allow the I_{Na}-mediated rotor to become stable before it happened to collide with a tissue border and self-terminate (Supplemental Movie 5-2, supplemental material). If the tissue size was increased to prolong the lifetime of the I_{Na}-mediated rotor when the $I_{Ca,L}$-mediated rotor terminated, the percentage of trials that resulted in termination for the same time course of I_{KATP} activation decreased.

Supplemental Movie 5-1

Supplemental Movie 5-1. Termination of $I_{Ca,L}$-mediated reentry by slow activation of I_{KATP} over 5 minutes (first 90 s shown). A stable $I_{Ca,L}$-mediated spiral wave is initially present in the center of heterogeneous bi-excitable tissue (4.5 x 4.5 cm), with intermittent I_{Na}-mediated wavefronts appearing in the periphery, as indicated by the transient rapidly-conducting bulges along the spiral arm. Slow I_{KATP} activation gradually converts the stable $I_{Ca,L}$-mediated spiral to a meandering $I_{Na,L}$-mediated spiral wave, which eventually terminates by collision with the tissue border (near 86,000 ms).

Supplemental Movie 5-2

Supplemental Movie 5-2. Conversion of $I_{Ca,L}$-mediated reentry to I_{Na}-mediated reentry by rapid activation of I_{KATP} over 50 ms. A stable $I_{Ca,L}$-mediated spiral wave is initially present in the center of heterogeneous bi-excitable tissue (4.5 x 4.5 cm), with intermittent I_{Na}-mediated wavefronts appearing in the periphery, as indicated by the transient rapidly-conducting bulges along the spiral arm. Rapid I_{KATP} activation over 50 ms (beginning at 500 ms) rapidly shortens APD and converts the stable $I_{Ca,L}$-mediated spiral to a stable $I_{Na,L}$-mediated spiral wave.

If random cell-to-cell variability in the number of K_{ATP} channels was introduced into the tissue model to simulate a heterogeneous distribution of K_{ATP} channels among cardiac myocytes, then for the cases in which I_{Na}-mediated rotors did not terminate during I_{KATP} activation, the increased dispersion of repolarization led to unidirectional conduction block, causing the I_{Na}-mediated rotor to break up into multi-wavelet VF (Fig 7C). This was similar to the finding in monolayers in which pinacidil increased arrhythmia complexity (Fig. 4B).

In summary, these simulations show that I_{KATP} activation can either terminate $I_{Ca,L}$-mediated reentry or convert it to more complex I_{Na}-mediated reentry in heterogeneous tissue, depending on the timing and speed of I_{KATP} activation, with slower I_{KATP} activation favoring termination.

5.5 Discussion and conclusions

Activation of sarcolemmal K_{ATP} channels shortens the cardiac AP duration and generally suppresses EAD's by increasing repolarization reserve, as demonstrated previously in many studies [130-137]. Therefore, when ventricular arrhythmias such as PVT and TdP are caused by EAD-mediated triggered activity arising from one or more focal sites, I_{KATP} activation tends to be antiarrhythmic by suppressing EAD formation. However, the extent to which EAD-mediated arrhythmias are focal or reentrant remains controversial [142, 143]. We recently demonstrated that under EAD-promoting conditions, cardiac tissue can become bi-excitable, i.e.

capable of supporting both I_{Na}- and $I_{Ca,L}$-mediated wavefronts [129]. Moreover, $I_{Ca,L}$-mediated rotors which can form under these conditions exhibit electrocardiographic features and cycle lengths resembling PVT and TdP [129]. Given the possibility that $I_{Ca,L}$-mediated reentry may be involved in the pathogenesis of PVT or TdP, the question arises as to whether I_{KATP} activation has exclusively antiarrhythmic effects on this form of reentry (as it does on EAD-mediated triggered activity), or whether it can be pro-arrhythmic as well. This is an important question, because I_{KATP} activation agonists have been proposed as therapeutic agents for TdP, and also because hypotension associated with prolonged episodes of PVT and TdP may result in I_{KATP} activation physiologically. We hoped that investigation of this issue might provide insight into why PVT and TdP episodes, which usually self-terminate, occasionally degenerate to VF to cause sudden cardiac death [108, 109, 138].

5.5.1 Pro- and Anti-Arrhythmic Effects of I_{KATP} Activation on EAD-mediated Arrhythmias

Using pinacidil to activate I_{KATP} in NRVM monolayers, we found I_{KATP} activation often converted $I_{Ca,L}$-mediated anatomic or functional reentry to I_{Na}-mediated reentry with faster conduction velocity, accelerating the rate of the tachycardia. These findings imply that if $I_{Ca,L}$-mediated reentry is present during PVT or TdP, activation of I_{KATP} by drugs or ischemia might accelerate the

tachycardia, potentially resulting in wavebreak and precipitating multi-wavelet or mother rotor VF. We consistently observed that anatomic $I_{Ca,L}$-mediated reentry around a central obstacle was converted to anatomic I_{Na}-mediated reentry. For functional $I_{Ca,L}$-mediated rotors in which $I_{Ca,L}$- and I_{Na}-mediated wavefronts co-existed, however, the effects of I_{KATP} activation were probabilistic. As elucidated in computer simulations, if I_{KATP} was activated during an epoch when no I_{Na}-mediated wavefronts happened to be present in the tissue, reentry terminated. However, if I_{KATP} was activated when both $I_{Ca,L}$- and I_{Na}-mediated wavefronts were present, the $I_{Ca,L}$-mediated wavefronts were eliminated, but the I_{Na}-mediated wavefronts were unaffected, allowing I_{Na}-mediated rotors to form and potentially break up into multiwavelet VF (Fig. 7). An important factor influencing whether functional $I_{Ca,L}$-mediated rotors terminated or were converted to I_{Na}-mediated reentry and VF was the rapidity with which I_{KATP} was activated. As I_{KATP} was activated more slowly, the probability of termination progressively increased and the probability of degeneration to VF concomitantly decreased. This was because the tissue size was not large enough to support a stable I_{Na}-mediated rotor when I_{KATP} first became large enough to eliminate the $I_{Ca,L}$-mediated rotor. Only if subsequent I_{KATP} activation was rapid did the APD and wavelength subsequently shorten quickly enough to stabilize the I_{Na}-mediated rotor before it meandered to a tissue border and self-terminated. This implies that tissue size, relative to wavelength, is also an important determinant of whether functional $I_{Ca,L}$-mediated rotors terminate or are

converted to sustained I_{Na}-mediated reentry, with termination being favored by smaller tissue size. However, even for the large tissue size (4.5 x 4.5 cm) that we simulated, the incidence of termination was still 41% even with very rapid I_{KATP} activation over 50 ms, and 100% for slow activation over 5 mins. Given that spontaneous I_{KATP} activation due to systemic hypotension during PVT or TdP occurs gradually over minutes, our findings suggest that hypotension in this setting is more likely to favor termination of these arrhythmias than promote degeneration to VF, but the latter still has a finite probability. In addition, there are many other reasons why episodes of PVT or TdP due to $I_{Ca,L}$-mediated reentry might spontaneously terminate before I_{KATP} activation becomes significant, including heterogeneity-induced spiral drifting, wave collision, and dynamical instabilities [144-147]. Also, under conditions in which PVT or TdP are maintained primarily by focal activation, rather than $I_{Ca,L}$-mediated reentry, I_{KATP} activation would be expected to suppress the arrhythmia, whether activated rapidly or slowly. However, our findings raise the possibility that acute intravenous administration of an I_{KATP} agonist to terminate PVT or TdP in the clinical setting could run a significant risk of converting the arrhythmia to VF, if the arrhythmia involved $I_{Ca,L}$-mediated reentry and the drug was administered rapidly. Our study shows that this occurs as a result of "flipping of the switch" of bi-excitable tissue, converting low frequency I_{Ca}-mediated reentries to high frequency I_{Na}-mediated reentries.

5.5.2 Limitations

In extrapolating to the clinical relevance of the present findings, however, a number of caveats and limitations should be recognized. $I_{Ca,L}$-mediated reentry was induced using BayK + Iso in NRVM monolayers, which, despite the advantages for optical mapping, have important electrophysiological differences with human myocardium. BayK + Iso are an artificial means of inducing EADs, with arguably limited direct physiological relevance, although Iso alone has been shown to generate EAD bursting in this preparation [141], and is well-known to be a potentiating arrhythmogenic factor in long QT syndromes [59, 60]. Among many other effects, BayK and Iso both accentuate mode 2 gating of L-type Ca channels, which is believed to the genetic defect in LQT8 [148]. In addition, $I_{Ca,L}$-mediated rotors due to bi-excitability have yet to be documented experimentally in intact native animal or human cardiac tissues subjected to more physiologically-relevant stressors causing EADs. The experimental model (NVRM) and computer AP model (rabbit ventricle) also represented different species. On the other hand, the observation that different experimental and computer models yielded consistent results increases our confidence that these findings are generalizable, and may have relevance to clinical EAD-mediated arrhythmias such as TdP and PVT.

6 Concluding Remarks

The purpose of this dissertation is to provide its readers with a new perspective on EAD-mediated arrhythmias. It is my hope that in the process of doing so, it has given its readers a newfound appreciation for nonlinear dynamics in answering questions related to medicine and the biological sciences. If only this is accomplished, the time and effort taken to write this dissertation was well worth it.

If there is one major theme I would like to leave the reader with is the *importance of timing* in EAD-mediated arrhythmias.

In the case of the EAD burst study (Chapter 3), it is clear that conventional explanations based on magnitude are insufficient to explain the occurrence of EADs, but rather, the time constants (and magnitude) of the ion channels have to be in the correct resonance relations to each other. Take the analogy of two people arm wrestling. Oscillations do not occur when one individual massively overpowers the other. Rather, oscillations can only occur when the strengths of the individuals fluctuate out of phase with one another. That is the essence of the Hopf-Homoclinic bifurcation mechanism for EADs

In the case of the biexcitability study (Chapter 4), the timing (and magnitude) of the stimulus is important in the *initiation* of either a I_{Na}-dependent or I_{Ca}-dependent (ie. EAD-mediated) spiral wave in certain pathological tissue substrates. While EADs are self-limited at the single cell level, the timing (and magnitude) of the electrotonic current present in tissue as a result of cell-to-cell coupling, facilitates

the *maintenance* of EADs (ie. I_{Ca}-dependent spiral waves) at the tissue level. In heterogeneous tissue, these I_{Ca}-dependent spiral waves meander while "spewing" both I_{Ca}- and I_{Na}-mediated wavefronts along the arm of the spiral wave, giving rise to the classic heart rate and ECG appearance of TdP.

In the case of the K_{ATP} channel activation "flipping the switch" study (Chapter 5), whether a I_{Ca}-dependent reentry either spontaneously terminates or converts to a I_{Na}-dependent reentry is dependent on the timing of K_{ATP} channel activation. More specifically, the outcome is dependent on the presence of I_{Na}-dependent wavefronts being present in the tissue at the time of K_{ATP} channel activation. These results are consistent with clinical observations of PVT and TdP, suggesting that in the clinical setting, K_{ATP} channels may serve to not only spontaneously terminate these I_{Ca}-dependent arrhythmias, but also to facilitate their degeneration to I_{Na}-dependent VT/VF.

I hope that this new perspective of EADs ("born by Hopf and die by Homoclinic") that emphasizes timing, will lead to new therapeutic targets, and a new paradigm for drug development to prevent cardiac arrhythmias by targeting the time dependent properties of specific channels, rather than focusing on blocking their magnitude, often times with lackluster clinical efficacy, severe systemic side effects, and significant consequences related to excitation-contraction coupling

7 Bibliography

1. Tran, D.X., et al., *Bifurcation and chaos in a model of cardiac early afterdepolarizations.* Phys Rev Lett, 2009. **102**(25): p. 258103.
2. Council, N.R. *2010 National Research Council Data-Based Assessment of Research Doctorate Programs*. 2010; Available from: http://www.graduate.ku.edu/-downloads/NRC/MolecularandIntegrativePhysiology_102910.pdf.
3. FDA, *Guidance for Industry: E14 Clinical Evaluation of QT/QTc Interval Prolongation and Proarrhythmic Potential for Non-Antiarrhythmic Drugs*, F.a.D. Administration, Editor 2005, E14 Clinical Evaluation of QT/QTc Interval Prolongation and Proarrhythmic Potential for Non-Antiarrhythmic Drugs: Rockville, MD.
4. Strogatz, S.H., *Nonlinear dynamics and Chaos : with applications to physics, biology, chemistry, and engineering*. Studies in nonlinearity1994, Reading, Mass.: Addison-Wesley Pub. xi, 498 p.
5. Shaw, R.M. and Y. Rudy, *Electrophysiologic effects of acute myocardial ischemia. A mechanistic investigation of action potential conduction and conduction failure.* Circ Res, 1997. **80**(1): p. 124-38.
6. Chang, M.G., et al., *Spiral waves and reentry dynamics in an in vitro model of the healed infarct border zone.* Circ Res, 2009. **105**(11): p. 1062-71.

7. Shaw, R.M. and Y. Rudy, *Ionic mechanisms of propagation in cardiac tissue. Roles of the sodium and L-type calcium currents during reduced excitability and decreased gap junction coupling.* Circ Res, 1997. **81**(5): p. 727-41.

8. Quasar. *Basic cardiac action potential (with labels)*. 2009 [cited 2011 August 6]; Available from: http://en.wikipedia.org/wiki/File:Action_potential_ventr_myocyte.gif.

9. Marban, E., *Cardiac channelopathies.* Nature, 2002. **415**(6868): p. 213-8.

10. Wetzel, G.T. and T.S. Klitzner, *Developmental cardiac electrophysiology recent advances in cellular physiology.* Cardiovasc Res, 1996. **31 Spec No**: p. E52-60.

11. Bers, D.M., *Cardiac excitation-contraction coupling.* Nature, 2002. **415**(6868): p. 198-205.

12. Calmettes, G., *System's Biology Analysis of Chronic Hypoxia-Induced Heart Energetics Adaptation*, in *Laboratory of Magnetic Resonance for the study of Biological Systems*2010, CNRS-University of Bordeaux 2.

13. Franzini-Armstrong, C., F. Protasi, and V. Ramesh, *Shape, size, and distribution of Ca(2+) release units and couplons in skeletal and cardiac muscles.* Biophys J, 1999. **77**(3): p. 1528-39.

14. Alseikhan, B.A., et al., *Engineered calmodulins reveal the unexpected eminence of Ca2+ channel inactivation in controlling heart excitation.* Proc Natl Acad Sci U S A, 2002. **99**(26): p. 17185-90.

15. Moss, R.L., M. Razumova, and D.P. Fitzsimons, *Myosin crossbridge activation of cardiac thin filaments: implications for myocardial function in health and disease.* Circ Res, 2004. **94**(10): p. 1290-300.

16. !!! INVALID CITATION !!!

17. Reuter, H., et al., *Na(+)--Ca2+ exchange in the regulation of cardiac excitation-contraction coupling.* Cardiovasc Res, 2005. **67**(2): p. 198-207.

18. Schotten, U., et al., *Pathophysiological mechanisms of atrial fibrillation: a translational appraisal.* Physiol Rev, 2011. **91**(1): p. 265-325.

19. Sung, R.J., et al., *Electrophysiological mechanisms of ventricular arrhythmias in relation to Andersen-Tawil syndrome under conditions of reduced IK1: a simulation study.* Am J Physiol Heart Circ Physiol, 2006. **291**(6): p. H2597-605.

20. Volders, P.G., et al., *Progress in the understanding of cardiac early afterdepolarizations and torsades de pointes: time to revise current concepts.* Cardiovasc Res, 2000. **46**(3): p. 376-92.

21. Milberg, P., et al., *Inhibition of the Na+/Ca2+ exchanger suppresses torsades de pointes in an intact heart model of long QT syndrome-2 and long QT syndrome-3.* Heart Rhythm, 2008. **5**(10): p. 1444-52.

22. Luo, C.H. and Y. Rudy, *A dynamic model of the cardiac ventricular action potential. II. Afterdepolarizations, triggered activity, and potentiation.* Circ Res, 1994. **74**(6): p. 1097-113.

23. van Helvete, H. *Molecular mechanism of muscle contraction in skeletal muscle.* 2010 [cited 2011 August 6,]; Available from: http://en.wikipedia.org/wiki/File:Muskel-molekulartranslation.png.

24. Langer, G.A., *The myocardium*. 2nd ed1997, San Diego: Academic Press. xviii, 405 p., 3 p. of plates.

25. Ter Keurs, H.E. and P.A. Boyden, *Calcium and arrhythmogenesis.* Physiol Rev, 2007. **87**(2): p. 457-506.

26. *National Heart & Lung Institute (NHLI) -- Glossary*. 2011 [cited 2011 August 6,]; Available from: http://www1.imperial.ac.uk/nhli/cardio/heart/ccir/glossary/.

27. Doedel, E.J., Paffenroth, R.C., Champneys, A.R., Fairgrieve, T.F., Kuznetsov, Yu.A., Sandstede, B., & Wang, X., *AUTO 2000: Continuation and bifurcation software for ordinary differential equations (with HomCont)*, in *Technical Report, Caltech*February 2001.

28. Xie, Y., et al., *So little source, so much sink: requirements for afterdepolarizations to propagate in tissue.* Biophys J, 2010. **99**(5): p. 1408-15.

29. Munoz, V., et al., *Adenoviral expression of IKs contributes to wavebreak and fibrillatory conduction in neonatal rat ventricular cardiomyocyte monolayers.* Circ Res, 2007. **101**(5): p. 475-83.

30. Beauchamp, P., et al., *Relative contributions of connexins 40 and 43 to atrial impulse propagation in synthetic strands of neonatal and fetal murine cardiomyocytes.* Circ Res, 2006. **99**(11): p. 1216-24.

31. Kleber, A.G. and Y. Rudy, *Basic mechanisms of cardiac impulse propagation and associated arrhythmias.* Physiol Rev, 2004. **84**(2): p. 431-88.

32. Beauchamp, P., et al., *Electrical propagation in synthetic ventricular myocyte strands from germline connexin43 knockout mice.* Circ Res, 2004. **95**(2): p. 170-8.

33. Thomas, S.P., et al., *Impulse propagation in synthetic strands of neonatal cardiac myocytes with genetically reduced levels of connexin43.* Circ Res, 2003. **92**(11): p. 1209-16.

34. Pimentel, R.C., et al., *Autocrine regulation of myocyte Cx43 expression by VEGF.* Circ Res, 2002. **90**(6): p. 671-7.

35. Kucera, J.P., A.G. Kleber, and S. Rohr, *Slow conduction in cardiac tissue: insights from optical mapping at the cellular level.* J Electrocardiol, 2001. **34 Suppl**: p. 57-64.

36. Zhuang, J., et al., *Pulsatile stretch remodels cell-to-cell communication in cultured myocytes.* Circ Res, 2000. **87**(4): p. 316-22.

37. Tung, L. and A.G. Kleber, *Virtual sources associated with linear and curved strands of cardiac cells.* Am J Physiol Heart Circ Physiol, 2000. **279**(4): p. H1579-90.

38. Gillis, A.M., et al., *Mechanism of ventricular defibrillation. The role of tissue geometry in the changes in transmembrane potential in patterned myocyte cultures.* Circulation, 2000. **101**(20): p. 2438-45.

39. Beardslee, M.A., et al., *Dephosphorylation and intracellular redistribution of ventricular connexin43 during electrical uncoupling induced by ischemia.* Circ Res, 2000. **87**(8): p. 656-62.

40. Rohr, S., A.G. Kleber, and J.P. Kucera, *Optical recording of impulse propagation in designer cultures. Cardiac tissue architectures inducing ultra-slow conduction.* Trends Cardiovasc Med, 1999. **9**(7): p. 173-9.

41. Kleber, A.G., *Discontinuous propagation of the cardiac impulse and arrhythmogenesis.* J Cardiovasc Electrophysiol, 1999. **10**(7): p. 1025-7.

42. Rohr, S., J.P. Kucera, and A.G. Kleber, *Slow conduction in cardiac tissue, I: effects of a reduction of excitability versus a reduction of electrical coupling on microconduction.* Circ Res, 1998. **83**(8): p. 781-94.

43. Kucera, J.P., A.G. Kleber, and S. Rohr, *Slow conduction in cardiac tissue, II: effects of branching tissue geometry.* Circ Res, 1998. **83**(8): p. 795-805.

44. Fast, V.G., et al., *Activation of cardiac tissue by extracellular electrical shocks: formation of 'secondary sources' at intercellular clefts in monolayers of cultured myocytes.* Circ Res, 1998. **82**(3): p. 375-85.

45. Rohr, S., et al., *Paradoxical improvement of impulse conduction in cardiac tissue by partial cellular uncoupling.* Science, 1997. **275**(5301): p. 841-4.

46. Kleber, A.G. and V. Fast, *Molecular and cellular aspects of re-entrant arrhythmias.* Basic Res Cardiol, 1997. **92 Suppl 1**: p. 111-9.

47. Seki, S., et al., *Fetal and postnatal development of Ca2+ transients and Ca2+ sparks in rat cardiomyocytes.* Cardiovasc Res, 2003. **58**(3): p. 535-48.

48. Kleber, A.G., *The shape of the electrical action-potential upstroke: a new aspect from optical measurements on the surface of the heart.* Circ Res, 2005. **97**(3): p. 204-6.

49. Bishop, M.J., et al., *Photon scattering effects in optical mapping of propagation and arrhythmogenesis in the heart.* J Electrocardiol, 2007. **40**(6 Suppl): p. S75-80.

50. Abraham, M.R., et al., *Antiarrhythmic engineering of skeletal myoblasts for cardiac transplantation.* Circ Res, 2005. **97**(2): p. 159-67.

51. Kizana, E., et al., *Gene transfer of connexin43 mutants attenuates coupling in cardiomyocytes: novel basis for modulation of cardiac conduction by gene therapy.* Circ Res, 2007. **100**(11): p. 1597-604.

52. Sekar, R.B., et al., *IK1 heterogeneity affects genesis and stability of spiral waves in cardiac myocyte monolayers.* Circ Res, 2009. **104**(3): p. 355-64.

53. Sekar, R.B., et al., *Lentiviral vector-mediated expression of GFP or Kir2.1 alters the electrophysiology of neonatal rat ventricular myocytes without inducing cytotoxicity.* Am J Physiol Heart Circ Physiol, 2007. **293**(5): p. H2757-70.

54. Chang, M.G., et al., *Proarrhythmic potential of mesenchymal stem cell transplantation revealed in an in vitro coculture model.* Circulation, 2006. **113**(15): p. 1832-41.

55. Rohr, S., *Cardiac fibroblasts in cell culture systems: myofibroblasts all along?* J Cardiovasc Pharmacol, 2011. **57**(4): p. 389-99.

56. Rohr, S., *Myofibroblasts in diseased hearts: new players in cardiac arrhythmias?* Heart Rhythm, 2009. **6**(6): p. 848-56.

57. Miragoli, M., N. Salvarani, and S. Rohr, *Myofibroblasts induce ectopic activity in cardiac tissue.* Circ Res, 2007. **101**(8): p. 755-8.

58. Lewandowski, R., et al., *RXP-E: a connexin43-binding peptide that prevents action potential propagation block.* Circ Res, 2008. **103**(5): p. 519-26.

59. Kossmann, C.E., *The long Q-T interval and syndromes.* Adv Intern Med, 1987. **32**: p. 87-110.

60. Vermeulen, J.T., *Mechanisms of arrhythmias in heart failure.* J Cardiovasc Electrophysiol, 1998. **9**(2): p. 208-21.

61. Marban, E., S.W. Robinson, and W.G. Wier, *Mechanisms of arrhythmogenic delayed and early afterdepolarizations in ferret ventricular muscle.* Journal of Clinical Investigation, 1986. **78**(5): p. 1185-92.

62. Hirano, Y., A. Moscucci, and C.T. January, *Direct measurement of L-type Ca2+ window current in heart cells.* Circ Res, 1992. **70**(3): p. 445-55.

63. Shorofsky, S.R. and C.T. January, *L- and T-type Ca2+ channels in canine cardiac Purkinje cells. Single-channel demonstration of L-type Ca2+ window current.* Circ Res, 1992. **70**(3): p. 456-64.

64. January, C.T. and J.M. Riddle, *Early afterdepolarizations: mechanism of induction and block. A role for L-type Ca2+ current.* Circ Res, 1989. **64**(5): p. 977-90.

65. Roden, D.M., *Long QT syndrome: reduced repolarization reserve and the genetic link.* J Intern Med, 2006. **259**(1): p. 59-69.

66. Kannankeril, P.J. and D.M. Roden, *Drug-induced long QT and torsade de pointes: recent advances.* Curr Opin Cardiol, 2007. **22**(1): p. 39-43.

67. Michael, G., et al., *Remodelling of cardiac repolarization: how homeostatic responses can lead to arrhythmogenesis.* Cardiovasc Res, 2009. **81**(3): p. 491-9.

68. Roden, D.M., *Taking the "idio" out of "idiosyncratic": predicting torsades de pointes.* Pacing Clin Electrophysiol, 1998. **21**(5): p. 1029-34.

69. Guevara, M.R. and H.J. Jongsma, *Three ways of abolishing automaticity in sinoatrial node: ionic modeling and nonlinear dynamics.* American Journal of Physiology, 1992. **262**: p. 1268-1286.

70. Qu, Z., W.R. MacLellan, and J.N. Weiss, *Dynamics of the cell cycle--checkpoints, sizers and timers.* Biophysical Journal, 2003. **85**: p. 3600-3611.

71. Goldbeter, A. and R. Lefever, *Dissipative structures for an allosteric model. Application to glycolytic oscillations.* Biophysical Journal, 1972. **12**(10): p. 1302-15.

72. Goldbeter, A., *A model for circadian oscillations in the Drosophila period protein (PER).* Proc Biol Sci, 1995. **261**(1362): p. 319-24.

73. Eschenhagen, T., et al., *Cardiac tissue engineering.* Transpl Immunol, 2002. **9**(2-4): p. 315-21.

74. Husse, B. and M. Wussling, *Developmental changes of calcium transients and contractility during the cultivation of rat neonatal cardiomyocytes.* Mol Cell Biochem, 1996. **163-164**: p. 13-21.

75. Zimmermann, W.H., et al., *Tissue engineering of a differentiated cardiac muscle construct.* Circ Res, 2002. **90**(2): p. 223-30.

76. Goldhaber, J.I., et al., *Action potential duration restitution and alternans in rabbit ventricular myocytes: the key role of intracellular calcium cycling.* Circ Res, 2005. **96**(4): p. 459-66.

77. Dipla, K., et al., *The sarcoplasmic reticulum and the Na+/Ca2+ exchanger both contribute to the Ca2+ transient of failing human ventricular myocytes.* Circ Res, 1999. **84**(4): p. 435-44.

78. Negretti, N., S.C. O'Neill, and D.A. Eisner, *The effects of inhibitors of sarcoplasmic reticulum function on the systolic Ca2+ transient in rat ventricular myocytes.* J Physiol, 1993. **468**: p. 35-52.

79. Lukyanenko, V., et al., *Dynamic regulation of sarcoplasmic reticulum Ca(2+) content and release by luminal Ca(2+)-sensitive leak in rat ventricular myocytes.* Biophys J, 2001. **81**(2): p. 785-98.

80. Mahajan, A., et al., *Modifying L-Type Calcium Current Kinetics: Consequences for Cardiac Excitation and Arrhythmia Dynamics.* Biophysical Journal, 2008. **94**(2): p. 411-423.

81. Malmivuo, J. and R. Plonsey, *Bioelectromagnetism*1995, New York: Oxford University Press.

82. Mahajan, A., et al., *A rabbit ventricular action potential model replicating cardiac dynamics at rapid heart rates.* Biophys J, 2008. **94**(2): p. 392-410.

83. Chang, M.G., et al., *Bi-stable wave propagation and early afterdepolarization-mediated cardiac arrhythmias.* Heart Rhythm, 2012. **9**: p. 115-122.

84. Cohen, S.D. and A.C. Hindmarsh, *CVODE, A Stiff/Nonstiff ODE Solver in C.* Computers in Physics, 1996. **10**(2): p. 138-143.

85. Xie, Y., et al., *The Transient Outward Current Ito Promotes Early Afterdepolarizations.* Biophysical Journal, 2010. **98**(3): p. 531a (abstract).

86. Sato, D., et al., *Synchronization of chaotic early afterdepolarizations in the genesis of cardiac arrhythmias.* Proc Natl Acad Sci U S A, 2009. **106**(9): p. 2983-8.

87. Landau, M., et al., *Bistabilities and annihilation phenomena in electrophysiological cardiac models.* Circ Res, 1990. **66**(6): p. 1658-72.

88. Holmes, P., Marsden, JE, *Bifurcations of dynamical systems and nonlinear oscillations in engineering systems*, in *Nonlinear Partial Differential Equations and Applications. Lecture Notes in Mathematics, Volume 648*1978, Springer-Verlag: New York. p. 163-206.

89. January, C.T., J.M. Riddle, and J.J. Salata, *A model for early afterdepolarizations: induction with the Ca2+ channel agonist Bay K 8644.* Circulation Research, 1988. **62**(3): p. 563-71.

90. Kass, R.S., *Voltage-dependent modulation of cardiac calcium channel current by optical isomers of Bay K 8644: implications for channel gating.* Circulation Research, 1987. **61**(4 Pt 2): p. I1-5.

91. Sanguinetti, M.C., D.S. Krafte, and R.S. Kass, *Voltage-dependent modulation of Ca channel current in heart cells by Bay K8644.* Journal of General Physiology, 1986. **88**(3): p. 369-92.

92. Faber, G.M. and Y. Rudy, *Action potential and contractility changes in [Na(+)](i) overloaded cardiac myocytes: a simulation study.* Biophys J, 2000. **78**(5): p. 2392-404.

93. Shannon, T.R., et al., *A mathematical treatment of integrated Ca dynamics within the ventricular myocyte.* Biophysical Journal, 2004. **87**(5): p. 3351-71.

94. Shaw, R.M. and Y. Rudy, *Electrophysiologic effects of acute myocardial ischemia: A mechanistic investigation of action potential conduction and conduction failure.* Circ. Res., 1997. **80**(1): p. 124-138.

95. Chang, M.G., et al., *Spiral Waves and Reentry Dynamics in an In Vitro Model of the Healed Infarct Border Zone.* Circulation Research, 2009. **105**(11): p. 1062-1071.

96. Shaw, R.M. and Y. Rudy, *Ionic mechanisms of propagation in cardiac tissue: Roles of the sodium and L-type calcium currents during reduced excitability and decreased gap junction coupling.* Circ. Res., 1997. **81**: p. 727-741.

97. Strogatz, S.H., *Nonlinear dynamics and Chaos: with applications to physics, biology, chemistry, and engineering*. Studies in nonlinearity2000, Cambridge: Westview Press. xi, 498.

98. Gardner, T.S., C.R. Cantor, and J.J. Collins, *Construction of a genetic toggle switch in Escherichia coli.* Nature, 2000. **403**(6767): p. 339-42.

99. Sha, W., et al., *Hysteresis drives cell-cycle transitions in Xenopus laevis egg extracts.* Proc Natl Acad Sci U S A, 2003. **100**(3): p. 975-80.

100. Keating, M.T. and M.C. Sanguinetti, *Molecular and cellular mechanisms of cardiac arrhythmias.* Cell, 2001. **104**(4): p. 569-80.

101. Li, G.R., et al., *Transmural action potential and ionic current remodeling in ventricles of failing canine hearts.* Am J Physiol Heart Circ Physiol, 2002. **283**(3): p. H1031-41.

102. Saucerman, J.J., et al., *Proarrhythmic consequences of a KCNQ1 AKAP-binding domain mutation: computational models of whole cells and heterogeneous tissue.* Circulation Research, 2004. **95**(12): p. 1216-24.

103. Roden, D.M., *Drug-induced prolongation of the QT interval.* New England Journal of Medicine, 2004. **350**(10): p. 1013-22.

104. El-Sherif, N. and G. Turitto, *Torsade de pointes.* Current Opinion in Cardiology, 2003. **18**(1): p. 6-13.

105. Antzelevitch, C., *Ionic, molecular, and cellular bases of QT-interval prolongation and torsade de pointes.* Europace, 2007. **9 Suppl 4**: p. iv4-15.

106. Liu, J. and K.R. Laurita, *The mechanism of pause-induced torsade de pointes in long QT syndrome.* Journal of Cardiovascular Electrophysiology, 2005. **16**(9): p. 981-7.

107. Choi, B.R., F. Burton, and G. Salama, *Cytosolic Ca2+ triggers early afterdepolarizations and Torsade de Pointes in rabbit hearts with type 2 long QT syndrome.* J. Physiol., 2002. **543**(2): p. 615-631.

108. Krikler, D.M. and P.V. Curry, *Torsade De Pointes, an atypical ventricular tachycardia.* Br Heart J, 1976. **38**(2): p. 117-20.

109. Drew, B.J., et al., *Prevention of torsade de pointes in hospital settings: a scientific statement from the American Heart Association and the American College of Cardiology Foundation.* Circulation, 2010. **121**(8): p. 1047-60.

110. Mahajan, A., et al., *A rabbit ventricular action potential model replicating cardiac dynamics at rapid heart rates.* Biophysical Journal, 2008. **94**(2): p. 392-410.

111. Rohr, S., D.M. Scholly, and A.G. Kleber, *Patterned growth of neonatal rat heart cells in culture. Morphological and electrophysiological characterization.* Circulation Research, 1991. **68**(1): p. 114-30.

112. de Diego, C., et al., *Spatially discordant alternans in cardiomyocyte monolayers.* Am J Physiol Heart Circ Physiol, 2008. **294**(3): p. H1417-25.

113. Laurita, K.R., et al., *Transmural heterogeneity of calcium handling in canine.* Circulation Research, 2003. **92**(6): p. 668-75.

114. Akar, F.G. and D.S. Rosenbaum, *Transmural electrophysiological heterogeneities underlying arrhythmogenesis in heart failure.* Circulation Research, 2003. **93**(7): p. 638-45.

115. Pertsov, A.M., et al., *Spiral waves of excitation underlie reentrant activity in isolated cardiac muscle.* Circulation Research, 1993. **72**(3): p. 631-650.

116. Tran, D.X., et al., *Bifurcation and Chaos in a Model of Cardiac Early Afterdepolarizations.* Physical Review Letters, 2009. **102**(25): p. 258103.

117. Clancy, C.E. and Y. Rudy, *Linking a genetic defect to its cellular phenotype in a cardiac arrhythmia.* Nature, 1999. **400**(6744): p. 566-9.

118. Ten Tusscher, K.H., R. Hren, and A.V. Panfilov, *Organization of ventricular fibrillation in the human heart.* Circulation Research, 2007. **100**(12): p. e87-101.

119. Xie, F., et al., *A simulation study of the effects of cardiac anatomy in ventricular fibrillation.* Journal of Clinical Investigation, 2004. **113**(5): p. 686-93.

120. Valderrabano, M., et al., *Frequency analysis of ventricular fibrillation in swine ventricles.* Circulation Research, 2002. **90**(2): p. 213-222.

121. Choi, B.R., et al., *Life span of ventricular fibrillation frequencies.* Circulation Research, 2002. **91**(4): p. 339-345.

122. Ehara, T., A. Noma, and K. Ono, *Calcium-activated non-selective cation channel in ventricular cells isolated from adult guinea-pig hearts.* Journal of Physiology, 1988. **403**: p. 117-33.

123. Giles, W. and Y. Shimoni, *Comparison of sodium-calcium exchanger and transient inward currents in single cells from rabbit ventricle.* Journal of Physiology, 1989. **417**: p. 465-81.

124. Damiano, B.P. and M.R. Rosen, *Effects of pacing on triggered activity induced by early afterdepolarizations.* Circulation, 1984. **69**(5): p. 1013-25.

125. Panfilov, A.V. and A.V. Holden, *Computational Biology of the Heart*1997, New York: Wiley.

126. Qu, Z. and A. Garfinkel, *An advanced numerical algorithm for solving partial differential equation in cardiac conduction.* IEEE Trans. Biomed. Eng., 1999. **49**(9): p. 1166-1168.

127. Sato, D., et al., *Acceleration of cardiac tissue simulation with graphic processing units.* Medical and Biological Engineering and Computing, 2009. **47**(9): p. 1011-5.

128. Luo, C.H. and Y. Rudy, *A dynamical model of the cardiac ventricular action potential: I. simulations of ionic currents and concentration changes.* Circulation Research, 1994. **74**(6): p. 1071-1096.

129. Chang, M.G., et al., *Bi-stable wave propagation and early afterdepolarization-mediated cardiac arrhythmias.* Heart Rhythm, 2012. **9**(1): p. 115-22.

130. Fish, F.A., C. Prakash, and D.M. Roden, *Suppression of repolarization-related arrhythmias in vitro and in vivo by low-dose potassium channel activators.* Circulation Research, 1990. **82**: p. 1362-1369.

131. Spinelli, W., et al., *Antiarrhythmic actions of the ATP-regulated K+ current activated by pinacidil.* Circ Res, 1991. **68**(4): p. 1127-37.

132. Carlsson, L., et al., *Antiarrhythmic effects of potassium channel openers in rhythm abnormalities related to delayed repolarization.* Circulation, 1992. **85**(4): p. 1491-500.

133. Sato, T., et al., *Early afterdepolarization abolished by potassium channel opener in a patient with idiopathic long QT syndrome.* J Cardiovasc Electrophysiol, 1995. **6**(4): p. 279-82.

134. Riccioppo Neto, F., O. Mesquita Junior, and G.B. Olivera, *Antiarrhythmic and electrophysiological effects of the novel KATP channel opener, rilmakalim, in rabbit cardiac cells.* Gen Pharmacol, 1997. **29**(2): p. 201-5.

135. Watanabe, O., et al., *Nicorandil, a potassium channel opener, abolished torsades de pointes in a patient with complete atrioventricular block.* Pacing Clin Electrophysiol, 1999. **22**(4 Pt 1): p. 686-8.

136. Shimizu, W. and C. Antzelevitch, *Effects of a K(+) channel opener to reduce transmural dispersion of repolarization and prevent torsade de pointes in LQT1, LQT2, and LQT3 models of the long-QT syndrome.* Circulation, 2000. **102**(6): p. 706-12.

137. Chinushi, M., et al., *Triggers of ventricular tachyarrhythmias and therapeutic effects of nicorandil in canine models of LQT2 and LQT3 syndromes.* J Am Coll Cardiol, 2002. **40**(3): p. 555-62.

138. El-Sherif, N. and G. Turitto, *Torsade de pointes.* Curr Opin Cardiol, 2003. **18**(1): p. 6-13.

139. Calmettes, G., G.B. Drummond, and S.L. Vowler, *Making do with what we have: use your bootstraps.* J Physiol, 2012. **590**(Pt 15): p. 3403-6.

140. Ferrero, J.M., Jr., et al., *Simulation of action potentials from metabolically impaired cardiac myocytes. Role of ATP-sensitive K+ current.* Circ Res, 1996. **79**(2): p. 208-21.

141. Chang, M.G., et al., *Dynamics of early afterdepolarization-mediated triggered activity in cardiac monolayers.* Biophys J, 2012. **102**(12): p. 2706-14.

142. Asano, Y., et al., *Optical mapping of drug-induced polymorphic arrhythmias and torsade de pointes in the isolated rabbit heart.* J.Am.Coll.Cardiol., 1997. **29**: p. 831-842.

143. Choi, B.R., F. Burton, and G. Salama, *Cytosolic Ca2+ triggers early afterdepolarizations and Torsade de Pointes in rabbit hearts with type 2 long QT syndrome.* J Physiol, 2002. **543**(Pt 2): p. 615-31.

144. Nattel, S., et al., *Mechanisms of termination of atrial fibrillation by Class I antiarrhythmic drugs: evidence from clinical, experimental, and mathematical modeling studies.* J Cardiovasc Electrophysiol, 2003. **14**(10 Suppl): p. S133-9.

145. Qu, Z. and J.N. Weiss, *Effects of Na+ and K+ channel blockade on vulnerability to and termination of fibrillation in simulated normal cardiac tissue.* Am J Physiol Heart Circ Physiol, 2005. **289**(4): p. H1692-1701.

146. Qu, Z., *Critical mass hypothesis revisited: role of dynamical wave stability in spontaneous termination of cardiac fibrillation.* Am J Physiol, 2006. **290**(1): p. H255-63.

147. Yamazaki, M., et al., *Mechanisms of destabilization and early termination of spiral wave reentry in the ventricle by a class III antiarrhythmic agent, nifekalant.* Am J Physiol Heart Circ Physiol, 2007. **292**(1): p. H539-48.

148. Splawski, I., et al., *Inaugural Article: Severe arrhythmia disorder caused by cardiac L-type calcium channel mutations.* PNAS, 2005. **102**(23): p. 8089-8096.